HIGH PERFORMANCE SUPERCAPATTERY WITH RGO/TiO_2 NANOCOMPOSITES ANODE AND AN ACTIVATED CARBON CATHODE

IVY HENG

INSTITUE FOR ADVANCED STUDIES
UNIVERSITY OF MALAYA
KUALA LUMPUR

2019

HIGH PERFORMANCE SUPERCAPATTERY WITH RGO/TiO_2 ANODE AND AN ACTIVATED CARBON CATHODE

IVY HENG

**DISSERTATION SUBMITTED IN FULFILMENT OF
THE REQUIREMENTS FOR THE DEGREE OF MASTER
OF PHILOSOPHY**

**INSTITUTE FOR ADVANCED STUDIES
UNIVERSITY OF MALAYA
KUALA LUMPUR**

2019

UNIVERSITY OF MALAYA
ORIGINAL LITERARY WORK DECLARATION

Name of Candidate: Ivy Heng

Matric No: HMA170013

Name of Degree: Master of Philosophy

Title of Thesis ("this Work"): High performance supercapattery with rGO/TiO_2 nanocomposites anode and an activated carbon cathode.

Field of Study: Chemistry

I do solemnly and sincerely declare that:

(1) I am the sole author/writer of this Work;
(2) This Work is original;
(3) Any use of any work in which copyright exists was done by way of fair dealing and for permitted purposes and any excerpt or extract from, or reference to or reproduction of any copyright work has been disclosed expressly and sufficiently and the title of the Work and its authorship have been acknowledged in this Work;
(4) I do not have any actual knowledge nor do I ought reasonably to know that the making of this work constitutes an infringement of any copyright work;
(5) I hereby assign all and every rights in the copyright to this Work to the University of Malaya ("UM"), who henceforth shall be owner of the copyright in this Work and that any reproduction or use in any form or by any means whatsoever is prohibited without the written consent of UM having been first had and obtained;
(6) I am fully aware that if in the course of making this Work I have infringed any copyright whether intentionally or otherwise, I may be subject to legal action or any other action as may be determined by UM.

Candidate's Signature Date:

Subscribed and solemnly declared before,

Witness's Signature Date:

Name:

Designation:

ABSTRACT

Titanium dioxide (TiO_2) nanocrystals in intermediate phase of amorphous and anatase has been successfully synthesized through a simple, low temperature peroxo sol gel approach. Tranmission electron microscopy revealed that the TiO_2 nanocrystals obtained have an average diameter of 8-133 nm. The effects of calcination temperature on the morphology and phase transformation were studied by annealing the samples at 200-800 °C. TiO_2 nanocrystals annealed at 200 °C with diameter of 12 nm exhibited the highest specific capacitance of 26.46 C g^{-1} at current density of 0.2 A g^{-1} in 1M KOH as the electrolyte. The high specific capacity is attributed to the intermediate phase of amorphous and anatase structure which enhanced the redox active sites of the TiO_2 nanocrystals. A hybrid material of reduced graphene oxide/titanium dioxide (rGO/TiO_2) was successfully synthesized by facile hydrothermal technique. A different amount of GO ratios at 5%, 10%, 20%, and 30% were loaded with TiO_2. It is a well-known fact that porous structure and crystallinity of resultant rGO/TiO_2 play a crucial role in synergistic effect which facilitate electron transfer movement and reduce the volume changes during a charge-discharge cycle process. Based on the results obtained, an optimum of 10 wt. % GO loading with TiO_2 nanocrystals revealed that electrochemical performance achieved the highest specific capacity of 116.70 C g^{-1} with 0.2 A g^{-1} among the samples. This result inferred that high efficiency of ion diffusion was obtained with low charge transfer resistance between TiO_2 nanocrystals and rGO. The supercapattery was assembled in a configuration of optimized 10% rGO/TiO_2 nanocomposites as anode while activated carbon as cathode. The result obtained a superior energy density of 54.37 Wh kg^{-1} at power density of 420.48 W kg^{-1}. Additionally, the specific capacity still remained at 92% for 3000 charging-discharging cycles under a current density of 1 A g^{-1}. Hence, good life cycle stability, high specific capacity and low charge transfer resistance of rGO/TiO_2 nanocomposites electrode suggested that the prepared materials was a promising anode material for supercapattery application.

ABSTRAK

Nanokristal titanium dioksida (TiO_2) dalam fasa perantaraan amorf dan anatase telah berjaya disintesis dengan kaedah peroxo sol gel dalam suhu yang rendah. Mikroskop elektron mendedahkan bahawa nanokristal TiO_2 diperolehi mempunyai diameter purata 8-133 nm. Kesan morfologi dan transformasi fasa dikaji dengan merelaukan sampel pada suhu 200-800 °C. Nanokristals TiO_2 yang direlaukan pada suhu 200 °C mempunyai diameter 12 nm, mempamerkan spesifik kapasiti tertinggi iaitu 26.46 C g^{-1} pada ketumpatan arus 0.2 A g^{-1} dalam 1M KOH sebagai elektrolit.Spesifik kapasiti yang tinggi adalah disebabkan oleh fasa pertengahan struktur amorf dan anatase yang meningkatkan tapak aktif redoks dari nanokristals TiO_2. Bahan hibrida reduced graphene oxide/titanium dioxide (rGO/TiO_2) telah berjaya disintesis dengan teknik hidroterma yang mudah.Nisbah pembebanan GO berbeza pada 5%, 10%, 20% dan 30% dicampur dengan TiO_2. Struktur poros dan kristalografi rGO/TiO_2 yang dihasilkan menyebabkan kesan sinergi yang mempercepatkan pergerakan pemindahan elektron dan mengurangkan perubahan volum semasa proses kitaran pelepasan caj. Berdasarkan hasil yang diperoleh, optimum pemilihan 10 wt.% GO dengan nanokristals TiO_2 mendedahkan bahawa prestasi elektrokimia mencapai kapasiti spesifik tertinggi iaitu 116.70 C g^{-1} pada ketumpatan arus 0.2 A g^{-1}. Keputusan ini mencerminkan kecepatan penembusan ion dan kekurangan rintangan pemindahan caj antara nanokristals TiO_2 dan rGO, dan ini menghasilkan prestasi elektrokimia yang optimum.Superkapbateri dipasang berdasarkan 10% nanokomposit rGO/TiO_2 sebagai anod semasa karbon aktif sebagai katod. Hasilnya memperoleh ketumpatan tenaga tinggi 54.37 Wh kg^{-1} pada ketumpatan kuasa 420.48 W kg^{-1}. Di samping itu, kapasiti khusus masih kekal pada 92% untuk 3000 kitaran pada ketumpatan arus 1 A g^{-1}. Oleh itu, kestabilam kitaran hidup yang baik, spesifik kapasitif yang tinggi dan rintangan pemindahan caj rendah rGO/TiO_2 nanokomposit elektrod menyatakan bahawa bahan anod menjadi tumpuan dalam aplikasi superkapbateri yang berpotensi.

ACKNOWLEDGEMENTS

First and foremost, it is a genuine pleasure to express my deep sense of thanks and gratitude to my supervisors, Ir. Dr. Lai Chin Wei and Associate Prof. Juan Joon Ching on their dedication and keen interest above all their overwhelming attitude to help me completing my work. Their timely advice, meticulous scrutiny scholarly advice and scientific approach have helped me to a very great extent to accomplish this research.

This research was supported by a grant from the University Malaya Research Grant (UMRG) and Postgraduate Research Fund (PPP) for the sources of funding through this study.

I owe a deep sense of gratitude to all NANOCAT's technical and administrative staff for their keen interest on helping me at every stage of my research work and accommodation. I was extremely thankful to my NANOCAT's labmates for their kind help and cooperation throughout my research period.

Lastly, it is my privilege to thank my family for financial support and constant encouragement during my master study.

TABLE OF CONTENTS

LIST OF FIGURES

LIST OF TABLES

LIST OF SYMBOLS AND ABBREVIATIONS

A	:	Amperes
AC	:	Activated carbon
BET	:	Brunauer-Emmett-Teller
C	:	Capacity
cm	:	Centimetres
CV	:	Cyclic voltammetry
EDX	:	Energy dispersion X-ray spectroscope
EIS	:	Electrochemical impedance spectroscopy
Eq	:	Equation
ESR	:	Equivalent series resistance
F	:	Farads
FESEM	:	Field emission scanning electron microscope
FTIR	:	Fourier Transmission Infrared Spectroscopy
g	:	Grams
GCD	:	Galvanostatic charge/discharge
GO	:	Graphene oxide
H_2O_2	:	Hydrogen peroxide
Hz	:	Hertz
H	:	Hours
KOH	:	Potassium hydroxide
L	:	Litres
M	:	Molarity
M	:	Meter

N	:	Nano
R_{ct}	:	Charge transfer resistance
rGO	:	Reduced Graphene Oxide
rGO/TiO_2	:	Reduced Graphene Oxide/Titanium Dioxide
SCs	:	Supercapacitors
TiO_2	:	Titanium Dioxide
XRD	:	X-ray diffraction
Z'	:	Real impedance
Z"	:	Imaginary impedance
Ω	:	Ohm

CHAPTER 1: INTRODUCTION

1.1 Research Background

The main energy supply and energy demand are expected to grow with global population and economic growth in worldwide. The consumption of non-renewable energy sources such as fossil fuels introduce the large emission of carbon dioxide into the air. Causatively, the consumption of fossil fuels is the main driver for the climate change, ozone depletion and air pollution. Therefore, the recent policies in Malaysia have focused on development of novel devices to store or transform energy which has the potential to reduce air pollution and global warming (X. Liu et al., 2017).

Among the major electrochemical energy storage devices, batteries and supercapacitor are considered as potential candidates. Batteries can possess high energy density by using redox reactions throughout their electrodes, but their limitation is batteries have low power density (0.1-1 kW kg^{-1}) (Z. Wu, Li, Yan, & Zhang, 2017). Consequently, supercapacitor acquired exceptional merits due to high power output (1-10 kW kg^{-1}), fast charge and discharge rate capability and long cycling life compared to conventional batteries. (Jagadale et al., 2016). Nonetheless, supercapacitors suffered by low energy density in realizing in various applications compared to conventional batteries. In order to enhance energy density of supercapacitors without compromising the power density, hybrid energy storage devices are proposed to compliment characteristics either both of supercapacitor and batteries. These hybrid energy storage devices are described as supercapattery. The supercapattery (should not termed as asymmetric supercapacitor) , a latest version of hybrid energy storage device by utilizing high energy storage capability of redox active battery type materials as positive electrode accompanied by good power delivery potentiality of carbon materials as negative electrode (Iqbal et al., 2018).

High redox metal oxides were employed as positive electrode materials such as Fe_2O_3, Co_3O_4, V_2O_5, NiO etc have been widely reported as supercapacitor electrode. However, the electrochemical performance of titanium dioxide (TiO_2) is not widely investigated. TiO_2 has shown prominent advantages in photocatalysis applications provided that the affordable cost, good ability to exchange the ions, coupled with the stable chemical and thermal stability. However, irreversible redox process of transition metal oxide materials lead to poor electrochemical stability, declining gradual loss of electrochemical performance (J. Kim, Khoh, Wee, & Hong, 2015). To encounter the consideration, incorporation of carbon materials such as reduced graphene oxide (rGO) to TiO_2 are ideal platform to facilitate the charge transfer mechanism, leading to rising the cycling stability and electroactive sites (Thirugnanam & Sundara, 2018).

In this work, titanium dioxide (TiO_2) and reduced graphene oxide (rGO) has been used as the components of supercapattery. It is believed to able enhance assessable surface area and increase capacitance of electrodes. The present research study aims to investigate processing parameters including different calcination temperature on synthesis of TiO_2 and different loading amount of GO on formation of rGO/TiO_2 as well as their electrochemical performance.

1.2 Problem Statement

The low energy density (5-6 Wh kg^{-1}) depend on rGO or activated carbon is the fundamental demerit of supercapacitor, which is relatively lower compared to lithium ion battery (150 Wh kg^{-1}). Besides that, high agglomeration of rGO sheets due to Van der Waals attraction, results in reduction of effective surface area for electrolyte ions diffuse into rGO surface. These disadvantages make rGO unstable and unfavorable during rapid charge-discharge process and for the demand of outstanding cycle ability. Therefore, enormous efforts have been made to challenge these limitations such as enhance surface area to decline the resistance of diffusion, sustain the good density of packing, and enhance the conductivity.

In other words, the battery type materials such as TiO_2 metal oxide show some main drawbacks such as poor electric conductivity, swelling and shrinkage of active materials, results in instability during charge or discharge. To overcome these limitations, supercapattery was studied to bridge the energy density or power density gap between LIB and EDLC. The supercapattery consisting of capacitive- (eg. rGO) and battery type materials (eg. TiO_2) into one storage device.

Needless to say, hybrid nanocomposites provide synergic behavior and improves the relative properties such as electronic properties, chemical properties with respect to their individual components. However, one of the main issues for hybrid supercapacitors is the shortcoming in the power capacity between the active materials. Non-capacitive with faradaic reaction is is far more sluggish than EDLC capacitive reaction in hybrid nanocomposite. At normal running status of a hybrid supercapacitor, the shortcoming in the kinetics prevents full energy utilization of intercalation electrode and cause deteriorating the overall efficiency. Consequently, not any approach to mix hybrid nanocomposites are suitable to lead an optimal balance of kinetics configuration by improving the power capacity between the battery-type and capacitive electrode. Therefore, there is a need to future explore efforts on control of interfacial interaction between rGO and TiO_2 in order to improve the overall Faradaic processes across the interface. To provide the required optimal percolation preparation, right proportions of relative amount of active materials loading and particle sizes. In the present study, considerable efforts have been devoted to the synthesis of desired rGO/TiO_2 nanocomposite that could improve the electrochemical performance.

1.3 Objectives of Research

The objectives of this research are listed as below:

1. To study the effect of calcination temperature of TiO_2 nanocrystals produced on electrochemical performance of supercapacitor.
2. To optimize the different contents of GO loading incorporated with TiO_2 on electrochemical performance of rGO/TiO_2 nanocomposite.
3. To study the electrochemical properties of supercapattery with optimal rGO/TiO_2 nanocomposite as anode and an activated carbon as cathode.

1.4 Scope of Research

With rising interest in green nanomaterials, there is increasing attention paid to reduced graphene oxide/titanium dioxide nanocomposites (rGO/TiO_2) in these recent years due to minimum environmental impact and synergy effect between rGO and TiO_2. The composite material with rGO and TiO_2 shows the great advantage in different application especially in photocatalysis and photovoltaics application.

However, there is limited literatures on the formation of rGO/TiO_2 in supercapattery application. Taking this into consideration, detail studies regarding the relationship of particle size and crystallinity of TiO_2 at different calcination temperature on electrochemical performance and material characterization. Besides that, the effect of different amount of GO incorporated into TiO_2 to produce rGO/TiO_2 nanocomposites on electrochemical performance and material characterization has been established into this present work.

1.5 Outline Dissertation of Research Work

The thesis consists of five chapters. Chapter 1 included the research background, problem statement, research objective and research scope of the experiment. Chapter 2 offers a comprehensive literature survey on supercapacitors, components of supercapacitors such as working electrode, separator and electrolyte, TiO_2 based supercapacitor, rGO/TiO_2 based supercapacitor and the development fabrication methods for rGO/TiO_2 nanocomposites. The details of chemicals, preparation of working electrodes and experimental set up for supercapacitor purposes were stated in Chapter 3. Chapter 4 mainly discuss and interpret the research studies. Chapter 5 suggested several strategies for further improvement of supercapacitor. A series of processing parameters will be divided into four parts:

Part I: Synthesis of TiO_2 at different calcination temperature.

In this stage, TiO_2 nanocrystals powder was primarily synthesized through peroxo sol gel method with different calcination temperature. The calcination temperature influences the phase transition of TiO_2 and they were optimized to produce the desire electrode materials. The stability of peroxo TiO_2 was also studied.

Part II: Synthesis of rGO/TiO_2 nanocomposite with different GO loading.

Firstly, the synthesis of GO as starting materials. The synthesis of rGO/TiO_2 nanocomposite were carried out based on the reaction condition of TiO_2 with optimum calcination temperature in previous section (Part I). The peroxo sol gel hydrothermal method were used with different loading amount of GO into TiO_2 solution. The optimum amount of GO was also chosen as suitable materials for synthesis nanocomposite.

Part III: Material Characterization

The structural, morphological and electrochemical properties were characterized via characterization techniques. X-ray diffraction (XRD), Raman spectroscopy, Field Scanning Electron Microscope (FESEM), Transmission Electron Microscope (HRTEM), and Fourier Transform Infrared Spectroscopy (FTIR). In addition, Zeta Sizer was used to measure the particle size distribution and zeta potential of the nanoparticles produced. The measuring conditions of each measurement are discussed in Chapter 3.

Part IV: Electrochemical Performance Test

The measurement of each specific capacity was carried in three electrode system by using cyclic voltammetry test and charge discharge test. In the final stage, two electrodes system where optimum materials as anode electrode whereas activated carbon as cathode electrode will be carried out to calculate power and energy density.

CHAPTER 2: LITERATURE REVIEW

2.1 Introduction

Electric power generation is an integral part of the financial development of all countries. Generation and consumption of electricity rise with human population and economic development. In 2007, the population of 27.4 million is estimated to increase to 33.4 million in 2020 (Ali, Daut, & Taib, 2012).

Based on the report by Malaysia Energy Information Administration (EIA) in 2014 which is shown in Figure 2.1, fossil fuels contribute 86% of total electricity generation while hydropower and petroleum accounted for 11% and 1% respectively. The remaining 1% was accounted for different renewable energy resources. From the data analysis, the electricity sector in Malaysia is dominated by consumption of fossil fuels (Ashnani, Johari, Hashim, & Hasani, 2014). Unfortunately, limited sources of fossil fuels along with growing human population and technology development triggered the problem of insufficient energy. Besides that, the combustion of fossil fuels produces carbon dioxide gas (CO_2) which causes global warming. Malaysia is the highest CO_2 contributor among South East Asia countries, followed by Indonesia and Thailand.

Therefore, the aforementioned problem can be alleviated by replacing fossil fuels with devices that are able to store and deliver electric energy. Supercapacitors are considered as an alternative energy storage device which provide high power capability (Kate, Khalate, & Deokate, 2017; Xin Li & Wei, 2013). Supercapacitor is an energy storage device which contains two working electrodes consisting of carbon derivatives, metal oxide or conducting polymers that is pasted on the current collector, filled with electrolyte and one separator as sketched in Figure 2.2.

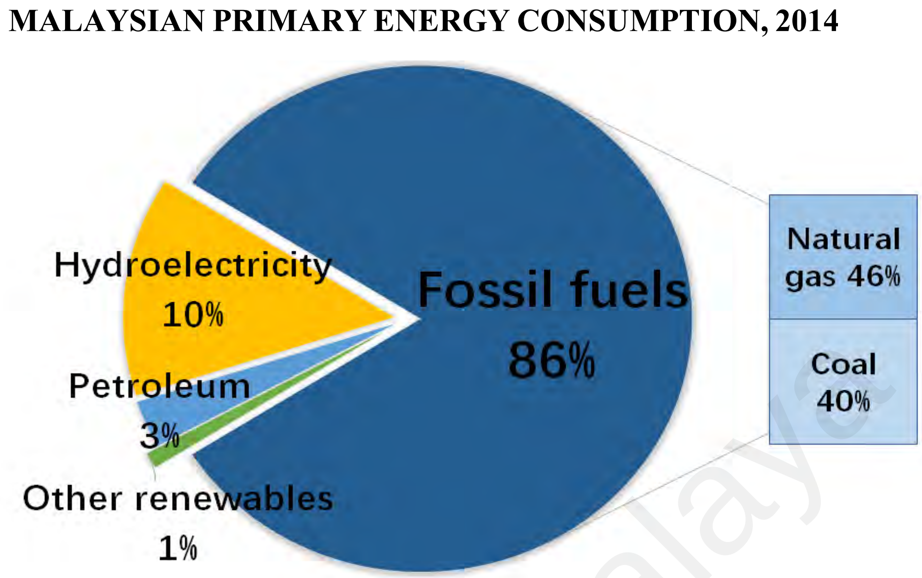

Figure 2.1: Different primary energy consumed in Malaysia for total electricity generation. Adapted from International Energy Agency (EIA). (Ashnani et al., 2014)

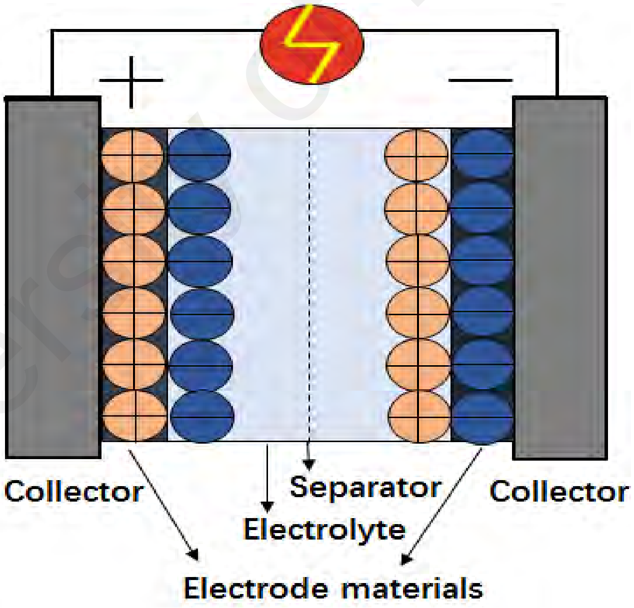

Figure 2.2: Construction of supercapacitor that comprised of two working electrodes immersed in electrolyte. Adapted from Materials Today (Fic, Platek, Piwek, & Frackowiak, 2018).

2.2 Different charge storage principle of electrodes

The electrochemical performance of supercapacitor is dependent on the different charge storage mechanism, type of electrolyte and active material used. Different active materials have different charge storage principle. Therefore, the active materials can be distinguished into three types according to the charge storage reaction: (1) Capacitive electrode, (2) Pseudocapacitive electrode and (3) Battery-type electrodes. Generally, pseudocapacitive and capacitive electrodes are controlled by surface reaction or near surface redox reaction and they offer higher energy density at high charge discharge rates compared with battery type electrodes (Augustyn, Simon, & Dunn, 2014). The charge storage mechanism of battery type electrode is restricted to ion diffusion inside the bulk of battery type material (Wang, Song, & Xia, 2016). Figure 2.3 (a) illustrates the influence of different charge storage mechanism with respect to the appearance of cyclic voltammograms (CV) and galvanostatic charge discharge (GCD) plots. The details of capacitive, pseudocapacitive and battery type electrodes are discussed in Section 2.2.1-2.2.3.

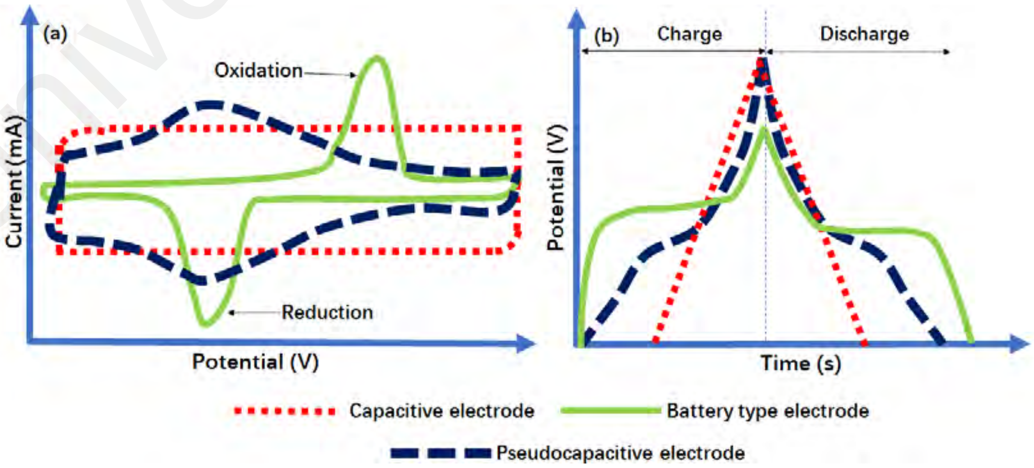

Figure 2.3: (a) CV for capacitive, pseudocapacitive and battery type electrodes. (b) GCD curves for capacitive, pseudocapacitive and battery type electrodes. Adapted from ACS Nano (Gogotsi & Penner, 2018)

2.2.1 Capacitive electrode

Capacitive electrode is also known as electrochemical double layer (EDL) electrode. Capacitive electrode stores its electrostatically where electrolyte ions adhere physically on electrode interface without ion diffusion limitations. Capacitive electrode store charge through bulk electrolyte ions separation towards high porosity of electrode materials. During the charging process, the anions and cations align themselves and diffuse toward positive and negative electrodes, respectively. Figure 2.4 shows the reversible ion absorption process which creates a thin electric double layer over the whole surface of the electrode material (Z. Zhang et al., 2017).

Generally, the capacitive electrode has higher energy storage than the conventional capacitor electrode because of the larger surface area (2000 m^2/g) which is a nature of carbon and carbon derivatives. The main drawback of capacitive electrodes is the charge accumulation happens from an electrostatic reaction, it leads to a lower energy density as compared to batteries (Saha, Samanta, Murmu, & Kuila, 2018).

The capacitive electrode shows the red dotted line of rectangular CV, indicating the capacitance is constant over a fixed voltage window (Figure 2.3 (a)). Capacitor electrode illustrates a red dotted line of linear time-dependent in voltage responses at a constant current during charging and discharging (Figure 2.3 (b)). Common capacitive electrode materials are such as activated carbon, carbon nanotube and graphene (Saha et al., 2018).

2.2.2 Pseudocapacitive electrode

Pseudocapacitive electrode is designed to store charge faradaically by using reversible and rapid redox reaction on the surface of the electrode-electrolyte interface without diffusion limitation (Figure 2.5). Pseudocapacitive electrodes include metal oxides (e.g., RuO_2, MnO_2, SbO_2 and V_2O_5) and conducting polymers (e.g,, PANI and PA) where the charge storage mechanism involves rapid electron transfer with superior conductivity and higher specific capacitance compared with capacitive electrodes. The challenge for pseudocapacitive electrode is it suffers from short-lived life span and experiences low electrical conductivity as compared to capacitive electrodes (Le et al., 2017).

There are three types of pseudocapacitive reactions, as identified by Conway (Conway, 2013); (i) Underpotential deposition where it happens when an absorbed layer is constructed on the surface of metal electrode of higher redox potential by a different metal ion. For example, copper or lead (metal) is adsorbed on the surface gold or platinum electrode (metal), (ii) Redox pseudocapacitance in which electrochemical adsorption of ions happens on the surface accompanied by chemical conversion between oxidation and reduction at redox active sites, (iii) Intercalation pseudocapacitance where the electrolyte ions intercalate into the electrode layers without changing the crystallographic phase.

In Figure 2.3 (a), the CV curve of pseudocapacitive electrode (shown in blue dotted line) displays the capacitive-like signature with additional broad redox peak, which deviates from the linear rectangular shape of GCD shown in Figure 2.3 (b). In short, the term of “Pseudo” and “capacitive” was used to describe an electrode involves redox reaction but it exhibits the electrochemical trademark of capacitive electrode (Brousse, Bélanger, & Long, 2015).

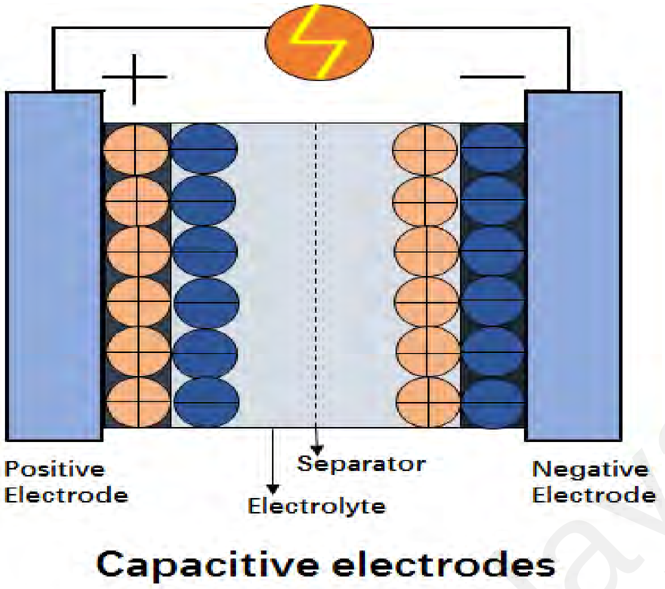

Figure 2.4: Storage mechanism of capacitive electrodes.
Adapted from Journal of Alloys and Compounds (Kate et al., 2017).

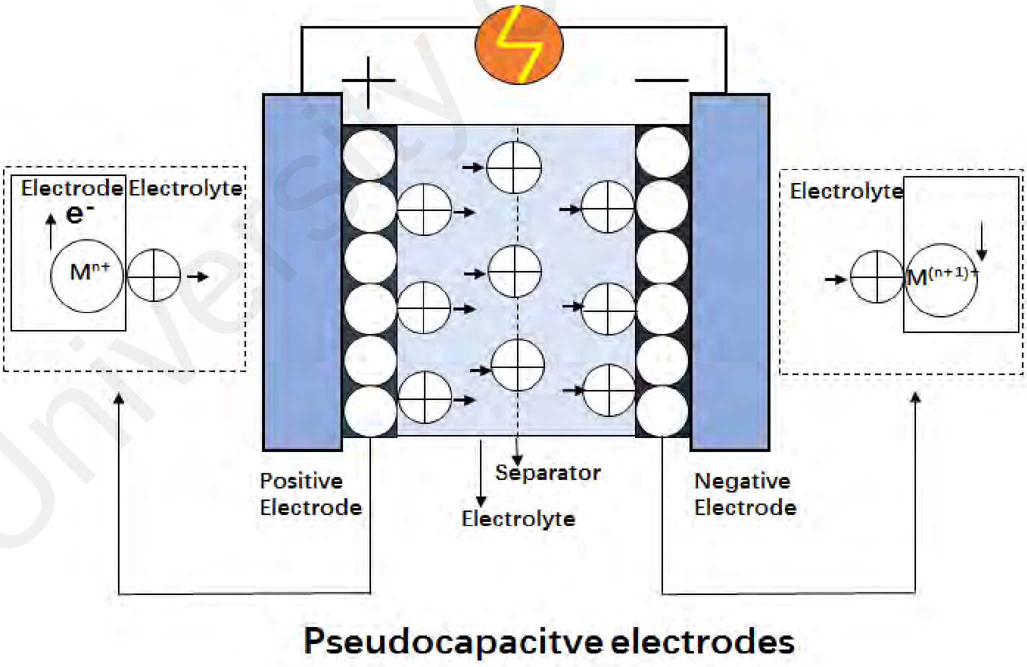

Figure 2.5: Storage mechanism of pseudocapacitive electrodes.
Note: M serves as a metal particle; Figure 2.5 showed anions get attracted and move towards the opposite direction to cations by the reversible redox reaction. Adapted from Journal of Alloys and Compounds (Kate et al., 2017).

2.2.3 Battery-type electrode

It is misleading and confusing that many authors consider the battery-type electrode as a pseudocapacitive electrode because the charge storage mechanism is based on the Faradaic reaction. Owing to recent review articles, few authors have critically commented on the confusion made by many reports on capacitance formula and farad (F) unit on battery type behavior of electrode materials (Brousse et al., 2015). As a matter of fact, battery-type electrode is considered as non-capacitive with purely faradaic properties and the process is rarely reversible. Basically, the typical battery properties display clear redox peaks in CV curves (green lines in Figure 2.3 (a)). Battery-type materials exhibit a plateau (whereby is the reason for larger energy storage of battery compared with supercapacitor) due to phase transformation of electroactive materials. Nickel, cobalt and iron should be classified as battery-type electrodes.

However, phase transformation of battery-type electrode is limited by diffusion which can cause to the distortion of the rate capability of the electrode. As the electrochemical signature (i.e. capacity is not constant over the working potential window) is different, the term “capacity” with the unit of “Coulomb” (C) or “milliamp hour” (mAh), should be the appropriate units used to report the charge stored in battery-type electrode instead of term “capacitance” (Farad F) which are used for capacitive and pseudocapacitive electrode.

2.3 Supercapacitor systems

Supercapacitors can be classified into three arrangements: symmetry, asymmetry and supercapattery. In symmetry hybrids, a device with two identical materials (capacitive/capacitive or pseudocapacitive/pseudocapacitive electrodes) are used on both electrodes.

Asymmetric hybrid exhibits two storage mechanisms (capacitive and faradaic process) in a different electrode. By employing two different materials on the electrodes, the electrochemical performance is enhanced as compared to the pure material in term of better cycling stability. Juchen and co-authors reported the asymmetric supercapacitor that consists of capacitive electrode (rGO and CB) and pseudocapacitive electrode (MnO_2) increase in specific capacitance. For instance, rGO/MnO_2/CB hybrid exhibited electrochemical performance of 154 F g^{-1} at 50 mV s^{-1}, which is a significant enhancement as compared to rGO/CB electrode (103 F g^{-1}) (J. Chen et al., 2015). Several asymmetric electrodes which have been reported include rGO/RuO_2/CNC//rGO; LNF//AC and MnO_2/MWCNT //AC (Cao, Lin, Sun, Yang, & Zhang, 2015; Rakhi & Lekshmi, 2017; Vinny, Chaitra, Venkatesh, Nagaraju, & Kathyayini, 2016).

Lastly, supercapattery (=**supercapa**citor + ba**ttery**) is the latest type of energy storage device which stores charge by means of electrostatic reaction at capacitive electrode and battery faradaic storage mechanism. In general, the cathode is made from carbon-based materials such as activated carbon while the anode consists of battery type material. As a matter of facts, literature study and complex step is required to balance the charges between cathode and anode (Lokhande, Lokhande, Lokhande, Kim, & Ji, 2016). Supercapattery provides higher volumetric and gravimetric energy density without losing cyclic stability compared with EDLC and pseudocapacitor. The synergistic effect of activated carbon and battery type electrode ($Ni_3(PO_4)_2$) resulted in high power capacity (599 W kg^{-1}) and energy capacity (76 Wh kg^{-1}) as well (Omar et al., 2016). Few studies have focused on supercapattery include; $MgCo_2O_4$//AC; $CoNi_2(PO_4)_2$//graphene and MnS/rGO//AC (Krishnan, Harilal, Pal, et al., 2017; Tao et al., 2018; X. Xu, Zhang, Zhao, & Hu, 2018). The classification of different supercapacitors is summarized in Figure 2.6.

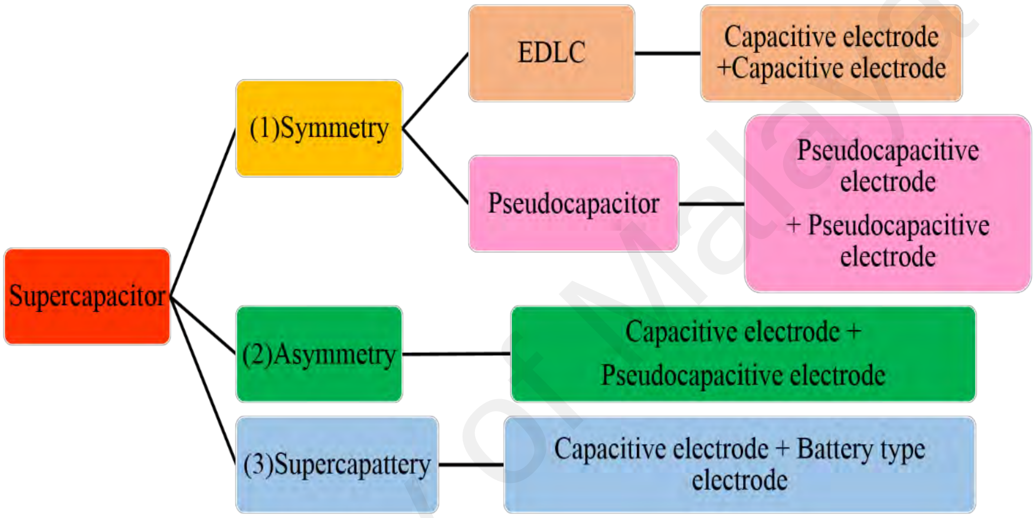

Figure 2.6: Different types of supercapacitors.

2.4 Electrolytes

Electrolyte is made up of electrolyte salt and solvent. Electrolyte facilitates the movement of cations and anions during the charging and discharging process. The energy storing process is related to the squared of operating voltage directly as shown in Equation 2.1.

$$\mathrm{E} = \frac{\mathrm{CV}^2}{2} \qquad \text{Eq 2.1}$$

Therefore, the potential window (V) of different electrolytes influence the capacitance, power density, energy density and life cycle of supercapacitor. The electrolytes used for supercapacitors are categorized into aqueous, organic or ionic liquids. An ideal electrolyte should have a wide potential window, low resistance and viscosity, is non-flammable and of reasonable cost. Table 2.1 summarizes main electrolytes currently used.

Previous recent literature studies have shown that the size of solvated ions in electrolytes are very important in determining the electrochemical characteristics of supercapacitors (H. Wu et al., 2013). For instance, Suhui Lu and co-authors (Lu et al., 2018) reported the symmetrical ordered mesoporous carbon/graphene composites (OMC/G) with several aqueous electrolytes which includes acidic electrolytes (H_2SO_4 and HCl), neutral (K_2SO_4 and Na_2SO_4) and alkaline electrolytes (NaOH, KCl, NaCl and KOH). It was found that OMC/G exhibited better specific capacitance in alkaline electrolytes (KOH) compared with electrodes immersed in acidic and neutral electrolytes due to the smaller solvated ions radius of OH^-, in addition larger pore size of OH^- allowed fast ionic diffusions, enhanced electric properties of graphene. Environmentally friendliness and high ionic conductivity of aqueous electrolytes are more favorable compared with non-aqueous electrolytes. Therefore, most research focused on determining suitable cathode and anode electroactive materials to form efficient composite electrodes in aqueous electrolytes (Zhong et al., 2015).

Wu and co-authors (H. Wu et al., 2013) reported that solvated ion has a smaller radius in aqueous electrolytes compared to organic electrolytes leading to lower conductivity and capacitance. Despite this, carbon based electrode with more macrospores is more suitable using organic solvents (H. Wu et al., 2013). Organic electrolyte possesses a wider electrochemical potential window that ranges between 0-2.5 V, however the issues of low viscosity, toxicity and electrolyte leakage lead to a limitation in supercapacitor applications (K. Xu, Ding, & Jow, 2001). Ionic liquid has considered replacing lower ionic of conventional organic electrolytes due to its high electrochemical and thermal stability. Nevertheless, the ionic liquid is sensitive to temperature and expensive, thereby limiting their use in supercapacitor (Galiński, Lewandowski, & Stępniak, 2006; Yan, Wang, Wei, & Fan, 2014).

Table 2.1: The major electrolytes currently used in supercapacitors application.

Electrolytes	Voltage Window (V)
Aqueous Electrolytes	
H_2SO_4	1.0
KOH	1.0
Na_2SO_4	1.8
Organic Electrolytes	
$TEABF_4$/PC	3.5
Ionic liquids	
$LiPF_6$	3.0

Note: H_2SO_4 (Sulphuric acid), KOH (potassium hydroxide), Na_2SO_4 (sodium sulphate), $TEABF_4$/PC (Tetraethylammonium tetrafluoroborate in propylene carbonate), $LiPF_6$ (Lithium hexafluorophoshate)(Mirzaeian et al., 2017).

2.5 Electrode Material

The main objective behind the research on supercapattery is to connect the gap between supercapacitor and batteries in terms of power and energy performance Material selection is very important in determining the supercapattery performance. Therefore, two factors in determining the performance of devices are summarized as follows:

-A high surface area of the material is the main criteria for electrode selection which facilitate sufficient fast reaction kinetics from the interaction between the electrolyte and electroactive materials (Heimböckel, Kraas, Hoffmann, & Fröba, 2018).

- The pore size distribution remains significant and a close size to the electrolyte ion is necessary to achieve maximum capacitance. Larger pore size will increase the gap between the center of electrolyte ion and pore wall, resulting in a decrease of capacitance (Abdollahifar et al., 2018).

The following Sections 2.5.1-2.5.4 discuss the characteristics and recent literatures of activated carbon, titanium dioxide, reduced graphene oxide and reduced graphene oxide/titanium dioxide nanocomposites as electrode materials.

2.5.1 Activated Carbon (AC)

There has been great interest in the production of AC as capacitive electrode material due to its adsorptive property, highly porous structure and economical cost (L. Zhang et al., 2013). ACs originate from various carbonaceous materials such as wood, coal, nuts, shell, coffee and more. The properties of ACs depend on production methods used (physical or chemical activation) and the nature of carbon precursors. It is well known that the porous structure of ACs have a broad pore size distribution of micropores (<2nm), mesopores (2-50nm) and macropores (>50nm).

According to the storage mechanism of capacitive electrode, the specific surface area of AC is directly proportional to the specific capacitance. Table 2.2 reports the performance of ACs with respect to their specific surface area. However, the practical situations do not fit the theory perfectly, especially at high current rate due to a heterogeneous pore size distribution, showing that not every pore are directly involved in charge accumulation (Kierzek, Frackowiak, Lota, Gryglewicz, & Machnikowski, 2004). Generally, some of the electrolytes ions are larger than the micropores of AC. As a result, the electrode material cannot fully interact with electrolyte ions. Therefore, in order to obtain high power density, AC electrodes should possess an extensive number of mesopores which allow improved penetration of electrolyte ions into the carbon. It is conclusively shown that a good capacitive performance result is in agreement with the optimized pore size.

Table 2.2: Electrochemical performance of various AC electrodes using different resources for supercapacitor application.

Materials	**Activation agent**	**BET surface area (m^2 g^{-1})**	**Electrolyte**	**Parameter**	**Specific Capacitance (F g^{-1})**	**Ref**
Dead gingko leaves	KOH	835	1 M H_2SO_4	0.5 A g^{-1}	374	(X. Zhu et al., 2018)
Argy wormwood	H_3PO_4 + KOH	927	6 M KOH	1 A g^{-1}	344	(Dai et al., 2018)
Kapok Shell	NaCl + KCl	1260	6 M KOH	20 mV s^{-1}	169	(K. T. Kumar et al., 2018)
Tobacco	KOH	1297	6 M KOH	0.5 A g^{-1}	148	(H. Chen et al., 2018)

2.5.2 Reduced Graphene Oxide (rGO)

rGO consists of single-layered sp^2 bonded carbon atoms which are arranged in a honeycomb lattice with separation of 1.42 Å (Figure 2.7). rGO has useful application prospects in flexible energy storage due to excellent thermal conductivity, high electrochemical stability, large specific surface area (~2630 m^2 g^{-1}) and excellent mechanical stability. Through the database Scopus search analysis, the world has published a total of more than 3133 on rGO-related material for supercapacitor since 2011 (Scopus). Table 2.3 summarizes rGO as an electrode material in supercapacitor application.

Typically, the chemically modified precursor of rGO (natural graphite) is called graphite oxide whereas the exfoliated ones are known as graphene oxide (GO). GO can be synthesized using Brodie (Brodie, 1860), Staudenmaier (Staudenmaier, 1898) or Hummers method (Hummers Jr & Offeman, 1958). At present, the improved Hummers method is widely used and is shown in Figure 2.8. The first stage of improved Hummers method is the oxidation step which uses strong acids and oxidation agents. The oxidation process helps to increase the interlayer spacing by introducing different oxygen-related groups such as carboxylic, carbonyl, hydroxyl, and epoxide groups. The second stage is to add strong oxidants such as hydrogen peroxide in excess to the oxidized graphite and this results in the production of graphite oxide. Lastly, ultrasonication step helps to obtain dispersed graphene oxide. Since the oxygen-containing groups were presented between broken carbon chains during chemical modification, the graphene sheets lost the properties of intrinsic high electrical conductivity presented in the graphite. To recover the electrical conductivity, the reduction of GO is needed to eliminate the oxygen functional groups (Mu et al., 2016).

Thermal and chemical reduction methods are two common ways used for GO reduction (L. Chen et al., 2011). Chemical reduction procedures usually use chemical reductants such as hydrazine, hydroquinone and sodium borohydride ($NaBH_4$) (Shin et al., 2009; Zhou, Bao, Tang, Zhong, & Loh, 2009). These chemical reductants are mostly toxic and explosive hence other green reductants like green tea, polyphenol, caffeine etc. have been explored to reduce GO (Omid Akhavan, Ghaderi, Aghayee, Fereydooni, & Talebi, 2012; O Akhavan, Kalaee, Alavi, Ghiasi, & Esfandiar, 2012; Vu et al., 2015). Thermal reduction such as hydrothermal technique has several advantages over the chemical reduction due to its simple operation, higher specific surface area, less agglomeration, and it provides higher electrical conductivity (Bao et al., 2009; P. Guo, Song, & Chen, 2009). Besides that, the hydrothermal technique enables the recovery of the π-conjugation system from GO sheets after reduction, which reduces the defects contents. (Ghorbani, Abdizadeh, & Golobostanfard, 2015).

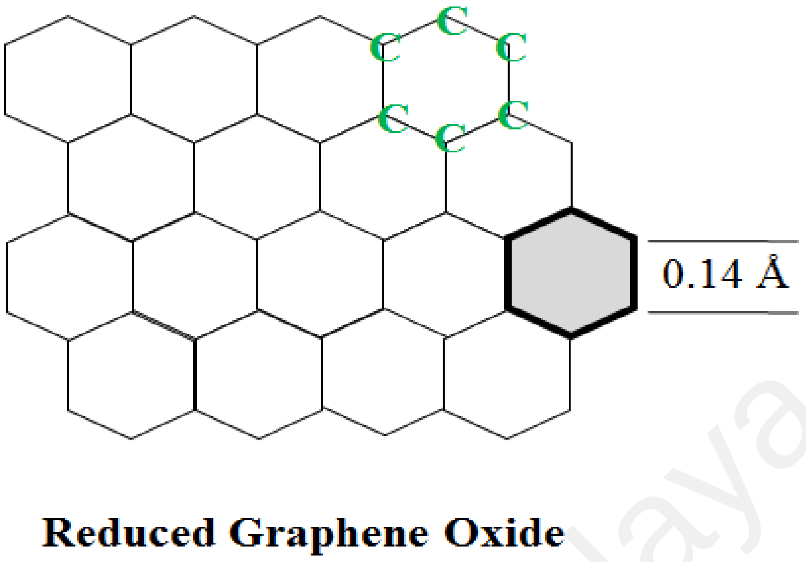

Figure 2.7: Structure of reduced graphene oxide.
Adapted from Nature (Morimoto, Kubo, & Nishina, 2016).

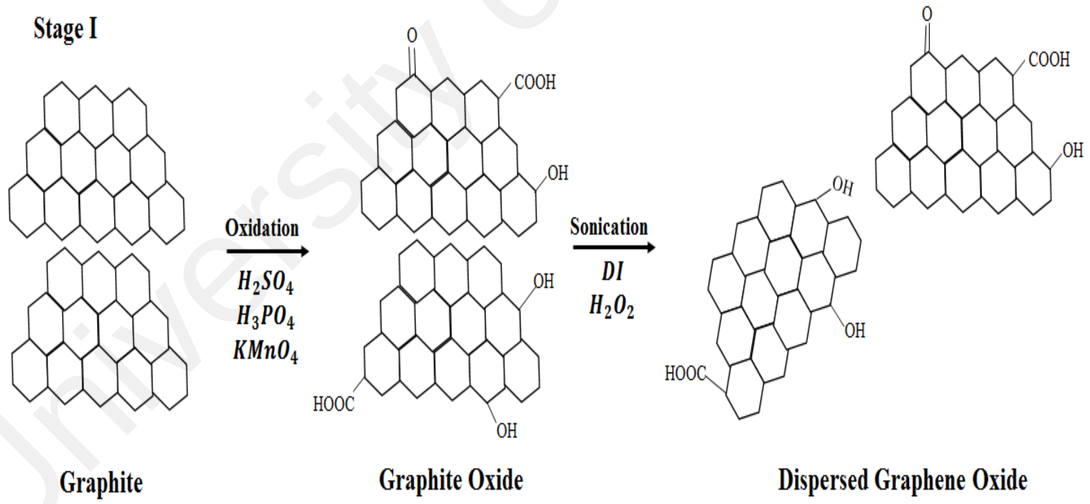

Figure 2.8: The process of improved modified Hummers method.
Adapted from ACS Applied Energy Journal (Down, Rowley-Neale, Smith, & Banks, 2018).

Table 2.3: rGO as an electrode material in supercapacitor application.

Synthesis method	**Specific Capacitance (F g^{-1} at a current density of 1 A g^{-1})**	**Cycling Stability**	**Electrolytes**	**Remarks**	**Ref**
Thermal reduction **It was conducted under N_2 atmosphere at 900°C for 2hr*	14	Not stated due to lower performance	1M H_2SO_4	Hydrothermal reduction method offers the highest specific capacitance due to it offers the most effective in removing oxygen-containing groups.	(Rasul, Alazmi, Jaouen, Hedhili, & Costa, 2017)
Chemical reduction **It was conducted at 100°C for 24hr*	136	70% retention after 2500 cycles	1M H_2SO_4		
Hydrothermal reduction **It was conducted at 180°C for 24hr*	274	60% retention after 2500 cycles	1M H_2SO_4		

Chemical reduction (Hydrazine Hydrate) _*It was conducted at room temperature_	112.6	97% retention after 500 cycles	1M Na_2SO_4	Room temperature hydrazine reduction is a cost saving and energy saving process.	(Sykam & Rao, 2017)
Chemical reduction (Hydrazine Hydrate) + Thermal reduction _*It was conducted at $85^{o}C$ for 1hr_ _*It was conducted at $900^{o}C$ for 2hr_	114	33% retention after 1000 cycles	1M H_2SO_4	Oxygen-containing functionalities of rGO are important to capacitance in organic-based supercapacitors.	(Navarro-Suárez et al., 2018)

2.5.3 Titanium dioxide (TiO_2)

Various investigations have been dedicated to an excellent capacitance value of metal oxide with respect to cheaper cost. Among the various metal oxides, TiO_2 has the merits of high specific surface area, environmental friendliness, physical and chemical stable, its intrinsic safety and cost-effectiveness due to an abundance of Ti element in our Earth's crust (Jung, Wang, & Hu, 2014). However, TiO_2 as battery type anode material in the practical application of energy storage is difficulty inferable from poor cycling rates as well as low theoretic capacity (Tang et al., 2013). For instance, low conductivity of bare TiO_2 electrode as anode presented in the capacity of 28.8 C g^{-1} at first cycle, later the capacity drops until 20.16 C g^{-1} after 3000 cycles as reported by Bhupender Pal et al (Pal et al., 2018). Besides that, Ling and co-author (L. Zhao, Tang, Chen, Feng, & Mi, 2018) reported the use of pristine TiO_2 electrode as anode resulted in rate capacity of 316.8 C g^{-1} at 2C, TiO_2 electrode shows poor rate capability as it maintains 59% of capacity after 1000 cycles. Therefore, different methods were endeavored to enhance the capacitive performance of TiO_2 electrode which includes the surface modifications of TiO_2, resulting in defects formation (production of vacancies, interstitial or substitutional aspects) which changes the color, conductivity, physical and chemical properties of TiO_2 (Yan Zhang et al., 2016). For the purpose of improving performance of TiO_2 anode, rGO coupling with TiO_2 was one of the effective way because of its high electrical conductivity and large specific surface area.

TiO_2 is an n-type semiconductor with three natural crystalline phases, namely anatase, brookite and rutile. The structure of the three main phases is well characterized by TiO_6 octahedron structure linked with different corners and edges. For anatase and rutile TiO_2, each octahedron is shared with four and two edges, to form a tetragonal structure.

Brookite's octahedron is shared with three edges to form an orthorhombic structure which is shown in Figure 2.9. In terms of electron transfer, anatase has faster electron transfer and has higher conductivity than amorphous TiO_2 while rutile has the lowest electron transfer rate and electronic conductivity (Jiang et al., 2015; Salari et al., 2012; Sawczak et al., 2015; Yun et al., 2012).

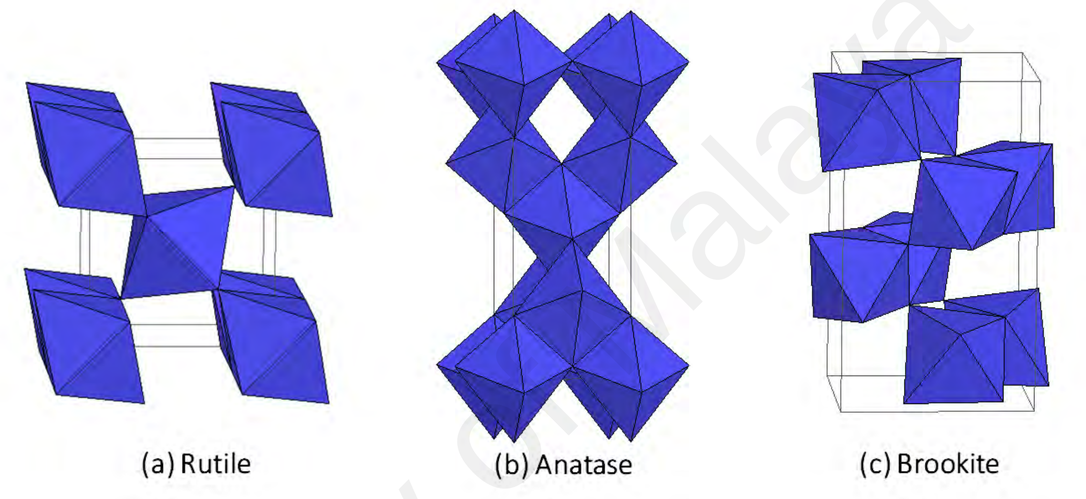

Figure 2.9: Structures of TiO_2 polymorphs : (a) Rutile, (b) Anatase, (c) Brookite Adapted from Journal of Materials Science and Engineering (Regonini, Bowen, Jaroenworaluck, & Stevens, 2013).

2.5.4 Reduced graphene oxide/ titanium dioxide (rGO/TiO_2) nanocomposites

As mentioned before, the properties of supercapacitor electrode based on pristine TiO_2 or rGO are not ideal due to the low electronic conductivity of carbon nanomaterials and limited storage capacity of TiO_2. The development of new binary nanocomposites by combining TiO_2 (battery type electrode) and rGO (capacitive electrode) are aimed at producing supercapattery with improved electrochemical properties. The rGO/TiO_2 nanocomposites are able to alleviate the inadequacies of a single material and accomplish ideal performance via synergistic effect. Table 2.4 depicts the summary of rGO/TiO_2 composites for sodium ion batteries. Table 2.5 shows the electrochemical performance of rGO/TiO_2 composites in supercapacitor application. The pioneer researchers in supercapacitor and sodium ion batteries application suggested that the enhancement in specific capacitance/capacity of rGO/TiO_2 composite is due to their new functionalities and properties as summarized below (Agharezaei, Abdizadeh, & Golobostanfard, 2018; S. Li et al., 2018; Thirugnanam & Sundara, 2018): (i) 2D graphene acted as a support to promote the growth and nucleation of metal oxide with well-defined structures (ii) Metal oxide anchored on rGO sheets can prevent the agglomeration of rGO, resulting in an increase of electroactive sites for fast electron transfer (iii) Highly conductive rGO also acts as an ion reservoir to enhance ion mobility. To the best of our knowledge, there is still no report on the fabrication of activated carbon as cathode and rGO/TiO_2 nanocomposites as an anode in the supercapattery application.

Table 2.4: Summary on rGO/TiO_2 based composites as anode electrodes for Na ion and Li ion batteries.

Materials	CD (A g^{-1})	First capacity (mAh g^{-1})	Cycle number	Remaining capacity (mAh g^{-1})	Ref
Na-ion batteries					
rGO/TiO_2	0.5	430	100	100	(Huang, Yan, Wang, Zhang, & Ju, 2016)
rGO/TiO_2	1	115	300	102	(Feng, Dong, Han, Li, & Li, 2016)
rGO/TiO_2	0.168	225	500	148	(J. H. Kim et al., 2017)
Li-ion batteries					
rGO/TiO_2	0.1	270	2000	180	(J. Li et al., 2017)
rGO/TiO_2	0.05	229	50	115	(Yoon et al., 2017)
NiO/rGO/TiO_2	0.02	320.6	200	255.8	(Z. Chen et al., 2019)

Note: CD-current density

Table 2.5: Electrochemical performance of rGO/TiO_2 composites in supercapacitor application.

Material	**SC (F g^{-1})**	**E**	**PW (V)**	**CD/SR**	**CR% (Cycles)**	**Ref**
Co/ rGO/TiO_2	34.8	0.5 M Na_2SO_4	-0.45-0.55	5 mV s^{-1}	Nil	(Xiao, Guo, Sun, Pei, & Zhou, 2016)
H/rGO/TiO_2	51	1 M Na_2SO_4	0-1.8	1 A g^{-1}	80 (10000)	(Pham et al., 2018)
rGO/TiO_2	22.1	6 M KOH	-0.7-1.0	0.8 A g^{-1}	77 (1000)	(Luo et al., 2013)
N/rGO/TiO_2	51.8	1 M Na_2SO_4	-0.2-0.8	0.1 A g^{-1}	78.8 (5000)	(Sharavath, Sarkar, & Ghosh, 2018)

Note: SC-specific capacitance; E-electrolyte; PW- potential window; CD-current density; CR-Capacity Retention; SR-scan rate

2.6 Preparation methods

2.6.1 Peroxo sol gel

The conventional sol gel method is one of the general methods used to produce a metal oxide. This method offers many merits which include simple operation, cost-efficient and the ability to control the crystallinity and desired morphology (Danks, Hall, & Schnepp, 2016). Notwithstanding, the use of toxic basic organic solvents or corrosive hydrochloric and nitric acid in the preparation of metal oxide are not environmentally friendly (M. Yang et al., 2018).

Herein, modified sol gel method such as peroxo sol gel method is introduced to solve the aforementioned problems in the production of metal oxide under neutral pH and low temperature (L. Zhang et al., 2013). Peroxo sol gel technique is also considered as an environmentally friendly technique as it does not require toxic alkoxides, organic ligands or solvents (Krivtsov et al., 2015). Ichninose and co-authors reported the synthesis of peroxotitanium acid hydrate and modified peroxo anatase TiO_2 sol from peroxotitanium solution. In this report, peroxotitanium complex sol was produced using TiO_2 precursor (e.g., $TiCl_4$ solution) and mixed with 30% H_2O_2 and ammonia, followed by a low temperature of hydrothermal treatment or calcination (Y.-J. Liu et al., 2008). Table 2.6 shows the crystal sizes of TiO_2 at a different heating time and temperatures by using the peroxo sol gel method. The size of TiO_2 crystal increased linearly with heating time and some spherical shape was observed, due to agglomeration of atoms when heating duration was increased. The result was showed in Table 2.6 revealed that TiO_2 particles crystallize easily with prolonged heating time (Sasirekha, Rajesh, & Chen, 2009).

Table 2.6: The crystal size and different preparation condition of TiO_2 by using peroxo sol gel method.

Metal Precursor	**Heating Time (h)**	**Temperature (°C)**	**Crystal size (nm)**	**Ref**
Titanyl sulfate ($TiOSO_4. nH_2O$)	2	100	5.0	(Ge, Xu, & Sun, 2006)
	6	100	33.0	
	10	100	40.0	
Titanium tetrachloride ($TiCl_4$)	2	88	2.0	(Sasirekha et al., 2009)
	2	95	3.2	
	4	88	9.0	
	4	95	12.0	
	8	88	12.7	
	8	95	14.0	
Titanium tetrachloride ($TiCl_4$)	2	90	2.0	(Sasirekha et al., 2009)
	2	97	3.8	
	4	90	4.0	
	4	97	9.0	
	8	90	11.0	
	8	97	12.0	
	12	90	14.0	
	12	97	10.0	
	16	90	13.0	

2.6.2 Hydrothermal

A hydrothermal method is a great tool due to its simplicity, ease of use and environmental friendliness. This technique employs high temperature and pressure in a stainless steel autoclave. Hydrothermal method is widely used to synthesize metal oxide of different nanosizes and it is normally carried out between 100-200 ºC. Besides that, GO products can be reduced to rGO by the hydrothermal method with or without reducing agents. For example, graphene was mixed with commercial TiO_2 to give rise elongated TiO_2 nanotubes in alkaline medium with hydrothermal treatment and simultaneously convert GO to rGO (Yimei Zhang, Wang, Zhu, Zhang, & Chen, 2017). Different morphologies such as noncubic, nanorod and flower-like structure can be obtained by controlling the preparation criterions such as temperature of reaction, pH of solution and heating duration. Nonetheless, nanomaterial agglomeration often happens in the absence of a surfactant agent.

2.6.3 Calcination

Nanoparticle synthesis using hydrothermal method usually requires subsequent heat treatment (calcination) to enhance the material properties. Calcination is a heat treatment process in the absence or insufficient supply of air or oxygen. Calcination is important for the phase transition, thermal decomposition and removal of volatile impurities. Calcination process is normally conducted in a muffle furnace and the heating temperature is below the melting point of materials. The morphology and crystallinity can be controlled by tuning the experimental conditions such as the treating temperature, heating time and rate of heating. The calcination process involves three stages: heating, soaking and cooling processes. The heating rate used in this experiment was 10ºC/min until it reached the desired temperature such as 200-800 ºC. Figure 2.10 shows the calcination profile for nanoparticle synthesis process. The merits and demerits of preparation methods are summarized in Table 2.7.

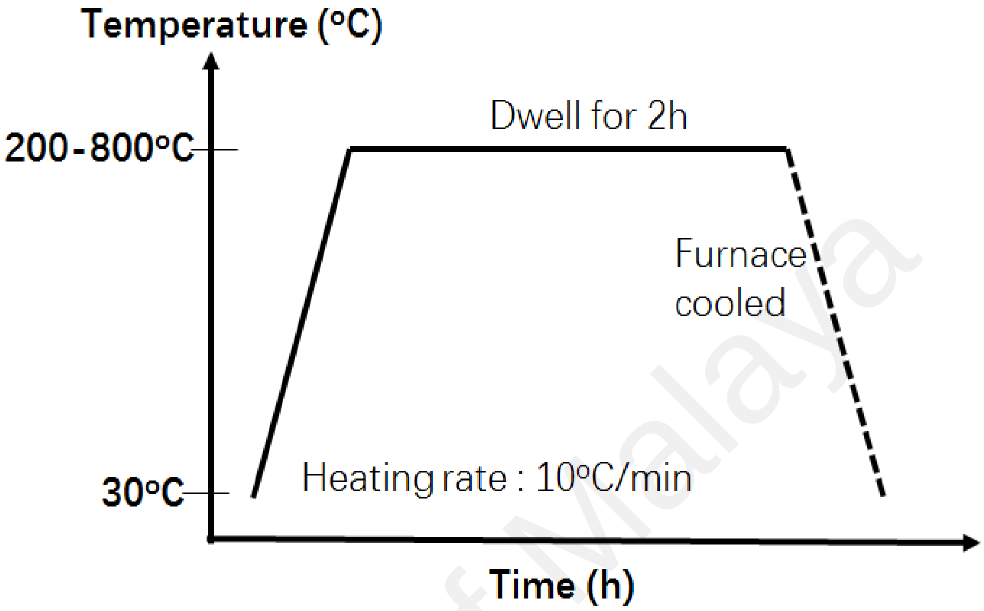

Figure 2.10: The calcination profile for nanoparticle synthesis process.

Table 2.7: Merits and demerits of different synthesis techniques.

Methods	**Merits**	**Demerits**	**References**
Peroxo Sol gel method	Simple, low temperature reaction, large yield and homogeneity	Long complete time	(Chang, Lee, & Chiu, 2013; S. Lee et al., 2010; Shavdina et al., 2015)
Calcination	Controlled morphology and crystallinity by tuning experimental conditions and controlling the preparation parameters.	Require expensive furnace	(H. Dong, Wang, & Koenig, 2018; Triampo, Yodyingyong, Panijpan, & Triampo, 2009)
Hydrothermal	Efficient and environmentally friendly, without the use of templates or reactants.	Low yield, a large amount of water has to be heated up and cooled down. High energy cost because of requiring heat exchangers and a high-pressure pump.	(Kruse & Dahmen, 2018; Munir et al., 2018)

2.7 Challenges and future perspective for rGO/TiO_2 nanocomposites in an energy storage field

rGO/TiO_2 nanocomposites have been investigated extensively in the energy storage and conversion field. The future opportunities in supercapacitor devices development are to search for flexible, high energy and power density, mechanical durability and stable packaging to rival with products in the current markets. rGO/TiO_2 nanocomposite is one of the prospective material to alleviate the aforementioned challenges and demand. The controlled synthesis of pristine rGO, TiO_2 and rGO/TiO_2 nanocomposites is one of the most critical direction for the supercapacitor’s further development. To date, numerous researches have been reported on the different synthesis method of rGO/TiO_2 nanocomposites. In order to reduce the equivalent series resistance, sol gel method and hydrothermal method are appropriate methods to homogeneously disperse TiO_2 onto rGO for better electrochemical performance. Furthermore, the proportion of between metal oxide and carbon nanomaterials should be optimized to achieve the desired properties. Finally, market commercialization is the critical issue where testing and regulation of rGO/TiO_2 are required to bridge the gap between industry application and academia lab research. Therefore, green and simpler cost-effective methods in the manufacturing of rGO/TiO_2 materials will be highly desirable.

2.8 Summary

In this review, we cover the work done on pure TiO_2 and rGO/TiO_2 as supercapacitor electrode materials. The various parameters related to the synthesis of nanomaterials have been reviewed. Besides that, the brief overview of electrolytes was also discussed. Factors such as energy density and power density are strongly dependent on the choice the electrolyte used and its potential window. In short, electrode materials and electrolyte selection will bring a significant impact to supercapacitor performance. The drawback with pristine carbon-based electrodes is that they have poor specific capacitance due to limited charge accumulation in the electric double layer. Besides that, pure metal oxide electrode has poor cycling stability. The limitations of metal oxides can be reduced by developing a composite TiO_2 electrode (eg, rGO/TiO_2) which will enhance the electrochemical performance. This is because composite electrodes provide larger specific surface area and higher specific capacitance as compared to the pristine materials. It is also important to optimize the loading amount of electroactive materials while synthesizing the composite materials. As a conclusion, it is clearly seen that the electrochemical performance of the electrode materials mainly relies on the conductivity, specific surface area and potential window of electrolyte used.

CHAPTER 3: METHODOLOGY

3.0 Chemicals and Materials

Chemical and material selection are very essential in designing fabrication of the electrodes for better electrochemical performance. Table 3.1 shows the general information of all materials and chemicals used in this research work.

3.1 Synthesis of TiO_2 nanocrystals

TiO_2 nanocrystals are synthesized by a peroxo sol-gel method employing titanium tetrachloride ($TiCl_4$) (Etacheri, Seery, Hinder, & Pillai, 2011; Sasirekha et al., 2009). In a typical synthesis of 1:2 peroxo-modified TiO_2 sol, 5.5 mL of $TiCl_4$ was slowly added into 150 mL cold distilled water to form titanium oxychloride ($TiOCl_2$). After 30 minutes constant stirring, a suitable amount of 30 wt% of ammonium hydroxide (NH_4OH) was then added drop by drop to form titanium hydroxide gel, $Ti(OH)_4$. During this process, the color of the solution changed to white. After aging for 12 h, $Ti(OH)_4$ gel was centrifuged and washed with distilled water several times.10 mL of H_2O_2 and 100 mL deionized water was then added into white $Ti(OH)_4$ gel to form yellow and transparent peroxotitanium complex solution. This peroxotitanium complex solution was heated at 50 ºC for 2 h for gelation followed by drying in an oven at 100 ºC for 24 h. The sample is denoted as TiO_2 nanocrystal. The resulting TiO_2 nanocrystals were calcined at different temperatures (200-800 ºC) for 2 h at a heating rate of 10 ºC min^{-1}. Figure 3.1 showed a flow diagram for preparation of TiO_2 by using peroxo sol gel method.

Table 3.1: Chemicals and materials used in the present study.

Materials/ Chemicals	**Function**	**Chemical Formula**	**Purity (%)**	**Manufacturer**
Titanium Tetrachloride	Precursor	$TiCl_4$	97.0%	Merck/United States
Graphite flakes	Raw material	C	<20 um	Sigma Aldrich
Potassium Permanganate	Oxidising agent	$KMnO_4$	99.0%	Friendemann Schmidt
Potassium hydroxide	Electrolyte	KOH	85%	Merck/United States
Ammonia	pH controller and reducing agent	NH_3	25%	Merck/United States
Hydrogen Peroxide	Oxidising agent	H_2O_2	30%	Friendemann Schmidt
Ethanol	Solvent and Cleaning agent	CH_3OH	95%	J. Kollin Chemicals
Carbon Black	Conductive material	C	Super P	Timcal
Polyvinylidine fluoride	Binder	$(C_2H_2F_2)_n$	N/A	Merck/ United States
N-Methyl-2-pyrrolidone	Solvent	C_5H_9NO	99.5%	Sigma Aldrich
Acetone	Cleaning agent	C_3H_6CO	Reagent	Merck/ United States
Sulphuric acid	Oxidising agent	H_2SO_4	98%	Merck/ United States
Phosphoric acid	Oxidising agent	H_3PO_4	85%	Merck/ United States
Hydrochloric acid	Washing agent	HCl	37%	Friendemann Schmidt

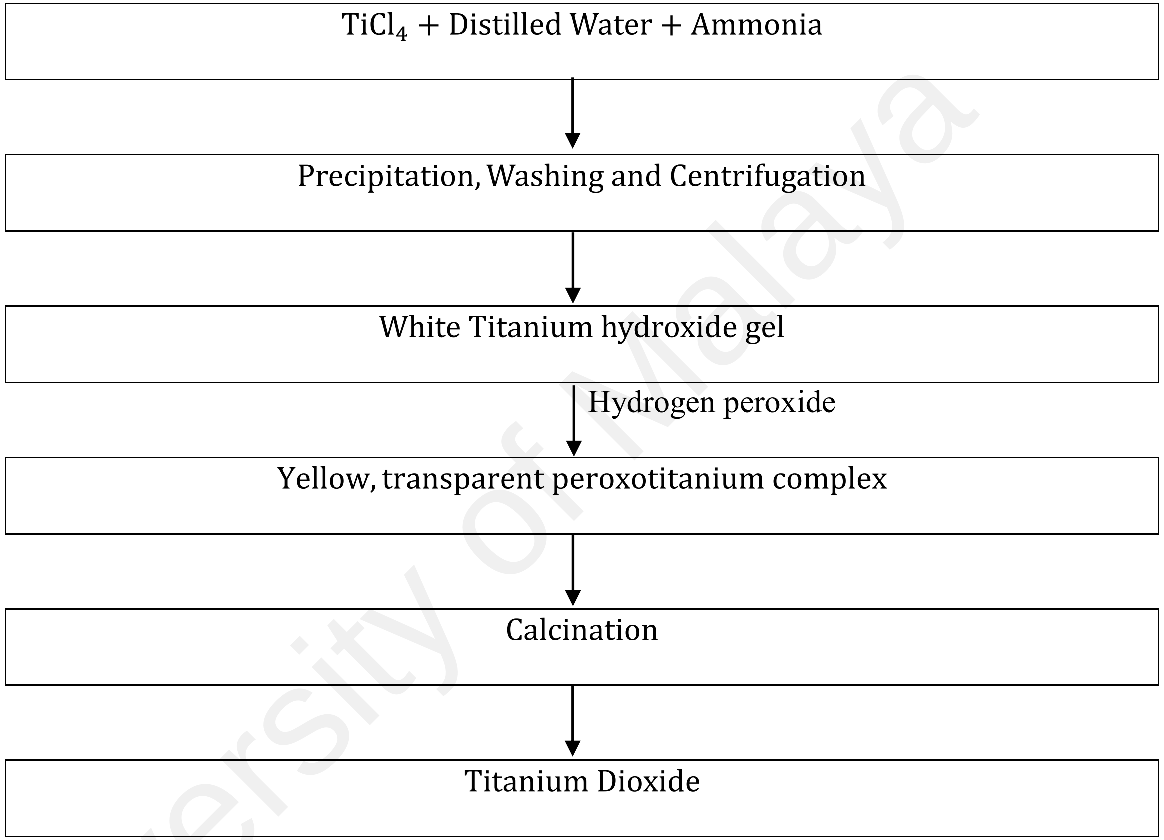

Figure 3.1: A flow diagram for preparation of TiO_2 by using peroxo sol gel method.

3.3 Synthesis of graphene oxide

Improved graphene oxide (GO) was synthesized from natural graphite flakes using a previously reported improved method (L. Dong et al., 2014; Hosseinpour, Abdizadeh, & Golobostanfard, 2017). Firstly, a 9:1 mixture of concentrated H_2SO_4/H_3PO_4 (180: 20mL) was dispersed into 3g of pristine graphite and 1g of $KMnO_4$ at room temperature. The green suspension was heated to 50 ºC and stirred for 15 h. For the observation view, the solution changed from dark purplish green colour to brick red brown colour. After that, the suspension will be cooled down to room temperature, 300 mL of ice cold deionized water solution along with 20 mL of 30% H_2O_2 was added in order to stop the reaction. The colour of solutions turned from brick red brownish to golden yellow, indicating completion of oxidation process. The product was centrifuged by using the Eppendorf Centrifuge 5430 R (500 rpm for 30 min), the supernatant was remained. The solution was centrifuged at 8000 rpm for 15 min and was washed in succession with 10% HCl and deionized water until the pH value of the filtrate was nearly neutral. Finally, the resulted brown GO obtained was oven-dried at 70 ºC overnight.

3.4 Synthesis of rGO/TiO_2 using peroxo sol gel hydrothermal method

Improved graphene oxide (GO) was synthesized from natural graphite flakes by using a modified Torr method (L. Dong et al., 2014; Hosseinpour et al., 2017). TiO_2 sol was synthesized by sol gel method, as reported in previous work (Heng et al., 2018).Then, a variable amount of GO powder (5wt. %, 10wt. %, 20wt %, and 30 wt. %) was dispersed separately in 40 mL distilled water under sonication for 1 h. The amount of GO was calculated from the total weight of TiO_2. Weight of TiO_2 was previously calculated from the weight of $TiCl_4$ as benchmark. Therefore, the samples were denoted as 5% rGO/TiO_2, 10% rGO/TiO_2, 20% rGO/TiO_2 and 30% rGO/TiO_2 nanocomposites, respectively. Next, 20 mL of TiO_2 sol was added into the GO solution. Then the solution was heated at 60 ºC for 2 h. The suspension was then transferred to a 100 mL Teflon-lined stainless-steel autoclave and hydrothermally reduced at 180ºC for 6 h. The resultant nanocomposite was then washed with deionized water and ethanol for several times and oven-dried at 70 ºC. Figure 3.2 showed a schematic presentation of rGO/TiO_2 synthesis from peroxo sol gel hydrothermal method.

Table 3.2: The composition of peroxo TiO_2 sol.

Chemical	Amount (mL)
Titanium Tetrachloride	1.5
Ammonia	3
Water	50
30% Hydrogen peroxide	2

Table 3.3: The composition of rGO/TiO_2 nanocomposite.

Precursor composite sol	**%Mass of GO (%)**	**Peroxo TiO_2 sol (mL)**	**Amount of GO (mg)**
5% rGO/TiO_2	5	20	21
10% rGO/TiO_2	10	20	44
20% rGO/TiO_2	20	20	100
30% rGO/TiO_2	30	20	171

Part I: Synthesis of Graphene Oxide

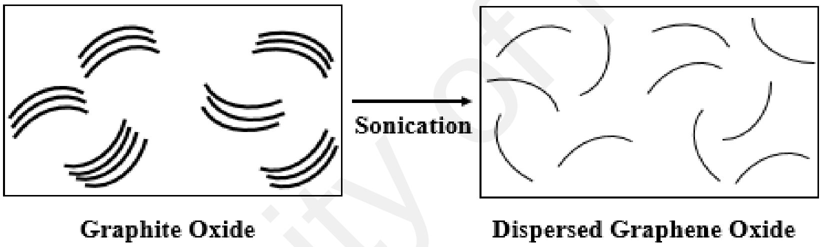

Part II: Synthesis of rGO/TiO_2

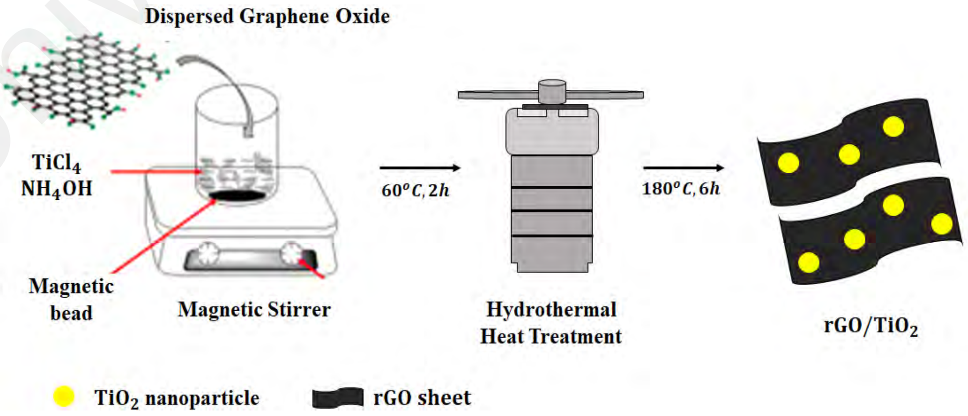

Figure 3.2: A schematic presentation of rGO/TiO_2 composite synthesis from peroxo sol gel hydrothermal method.

3.5 Material Characterization

3.5.1 Structural Analysis

The crystalline phases of the samples were determined via X-ray diffraction (Bruker axis D8 Advance diffractometer, Germany), using Cu Kλ radiation source (λ=1.5406 Å) at 40 kV and 30 mA with 0.02 s^{-1} scanning rate. The samples are scanned over in the 2θ range of 5-70°. The crystallite size of samples was calculated from the following Equation 3.1:

$$\mathrm{D} = \frac{\mathrm{K}\,\lambda}{\beta\cos\theta} \qquad \text{Eq 3.1}$$

Where K is Scherrer's constant (0.9), D is the diameter of grain, λ is the X-ray wavelength, θ is the diffraction angle, and B is the FWHM of the diffraction peak.

The zeta potential was measured by Malvern Zetasizer Nano ZS. FTIR spectrum was recorded in the range of 400-4000 cm^{-1} at a resolution of 4 cm^{-1} for every sample (Perkin Elmer Spectrum 400). The Raman spectra are recorded on a Renishaw (Gloucestershire, UK) in Via microscope with He Cd laser excitation source (λ=514.0 nm) at room temperature for functional group and structural identification. The scanning range is 400-4000 cm^{-1}.

The surface morphology and lattice of rGO, TiO_2, and rGO/TiO_2 nanocomposites were observed by using Field Emission Scanning Electron Microscope (FESEM; JEOL JSM-7600F at an accelerating voltage of 5.0 kV). The elemental analysis of rGO/TiO_2 was determined by using energy dispersion X-ray (EDX microanalysis) equipped in the FESEM. A high-resolution transmission electron microscope (HRTEM, JEOL model JEMP-2100 F instrument) was used to analyze the microstructures and morphologies of TiO_2 samples. Prior to TEM analysis, the samples were ultrasonically dispersed in ethanol for several hours. The N_2 adsorption/ desorption isotherms were analyzed by a surface area and porosity analyser (Tristar II 3020).

3.5.2 Fabrication of electrodes

Pretreatment of nickel foam (NF) was completed by an ultrasonic treatment with ethanol, dilute hydrochloric acid and distilled water respectively in the water bath, and then oven dried at 80 ºC (C. Zhao et al., 2016). The working electrodes were prepared by mixing electrode sample (TiO_2 or rGO/TiO_2 powder), carbon black, and PVDF in a weight ratio of 75:15:10 with NMP as the solvent. The mixture was then stirred for 12 h to form a homogeneous slurry. Briefly, the resulting slurry was pasted onto a sheet of nickel foam (1x1cm^2) and dried at 80 ºC for 12 h. The mass loading of the electrode materials on the single electrode was about 5.8 mg.

3.5.3 Electrochemical measurement

All electrochemical experiments were carried out using a three-electrode configuration in a 1M KOH electrolyte under normal atmosphere at room temperature. The Ag/AgCl was used as the reference electrode and Pt sheet as a counter electrode. Cyclic voltammetry (CV), galvanostatic charge-discharge (GCD) and electrochemical impedance spectroscopy (EIS) (0.01Hz to 100kHz) measurements were carried out by an electrochemical workstation (Metrohm Autolab PGSTAT 302N). The specific capacity (Cs) was calculated from CV curve according to Equation 3.2:

$$C_s(Cg^{-1}) = \frac{\int IdV}{\Delta V \times m \times v} \qquad \text{Eq 3.2}$$

Where $\int \mathrm{I}\,\mathrm{dV}$ is integral area under the CV curve, m is the mass of active sample material (g), and υ is the scan rate used in the experiment ($\mathrm{V\ s^{-1}}$), ΔV is the applied potential window.

Besides that, Cs of the electrodes were calculated from the galvanostatic discharge curves using the following Equation 3.3:

$$\mathrm{C_s(C\,g^{-1})} = \frac{\mathrm{I \times t}}{\mathrm{m}} \qquad \text{Eq 3.3}$$

Where I is the current of the system (A), t is the discharge time (s) and m is the mass of active sample material (g) and V is potential window.

Ultimately, $\mathrm{rGO/TiO_2}$ nanocomposite as positive electrode and activated carbon were prepared by a cellulose paper between two working electrodes to assemble a dual electrode cell soaked in the same 1M KOH electrolyte. The Cs is calculated based on Equation 3.3 but the m (g) serves as the total mass of both electroactive materials on two electrodes. The detailed energy density, and power density of single electrode and was calculated by the following Equations 3.4 and 3.5 (Jiao et al., 2016; J. Wang et al., 2017):

$$\mathrm{E(Wh\,kg^{-1})} = \frac{\mathrm{C \times \Delta V^2}}{2 \times 3.6} \qquad \text{Eq 3.4}$$

$$\mathrm{P(W\,kg^{-1})} = \frac{\mathrm{E\,x3600}}{\mathrm{t}} \qquad \text{Eq 3.5}$$

The overview of whole experiment was demonstrated as flow chart in Section 3.6.

3.6 Research Flow Chart

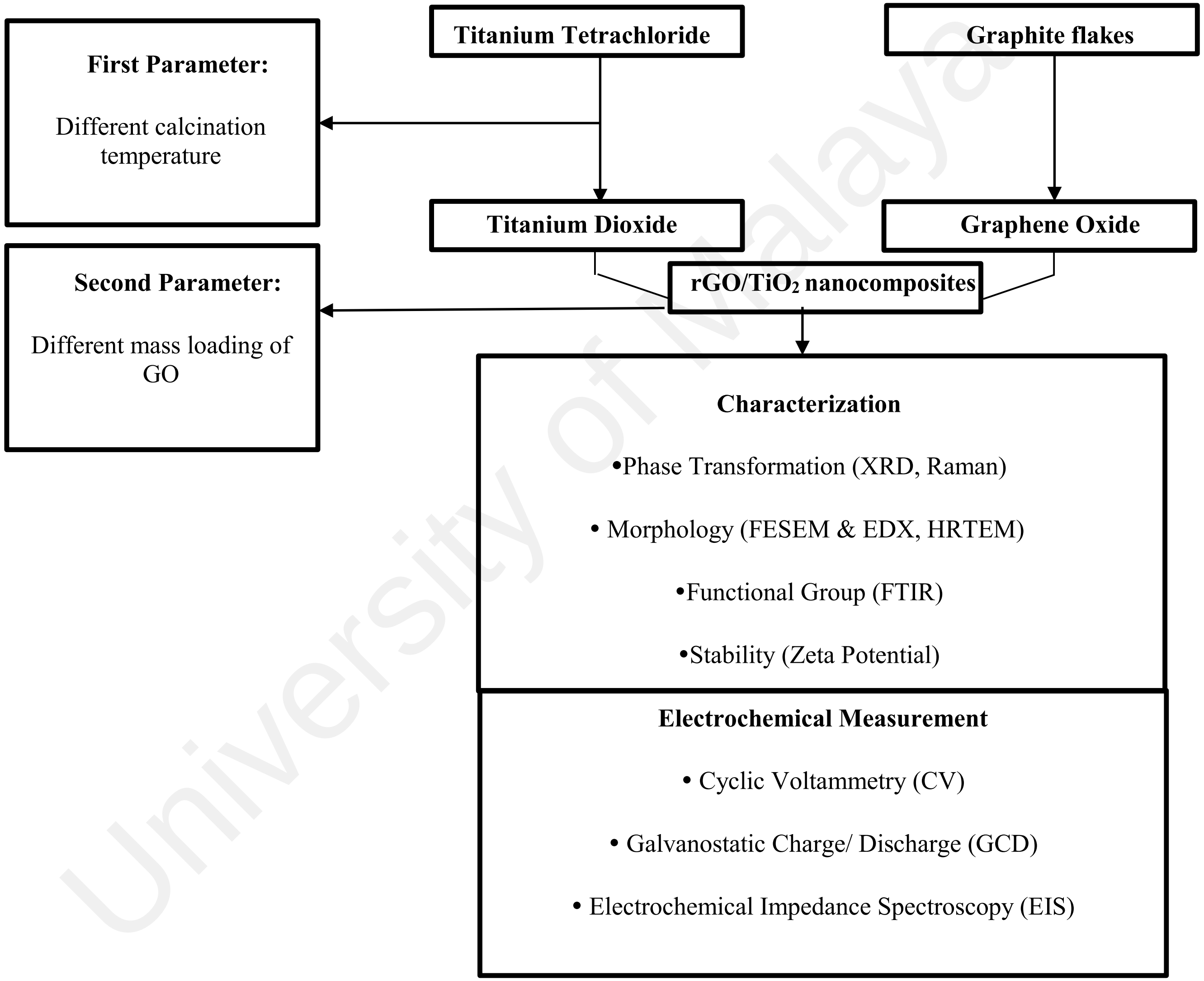

CHAPTER 4: RESULTS AND DISCUSSION

4.1 System 1: TiO_2 nanocrystals

4.1.1 Introduction

System 1 presents the information regarding the formation of TiO_2 nanocrystals and its electrochemical performance. The low temperature peroxo sol gel method for the preparation of the intermediate phase of amorphous and anatase TiO_2 nanocrystals is proposed. Besides that, the effect of different particle size and crystallinity of TiO_2 on the electrochemical performance of supercapacitor is not investigated. Therefore, in this study, the effect of different particle size and crystallinity of TiO_2 on electrochemical performance of supercapacitor is investigated. Additionally, the calcination temperatures are optimized to improve the charge-discharge of synthesized TiO_2 nanocrystals.

4.1.2 Stability Test

Sedimentation test and zeta potential were carried out to study the colloidal stability of TiO_2 nanocrystals and modified TiO_2 nanocrystals in water and H_2O_2 medium, respectively. Table 4.1 show the zeta potential and stability of TiO_2 nanocrystals in water and modified TiO_2 nanocrystals in H_2O_2 medium after sonication for 30 minutes. Sediments can be observed in unmodified TiO_2 nanocrystals colloidal solution after 14 days. Interestingly, the modified TiO_2 nanocrystals with H_2O_2 solution remained stable without visible precipitation under atmospheric conditions even after 21 days. This phenomenon can be explained by the coordination of peroxo group on the surface of Ti-O-Ti. The stability of TiO_2 nanocrystals colloidal systems is attributed to the equilibrium between the attractive and repulsive forces of the electrically charged particles (Ammam, 2012; Lorenzen, Rossi, Riegel-Vidotti, & Vidotti, 2018).

Zeta potential is a measurement which reflects the intensity of repulsive force between particles and stability of dispersion. It was found that TiO_2 nanocrystals in water showed basic pH. TiO_2 nanocrystals originally exhibited zeta potentials of -17.5 mV. The isoelectric point of TiO_2 ranged pH 4.5-6.8. If pH values vary from isoelectric point, TiO_2 nanocrystals would bear an electric charge (Y. Gao, Masuda, & Koumoto, 2004). Therefore, TiO_2 nanocrystals in water will turn less electronegativity and become positively charged when the pH value is higher than the isoelectric point.

For H_2O_2 solution modified TiO_2 nanocrystals, the addition of acidic H_2O_2 exists in the form of H_3O_2 and tends to contact with basic oxide sites. It was observed that the isoelectric point of modified TiO_2 nanocrystals shifted from basic to neutral pH. The surface traits of TiO_2 nanocrystal changed greatly after surface modification where the zeta potential of modified TiO_2 with H_2O_2 solution is -35.8 mV. The increase in zeta potential of modified TiO_2 is attributed due to protonation of H_2O_2 causing mutual repulsion of negative charge on the surfaces of TiO_2 nanocrystals (Y. Gao et al., 2004). The empty metal d-orbital (Ti^{4+} ion in TiO_2 sol) interact and accept electron density from antibonding H_2O_2 orbital to form peroxo complex. In short, a neutral impurity-free TiO_2 sol derived from $TiCl_4$ and H_2O_2 as bidentate ligand showing a better stability of dispersion in aqueous solution and improving the charge-discharge cycling stability of supercapacitor due to lower charge transfer resistance.

Table 4.1: Observation for unmodified TiO_2 nanocrystals colloidal solution in a water medium and modified TiO_2 nanocrystals colloidal solution in H_2O_2 medium and their zeta potential value

Duration **Samples**	Unmodified TiO_2 nanocrystals colloidal solution in a water medium	Modified TiO_2 nanocrystals colloidal solution in H_2O_2 medium
1 day		
14 days	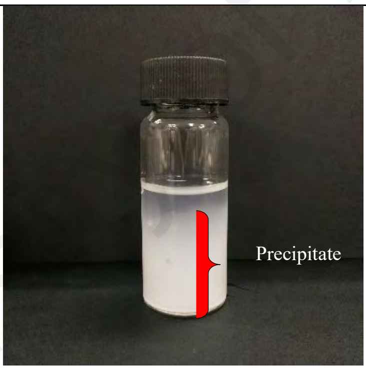	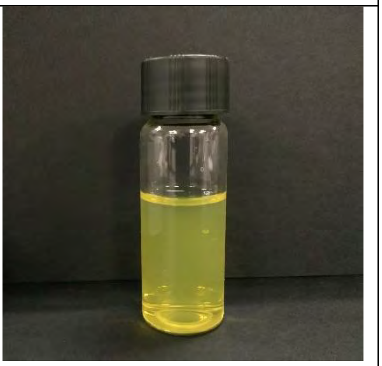
21 days	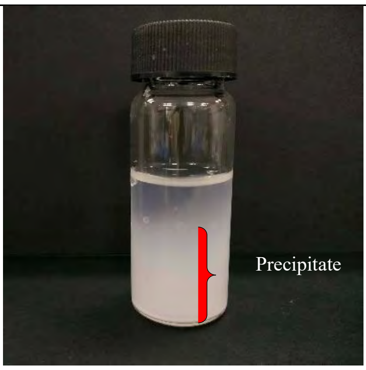	
Zeta Potential (mV)	-17.5 (Limited Stability)	-35.8 (Moderate Stability)

4.1.3 XRD

The effect of calcination temperature on the crystallization and phase transition of TiO_2 nanocrystals were analyzed using XRD. Figure 4.1 (a-e) shows the XRD pattern of TiO_2 nanocrystals and calcinated samples after annealing at various temperatures in the range of 200-800 ºC. The results clearly show that the crystallization rate of TiO_2 nanocrystals is determined by the calcination temperature (D.-S. Lee & Liu, 2002).

The TiO_2 nanocrystals are amorphous in nature (Z. Li et al., 2015; Tiron et al., 2016). Sobcyzk and co-authors (Sobczyk-Guzenda, Owczarek, Szymanowski, & Gazicki-Lipman, 2015) reported the X-ray diffractogram of non-annealed TiO_2 nanocrystals, amorphous states revealed a broad pattern with low intensity. However, weak anatase XRD peaks of TiO_2 nanocrystals is found in this experiment, which suggests peroxo sol gel method is able to promote crystallization of the anatase phase without calcination. Besides that, two weak peaks located at 25.6º and 48.8º are assigned to the (101) and (200) planes are observable for TiO_2 nanocrystals annealed at 200 ºC. Note here, our calcinated TiO_2 nanocrystals at 200 ºC may perform much better at lower annealing temperature containing intermediate amorphous and crystalline phase (Xiang Li, Zheng, Luo, Wu, & Lu, 2017). It is believed that the low temperature is favorable for the generation of finer crystallites with greater surface areas.

The XRD pattern of the calcinated TiO_2 nanocrystals at 400 ºC is shown in Figure 4.1 (c). As the calcination temperature was increased to 400 ºC, the anatase peaks intensity becomes stronger steadily whereas the peak width becomes narrower, indicating the formation of larger crystallites and promote crystallization. The obvious peaks are found at 2θ value of 25.6º, 38.4 º, 48.8 º, 54.8 º, 55.9º which are allocated to the (101), (004), (200), (105), and (211) planes of the tetragonal structure of TiO_2 (JCPDS card, No: 01-086-1157) respectively. This confirms that the calcination temperature at 400 ºC is sufficient to transform the amorphous phase into the crystallization phase (G. Li, Li, Boerio-Goates, & Woodfield, 2005). No other diffraction peaks were observed, indicating high purity of TiO_2 nanocrystals samples.

When the calcination temperature is further increased to 600 ºC, XRD pattern shows a lower the intensity of the anatase phase and rutile phase is observed at 27.4^o (110), 41.2^o (111), and 56.5^o (220) (Figure 4.1 (d)). At a high temperature of 600 ºC, the transformation mechanism involves sintering induced phase transformation and formation of oxygen vacancies which results in the formation of mix phase of anatase and rutile as observed (Sarma, Pal, Bailung, & Chutia, 2013). As sufficient thermal energy is present at 600 ºC, rearrangement of atoms happens when oxygen vacancies accelerates to break two of the six anatase Ti-O bonds leading to crystallite growth (Torres, Lindgren, Lu, Granqvist, & Lindquist, 2004). Besides that, the interfacial pressure of rutile particles absorbed and interact at the neighboring anatase particles' interface (Prasannalakshmi, Shanmugam, & Kannadasan, 2016).

Rutile as a major phase is observed at a higher annealing temperature of 800 ºC as presented in Figure 4.1 (e). Five common peaks corresponding to rutile phase where 2θ values are 27.4^o, 36.0^o, 41.2^o, 54.2^o, 56.5^o assigned to (110), (101), (111) ,(211), and (220) planes respectively (Sun & Gao, 2002; Tomita et al., 2006). Ghamsari and co-authors (Ghamsari, Radiman, Hamid, Mahshid, & Rahmani, 2013) concluded that the formation of the rutile phase transformed at 800 ºC is due to oxygen deficient atmosphere resulting structural rearrangement of anatase particles to a thermally more stable rutile formation . Sharp peaks observed in the XRD spectra of calcinated TiO_2 nanocrystals at 600 ºC and

800 ºC shows TiO_2 nanocrystals are highly crystalline. There was no other phase such as brookite phase observed among the five TiO_2 nanocrystal samples (Figure 4.1 (a-e)).

The crystallite size of different TiO_2 nanocrystals were calculated from the following Equation 3.1. The estimated crystallite sizes of TiO_2 nanocrystals by Scherrer's formula are 7.1 nm, 8.0 nm,14.1 nm, 28.3 nm, and 58.4 nm for TiO_2 nanocrystals, and calcinated TiO_2 nanocrystals at 200 ºC, 400 ºC, 600 ºC, and 800 ºC respectively. All samples show nanocrystalline properties.

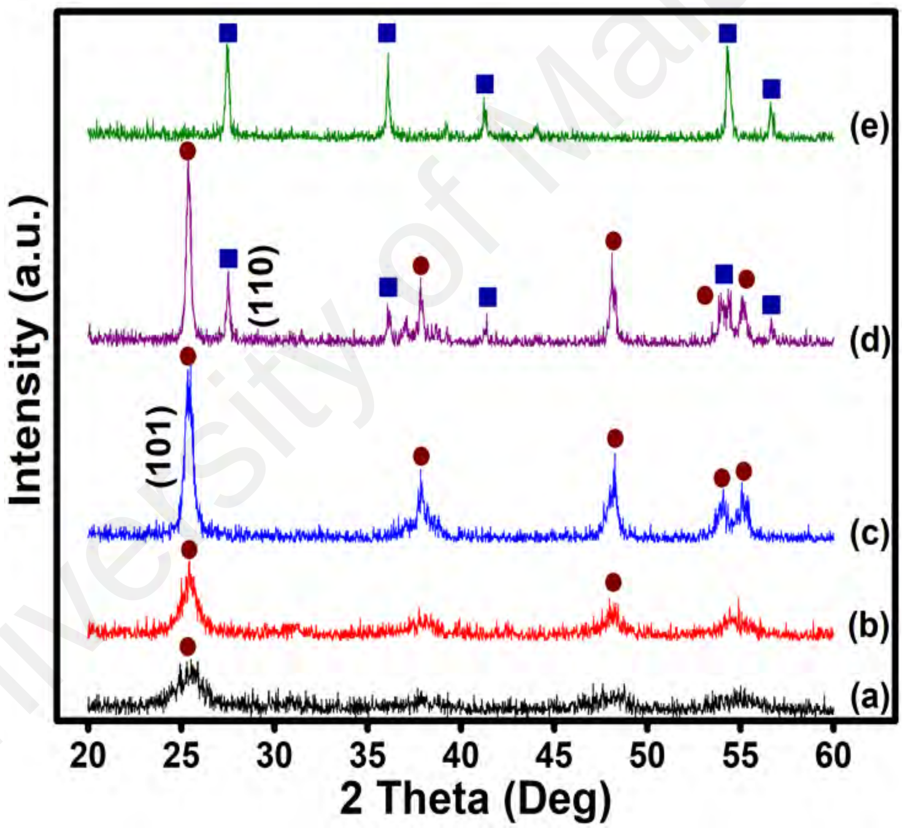

Figure 4.1: XRD of (a) TiO_2 nanocrystals before calcination and TiO_2 nanocrystals calcined at (b) 200 ºC, (c) 400 ºC, (d) 600 ºC, and (e) 800 ºC

[● = Anatase, ■ =Rutile]

4.1.4 FTIR

Figure 4.2 shows the FTIR identification spectra of TiO_2 samples taken in the range of 400-4000 cm^{-1}. The peak at 1400 cm^{-1} is attributed to the NH bond which indicated the presence of NH_4^+ (W. Low & Boonamnuayvitaya, 2013).The presence of vibration of OH^- groups and chemisorbed water are characterized by the peak at around 2900-3100 cm^{-1}. This shows that the presence of higher content of chemisorbed water compared to physiosorbed water on TiO_2 nanocrystals. The absorption band at around 1625 cm^{-1} is due to the bending vibration of physiosorbed water molecules (W. Low & Boonamnuayvitaya, 2013; Wellia et al., 2011). Meanwhile, the weak peak at 904cm^{-1} corresponds to O-O bond stretching vibrations (peroxo group), which indicates the presence of the peroxo groups in the Ti-O-O bond of the peroxotitanium complex. The disappearance of 904 cm^{-1} band after heat treatment from 400 ºC-800 ºC proved the thermal decomposition of peroxo groups (Sasirekha et al., 2009).

The transmission bands in the range of 450-690 cm^{-1} are identified as the formation of Ti-O-Ti lattice (Zou, Gao, & Xie, 2010).There is a decrease in Ti-O-Ti stretching frequency at 600 °C which may be caused by the formation of additional oxygen vacancies associated with loss of interstitial oxygen. An increase of oxygen content which strengthens theTi-O-Ti bond were also observed from heat treatment of TiO_2 at 200 ºC. This phenomenon can be attributed to the in-situ production of oxygen due to the low thermal decomposition of peroxotitanium complex, which blocks the oxygen vacancy formation and reduces the strength of Ti-O-Ti network. Stronger bonding of Ti-O-Ti shown in Figure 4.2 associated with smaller crystallite sizes of TiO_2 calcined at 200 ºC may be the vital reasons for the choice of supercapacitor.

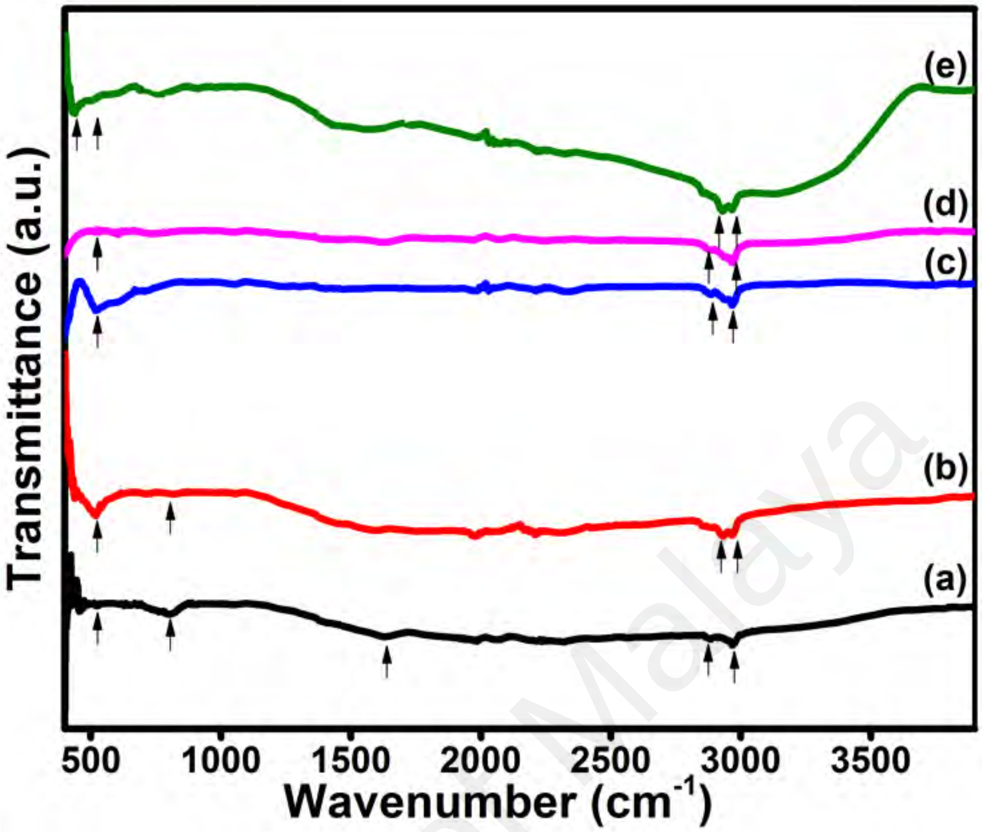

Figure 4.2: FTIR spectra of (a) TiO_2 nanocrystals before calcination and TiO_2 nanocrystals calcined at (b) 200 ºC, (c) 400 ºC, (d) 600 ºC, and (e) 800 ºC

4.1.5 FESEM & TEM

Figure 4.3 (a-e) shows FESEM and TEM morphological images of TiO_2 nanocrystals annealed at different temperatures. As shown in these images, the morphology of TiO_2 nanocrystals are dependent on the annealing temperature. The surface morphologies reveal the effect of annealing temperature on particle growth. The TiO_2 nanocrystals consist of spherical particles which has an average diameter of 8 nm as shown in Figure 4.3 (a). Some loose bulk of amorphous aggregates appeared are observed in the as prepared TiO_2 nanocrystals. Figure 4.3 (b) reveals the morphology of calcinated TiO_2 nanocrystals at 200 ºC have an average diameter of 12nm with smaller aggregates as compared to TiO_2 nanocrystals. This is believed to due to the reconstruction of TiO_2 nanocrystal during phase transition from some amorphous to anatase, increasing the particle size. The anatase TiO_2 nanocrystals which were calcined at 400 ºC are found to be spherical in shape with diameter of 22 nm.

The TEM images prove that the measured interplanar distance is about 0.35 nm which corresponding to anatase (101) spacing which is in good agreement with the reported XRD result. As observed in Figure 4.3 (d), calcinated TiO_2 nanocrystals at 600 ºC showed a morphology of densely packed particle distribution. It is believed that the primary TiO_2 particles interact and aggregate into bigger spherical particles when at high annealing temperature (J. Yu, Wang, Cheng, & Zhou, 2007). In addition, the TEM image of calcinated TiO_2 nanocrystals at 600 ºC displays growth behavior with the lattice spacing of the (101) and (004) with the interplanar distances of 0.350 and 0.237 nm, which further confirms that when the temperature was increased to 800 ºC, the morphology of TiO_2 nanocrystals showed formation of large non-porous and solid particles with diameter of 133 nm, which can be attributed to the thermally promoted crystallite growth (Figure 3 (e)). The calcinated TiO_2 nanocrystals at 800 ºC have an orientation along the (110) direction with a lattice spacing of 0.274 nm, corresponding to the rutile phase of TiO_2 nanocrystals. In other words, these results showed that the crystallinity increased linearly with calcination temperature, which is in good agreement with XRD and FTIR results.

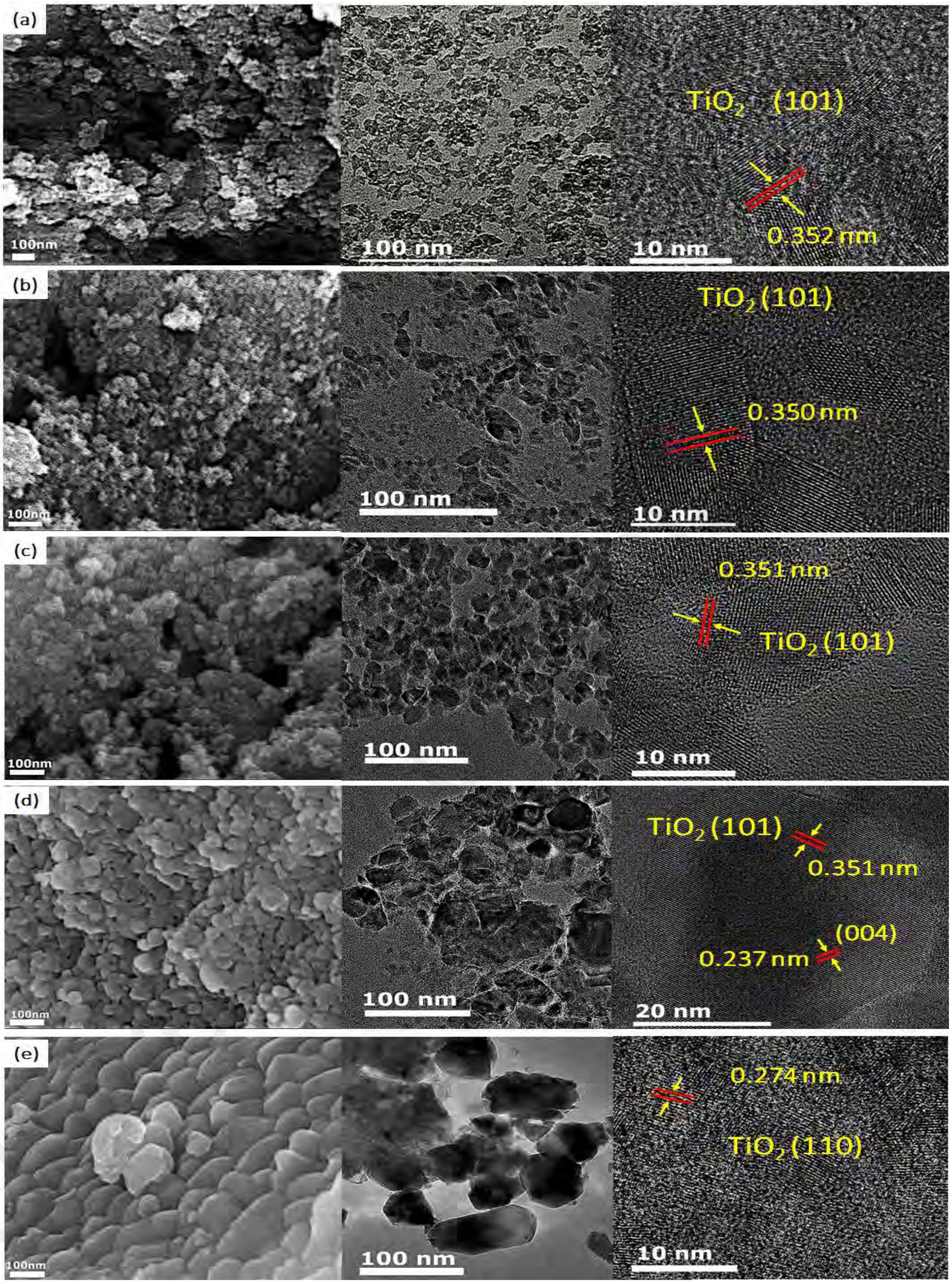

Figure 4.3: FESEM and TEM images of (a) TiO_2 nanocrystals before calcination and TiO_2 nanocrystals calcined at (b) 200 °C, (c) 400 °C, (d) 600 °C, and (e) 800 °C [Left = FE-SEM image, Middle= TEM image, Right=Lattice fringe of TiO_2]
*All the magnification of FESEM image was x120,000.

4.1.6 Electrochemistry analysis (Three-electrodes assembly)

4.1.6.1 CV analysis

The TiO_2 electrodes were analyzed in a range of 0.0-0.5 V using 1M KOH electrolyte. Figure 4.4 (a-e) show the CV curves of the TiO_2 electrodes at different scan rates (3-50 mV s^{-1}). Two strong peaks were observed, which indicates the pseudocapacitive behavior of TiO_2 (Poonguzhali et al., 2015). The existence of redox peaks can be explained by alkali K^+ cations intercalating in and out of the working electrode corresponding to reduction/ oxidation of the Ti ions (Pal et al., 2018). The redox reaction of TiO_2 in an alkaline medium can be explained with Equation 4.1.

$$xK^+ + TiO_2 + xe^- \Leftrightarrow K_xTiO_2 \qquad \text{Eq 4.1}$$

Note: x represents number of intercalation or de-intercalation of positive ions with an equal number of electrons (e^-)

Figure 4.5 showed a comparison curve between TiO_2, and calcinated TiO_2 nanocrystals at 200 ºC, 400 ºC, 600 ºC, and 800 ºC at a scan rate of 3 mV s^{-1}. The calculated specific capacity of TiO_2 and calcinated TiO_2 at 200 ºC, 400 ºC, 600 ºC, and 800 ºC at a scan rate of 3 mV s^{-1} were 72, 176, 44, 38, and 36 C g^{-1}, respectively. Among the five electrodes, TiO_2 nanocrystals calcined at 200 ºC have the maximum integrated area of CV curve, showing the largest capacity (Fu et al., 2015). The capacity decreased for TiO_2 nanocrystals calcined at 400-800 ºC due to lesser amorphous electroactive materials, leading to hindrance of charge transfer during Faradaic pseudocapacitance reaction.

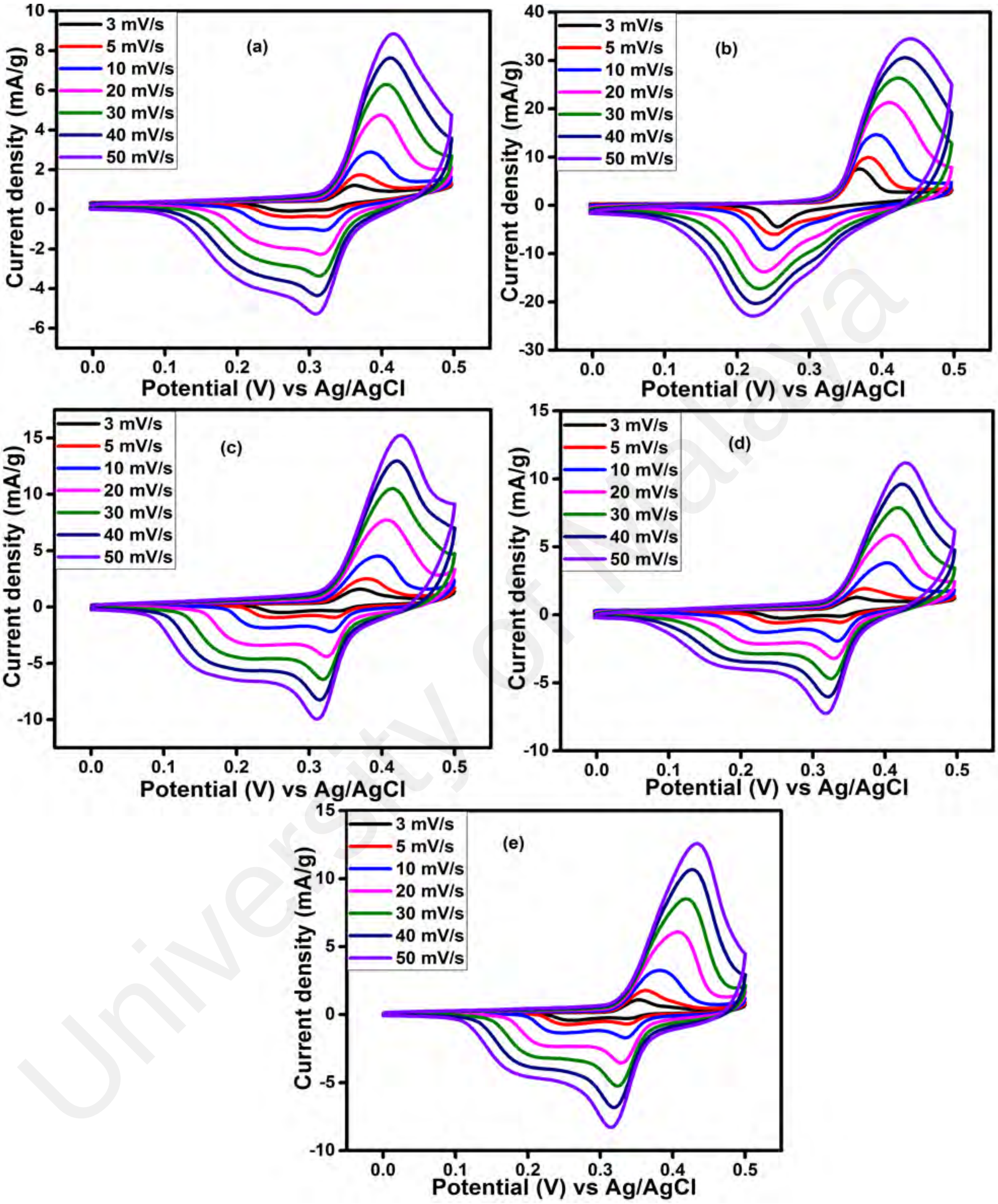

Figure 4.4: Cyclic voltammogram of (a)TiO_2 nanocrystals before calcination and TiO_2 nanocrystals calcined at (b) 200 ºC , (c) 400 ºC, (d) 600 ºC, and (e) 800 ºC at varied scan rate of (3-50 mV s^{-1}).

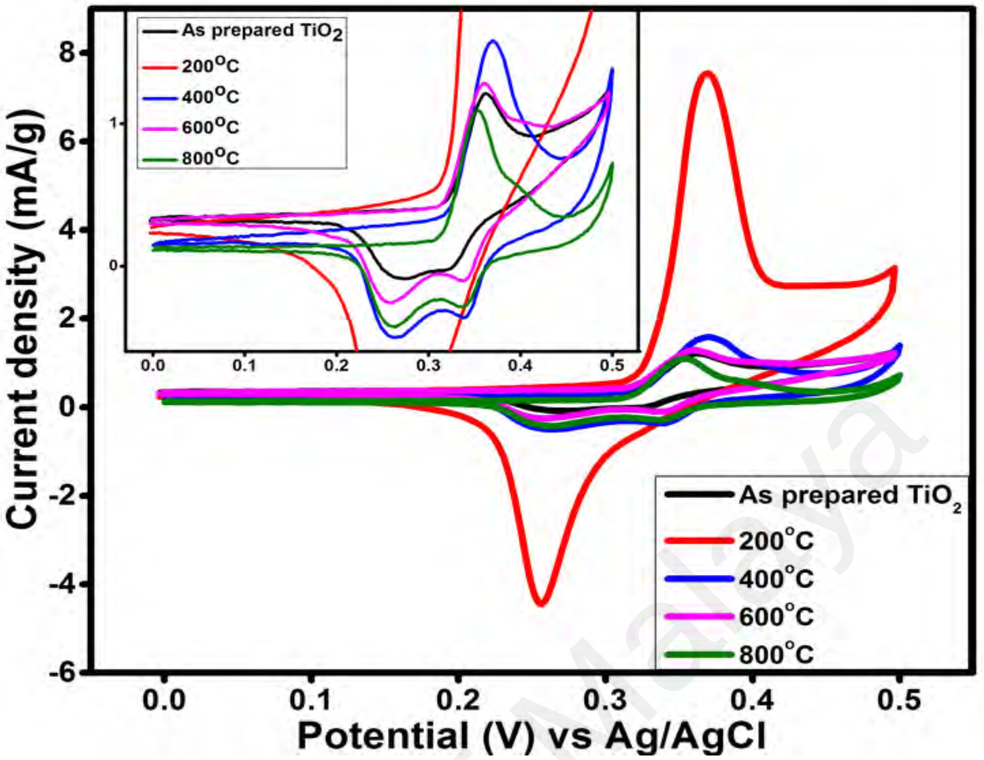

Figure 4.5: Cyclic voltammogram of TiO_2 nanocrystals before calcination and TiO_2 calcined at:200 ºC, 400 ºC, 600 ºC, and 800 ºC at a scan rate of 3 mV s^{-1}.

4.1.6.2 GCD analysis

Figure 4.6 (a-e) shows the galvanostatic charge-discharge profiles of the TiO_2 electrodes recorded in a stable potential window between 0-0.5 V at various current densities (0.2-1.0 A g^{-1}). Triangular shape with an obvious discharge plateau in every GCD curve was observed, which suggest a faradaic redox battery behavior (Gu, Ge, Wang, & Tu, 2015).When the current density was high, K^+ ions have time constraints to access and interact with the active material. Similarly, K^+ ions have sufficient time for diffusion through an electrode material occurs at a low current density, initiating the reaction with electrolyte species and electrode materials (Jahromi et al., 2015). In other words, the discharge time and specific capacitance increase linearly with the decrease of current density. The results showed that TiO_2 electrodes calcined at 200 ºC have a longer discharge time among the other five working electrodes.

At a low current density of 0.2 A g^{-1}, as-prepared TiO_2 electrodes and TiO_2 electrodes calcined at 200 ºC, 400 ºC, 600 ºC, and 800 ºC recorded capacitance value of 10.23,26.46, 70.26, 14.84, and 9.16 C g^{-1} respectively. Li and co-authors reported the optimal annealing parameters for supercapacitor applications should be chosen at a lower temperature (350 ºC) (X. Li et al., 2017). Interestingly, TiO_2 nanocrystals annealed at 200 ºC exhibited the best performance among with the samples.

The phase transition of TiO_2 nanocrystals from anatase to rutile is the key factor which influence the capacitance behavior. Intermediate phase of amorphous and anatase of the as-prepared TiO_2 nanocrystals and TiO_2 nanocrystals calcined at 200 ºC have a smaller particle size, leading to less particle aggregation. The lesser and smaller particle aggregation results in enhancement of K^+ insertion into redox active sites. As observed, when there is an increase in size of particles during the phase transformation of TiO_2

nanocrystals into rutile phase, redox active sites start to decrease. Lastly, irregular surfaces of TiO_2 nanocrystals that calcined at 200 ºC provide the larger surface area which promotes interaction between electrolyte and interfacial area of TiO_2 nanocrystals.

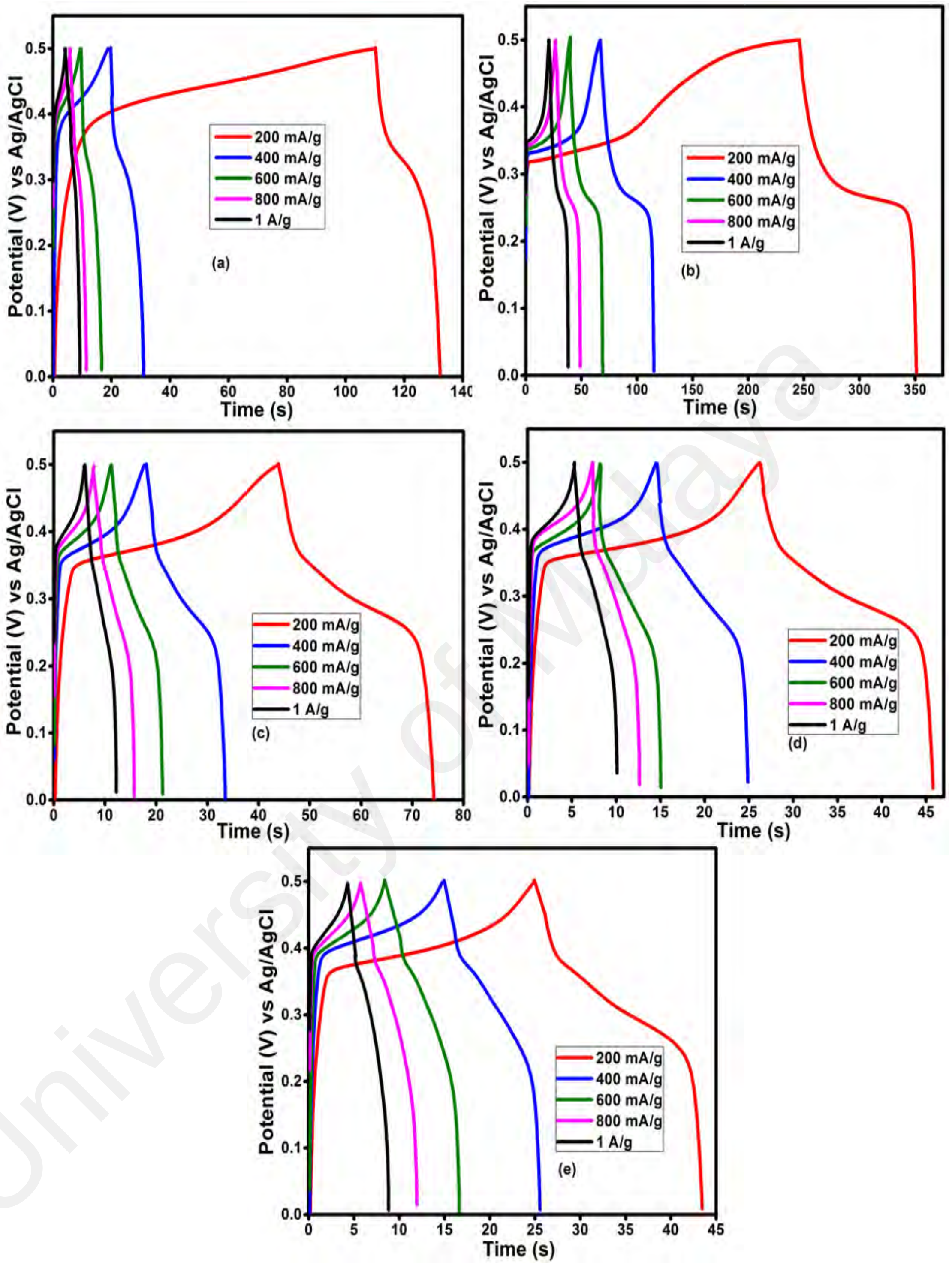

Figure 4.6: Galvanostatic discharge curves of (a) TiO_2 nanocrystals before calcination and TiO_2 nanocrystals calcined at (b) 200 ºC, (c) 400 ºC, (d) 600 ºC, and (e) 800 ºC at different current densities.

4.1.6.3 EIS analysis

To further investigate the relationship of charge transfer dynamics between electrode and electrolytes, EIS was performed on all working electrodes. It is well known that internal resistance between working electrode and electrolyte, the contact resistance between electrode and nickel foam are the important features which influence the capacitance. The EIS plots of the TiO_2 nanocrystals in a frequency range 0.01-100 kHz are illustrated in Figure 4.7 (a-e). There are two regions in the 0.01-100 kHz which are the high and low frequency regions.

The intercept of semicircle at higher frequency is observed in Figure 4.7 (a-e) is equivalent to the charge transfer resistance (R_{ct}). The observed R_{ct} values of TiO_2 and calcinated TiO_2 nanocrystals at 200 ºC, 400 ºC, 600 ºC, 800 ºC are 9.04, 3.83, 6.54, 8.10, and 13.79 Ω respectively. The lowest R_{ct} value of TiO_2 nanocrystals calcined at 200 ºC is attributed to the smaller particle size of TiO_2 nanocrystals with the higher electroactive surface area. At the same time, the good electrochemical utilization of TiO_2 nanocrystals electrodes can enhance the fast ions flow from electrolyte into the working electrode surface during the faradaic reaction (Fabregat-Santiago et al., 2008).

The straight-line slope observed in the low frequency region corresponding to the Warburg impedance (W), which reflects the diffusion resistance from electrolyte ions into the pore structure of TiO_2 nanocrystals electrode surface. TiO_2 nanocrystals calcined at 200 ºC possess lower slope, suggesting the enhancement in diffusion rate of electrolyte into working electrode surface. This may also be attributed to the presence of a more porous structure of TiO_2 nanocrystals calcined at low temperature of 200 ºC.

Based on EIS plots, the charge transfer resistance of as-prepared sample (9.04 Ω) is observed to be larger than the other samples except TiO_2 nanocrystals calcined at 800 ºC (13.79 Ω). This might be attributed to the defect of TiO_2 nanocrystals without calcination comprises impurities in the absence of calcination which results in a decrease of electrochemical performance. This suggests that calcination can effectively remove excess NH_4Cl and/or adsorbed organic ammonia molecules from the surface of titania particles due to the endothermic decomposition process (Danks et al., 2016; Kanezaki, Sakamoto, Ookubo, & Ooi, 1992; H. Xie, Zhang, Xi, Wang, & Liu, 2002). Heat treatment at high temperature (~800 ºC) introduces oxygen vacancies, which in turn accelerates the crystallite growth (Torres et al., 2004; H.-F. Yu, 2007).

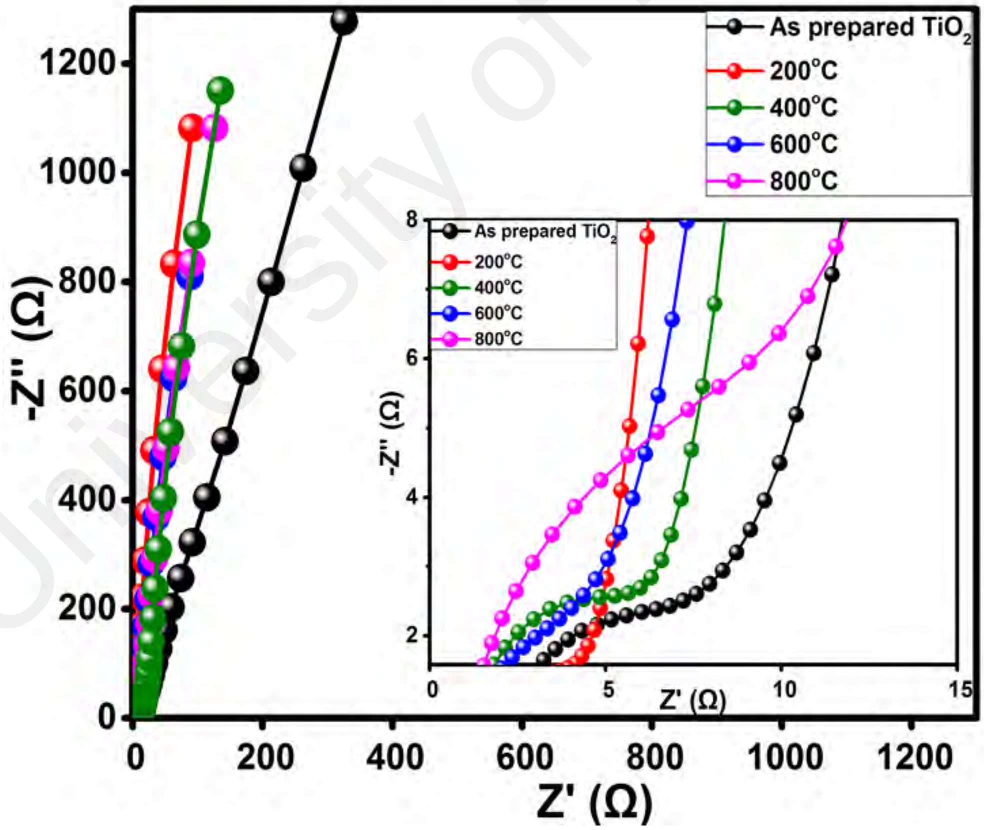

Figure 4.7: Nyquist plot for the TiO_2 electrodes before calcination, and TiO_2 nanocrystals calcined at 200 ºC , 400 ºC, 600 ºC, and 800 ºC with the enlarge view insert.

4.2 System 2

4.2.1 Introduction

System 2 presents the information regarding the formation of rGO/TiO_2 nanocomposites and its electrochemical performance. A variety of synthesis protocols were used in preparing rGO/TiO_2 nanocomposite electrodes, including hydrothermal with the addition of basic NaOH, vacuum-assisted filtration with thermal treatment and microwave-assisted method. However, these methods predominantly require toxic and strong alkaline reducing reagents, certain stabilizer and a complicated lengthy synthesis duration.

This study demonstrates an environmental friendly and one-step approach that combines sol-gel hydrothermal without the addition of any reducing agents for rGO/TiO_2 nanocomposites formation to further improve the electrochemical properties of capacitive wise. Remarkably, a pioneer work has been established in regard to supercapattery system which combined electrodes of capacitive-type and battery-type from the conventional supercapacitor concept research was reported. It is assured that the combination of battery-type materials with capacitive-type materials could improve the electrochemical performance of supercapacitors with excellent power density and satisfactory cycling stability performance.

4.2.2 Mechanism

This experiment described that the sample was prepared by direct gelation of TiO_2 sol into GO solution, followed by hydrothermal heat treatment at 180 °C. The process with its final product and chemical reaction for preparing rGO/TiO_2 nanocomposites is illustrated in Figure 4.8 (a). Theoretically, the charge carrier transportation from TiO_2 to rGO in rGO/TiO_2 nanocomposite is markedly subjected to the chemical interaction among TiO_2 and rGO. Generally, it begins with hydrolysis and condensation to produce TiO_2 sol. Next, TiO_2 sol is added into exfoliated GO solution. The electrostatic force of attraction happens between the negatively-charge oxide functional groups of GO (i.e. oxygen-containing groups) and the positively-charged Ti^{4+} ion species, self-assembly of TiO_2 is attached on the carbon plane of GO; hence, the formation of Ti-O-C bridge. After stirring for 2 h, the solution is autoclaved at 180 ºC for 6 h. Nucleation happens rapidly with the growth of TiO_2 nanocrystals on the 2D rGO nanosheets during heat treatment. The dark grey powder of the intermediate rGO/TiO_2 product was obtained after heat treatment. Besides, GO is simultaneously converted into rGO by the reduction in hydrogen radicals (H^+), producing black rGO/TiO_2 final product, which is shown in Figure 4.8 (b) (Mohammad-Rezaei & Razmi, 2016; Nguyen-Phan et al., 2016). The specific process is listed as in Equation 4.2:

$$\mathrm{GO} + \mathrm{H}^+ \rightarrow \mathrm{rGO} + \mathrm{H_2O} \qquad \text{Eq 4.2}$$

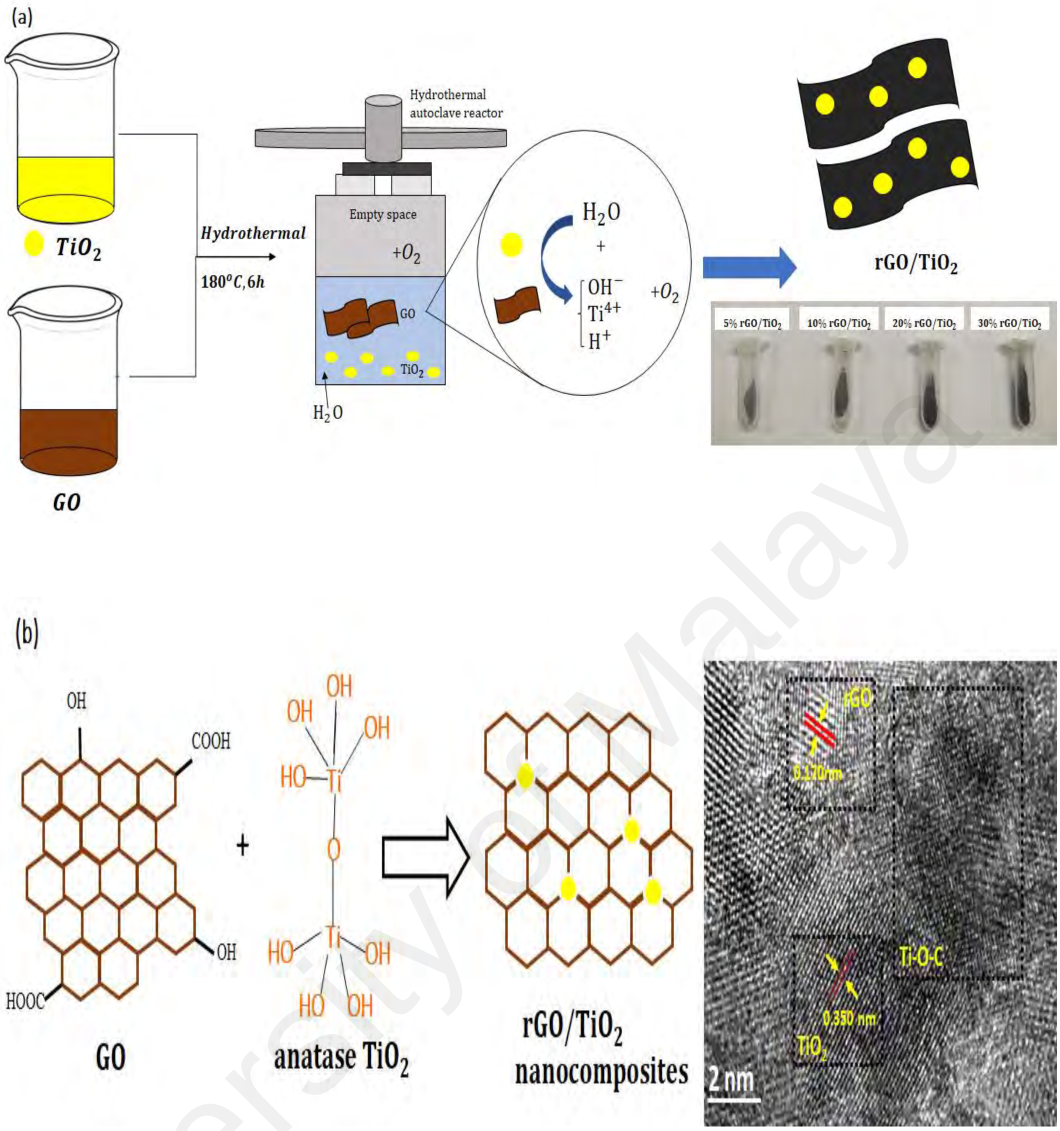

Figure 4.8: Schematic diagram of (a) Sol gel hydrothermal method for rGO/TiO_2 nanocomposites preparation and (b) Structure formation mechanism of rGO/TiO_2 nanocomposites

4.2.3 FESEM &EDX

FESEM morphological images and relative EDX mapping analysis of as-prepared rGO, TiO_2 and 10% rGO/TiO_2 nanocomposites are illustrated in Figure 4.9. Figure 4.9 (a) reveals the heterogeneous spheres that were produced in bundle of as-prepared TiO_2 with an average diameter of (~71.0 nm). Figure 4.9 (b) clearly displays a tissue-like monolayer rGO superthin layer (~ 46 nm) with the well-performed structure under synthesis reaction time of GO product (F. W. Low, Lai, & Hamid, 2015). Figure 4.9 (c) illustrates the images of 10 % rGO/TiO_2 nanocomposites. It clearly showed that the surface of rGO was scattered with TiO_2 nanocrystal. Surprisingly, the oxygen-containing groups (-COOH, -OH) of rGO retarded the growth of TiO_2 nanocrystals and subsequently formed an average size of TiO_2 nanocrystal (~59.43 nm). This phenomenon promoted an efficient electron charge transportation rate during the charge and discharge process in supercapattery application (J. Li et al., 2017). The EDX spectrum of 10% rGO/TiO_2 nanocomposites presented in Figure 4.9 (d) indicates the presence of C, O and Ti elements in 10% rGO/TiO_2 samples.

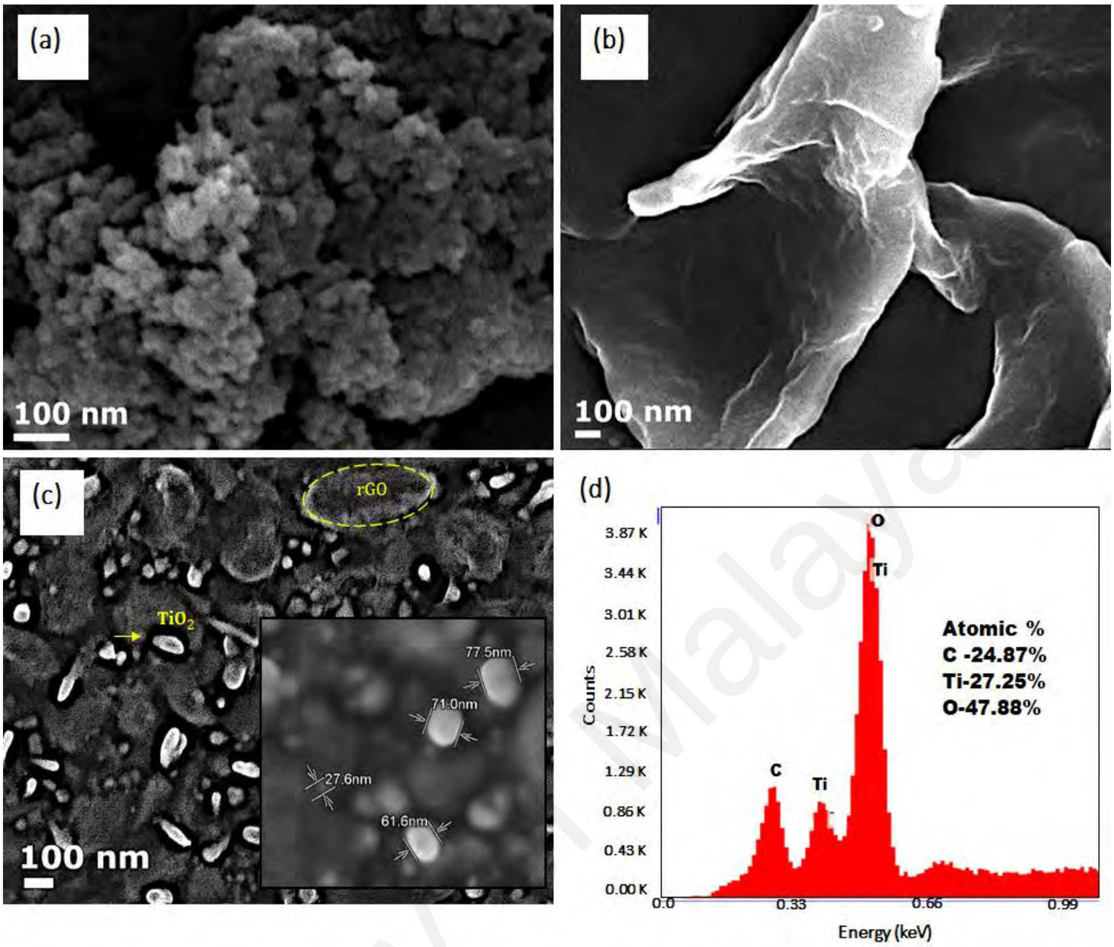

Figure 4.9: FESEM images of (a) TiO_2, (b) rGO nanosheet, (c) 10% rGO/TiO_2, and (d) EDX spectrum.

4.2.4 XRD

In the comprehensive work, XRD analysis was used to evaluate the crystal structure and justify the average spacing between TiO_2, GO, rGO, and rGO/TiO_2 nanocomposites. Figure 4.10 illustrates the XRD pattern of as-prepared GO, rGO, TiO_2 and rGO/TiO_2 nanocomposites. In Figure 4.10 (a), only one peak is detected at 2θ=10.5° along the 002 orientations. After hydrothermal reduction, the peak of GO at 10.5 ° was not perceived but a peak at 2θ=25.1° was detected and identified as rGO materials, as shown in Figure 4.10 (b). The d-spacing that was dramatically decreased from 0.703 nm (GO) to 0.38 nm (rGO) suggested that a poor arrangement or multi-layers of stacked situation has occurred between rGO materials. In other words, the disappearance peak at 10.5° is attributed to the oxygen-containing molecules that were thoroughly eliminated for the rGO samples (Thakur & Karak, 2012). These phenomena deduce that the interlayers between successive carbon layers are strengthened although lesser layers are formed.

In Figure 4.10 (c), some sharp crystalline peaks of 25.6°, 37.9°, 47.9°, 54.0° are implemented to (101), (004), (200) and (105) orientation which are signified as anatase TiO_2 (JCPDS card, No:01-086-1157). Meanwhile, the XRD patterns for the rGO/TiO_2 nanocomposites are shown in Figure 4.10 (d) – Figure 4.10 (g). The sharp crystalline peaks detected at 25.6°, 37.9°, 47.9°, 54.0°, 55.3° were implemented to (101), (004), (200), (105) and (211) orientation, which assignable to anatase TiO_2 (Hamid, Tan, Lai, & Samsudin, 2014). In addition, the absence of broad peaks along the 002 orientation for rGO/TiO_2 naocomposites suggested that there was a fine reduction of GO transformed rGO (refer Figure 4.10 (d) - Figure 4.10 (g). These peaks of anatase TiO_2 and rGO were observed to merge with each other at 2θ= ~25°, and the rGO and TiO_2 peaks were hardly distinguished in rGO/TiO_2 nanocomposites due to the strong reflection of (101) peak for the rGO/TiO_2 nanocomposites samples (Police et al., 2018; W. Wang et al., 2017). Notably, among the rGO/TiO_2 nanocomposites samples of 5% and 10% rGO/TiO_2 nanocomposites were observed to have a broader intensity as compared to the as-prepared TiO_2. This was attributed to the crystallinity of the as-prepared TiO_2 that was decreased by the interaction of TiO_2 in 5% and 10 % of GO. However, the (101) peak intensity was gradually increased with 20% and 30% of GO, which was ascribed to an increase in crystallinity of 20 % and 30% of rGO/TiO_2 nanocomposites. The results clearly determined that the crystal growth of TiO_2 nanocrystals was affected by the different weight percentage of GO. Increase of GO content provided a platform for more nucleation and crystallization of TiO_2, that lead to higher crystallinity as shown in Figure 4.10. According to Scherer's formula, the average crystallite size of as-prepared TiO_2 at 5%, 10%, 20%, and 30% of rGO/TiO_2 nanocomposites were 34.72 nm (F. W. Low, Lai, & Hamid, 2017).

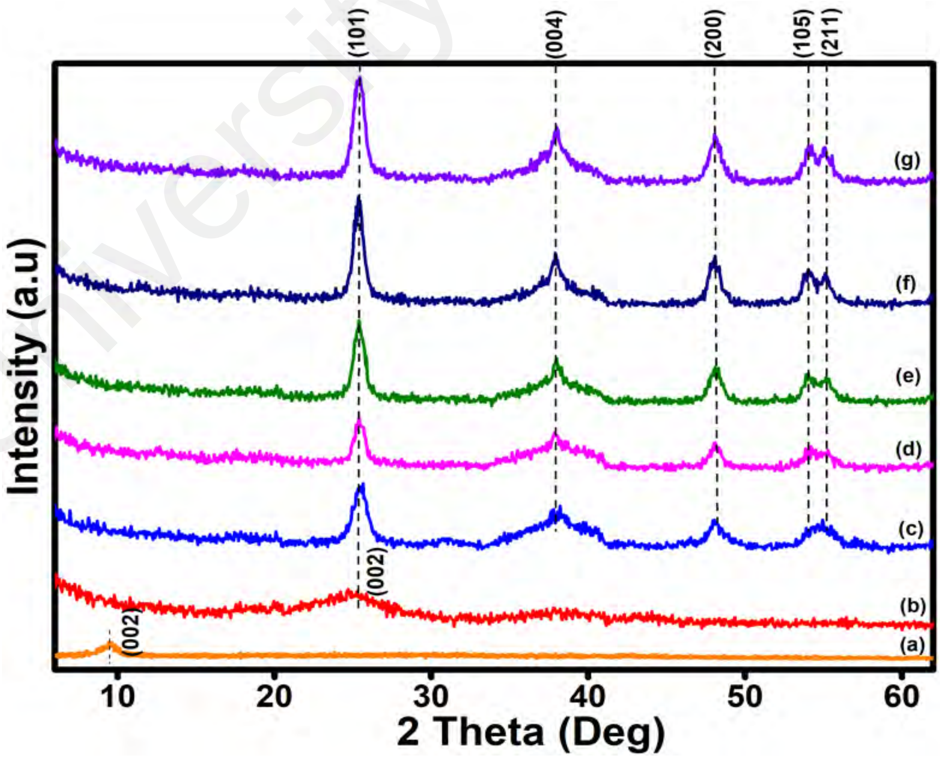

Figure 4.10: XRD pattern of (a) GO, (b) rGO, (c) TiO_2 and rGO/TiO_2 nanocomposites of (d) 5%, (e) 10%, (f) 20%, and (g) 30%.

4.2.5 Raman Spectroscopy

Raman spectroscopy is a non-destructive technique to understand the phase changes and vibration band of 5-30% rGO/TiO_2 nanocomposites. The Raman spectrum of rGO/TiO_2 nanocomposites in Figure 4.11 (a-d) with insert show two D-band peaks at 1351 cm^{-1} and G-band peak at 1593 cm^{-1} (Shaobin Yang et al., 2017). The D-band vibration referred to the sp^3 defects that were produced by the reduction process of GO (breathing mode of the K-point photos of A_{1g} symmetry), whereas the G-band was attributed to the in-plane vibration of sp^2 carbon bond (a first-order scattering of E_{2g} phonons) (Shoaib et al., 2017). The defect density of rGO in 5-30% rGO/TiO_2 nanocomposite samples could be represented by the intensity ratio between D-band and G-band (I_D/I_G). Generally, the I_D/I_G ratio is increased due to sp^2 carbon orientation during hydrothermal reduction. The I_D/I_G ratio for 5%, 10%, 20%, and 30% rGO/TiO_2 nanocomposites were 1.05, 0.8, 1.04 and 0.9, respectively. According to I_D/I_G ratio, 10% of rGO/TiO_2 nanocomposites obtained the lowest I_D/I_G value among composite samples, which attributed that the less structural defect among the composite samples and re-establishment of conjugated graphitic network during hydrothermal process, and thus resulting a higher degree of graphitisation and led enhanced charge transfer (Leong et al., 2015; J. Zhu et al., 2015). Moreover, typical peaks at 146.3 cm^{-1}, 400.30 cm^{-1}, 519.8 cm^{-1}, 638.7 cm^{-1} were attributed to the E_{g1}, $B1_g$, $A1_g$ and E_{g3} modes of anatase TiO_2, respectively (R. Zhang et al., 2018). In addition, the significant differences of vibration peak among the rGO/TiO_2 nanocomposite samples suggested that increased of crystal defects from GO to rGO transformation and also the difficulties on the thermal reduction control of TiO_2 during hydrothermal process (Shen et al., 2011).

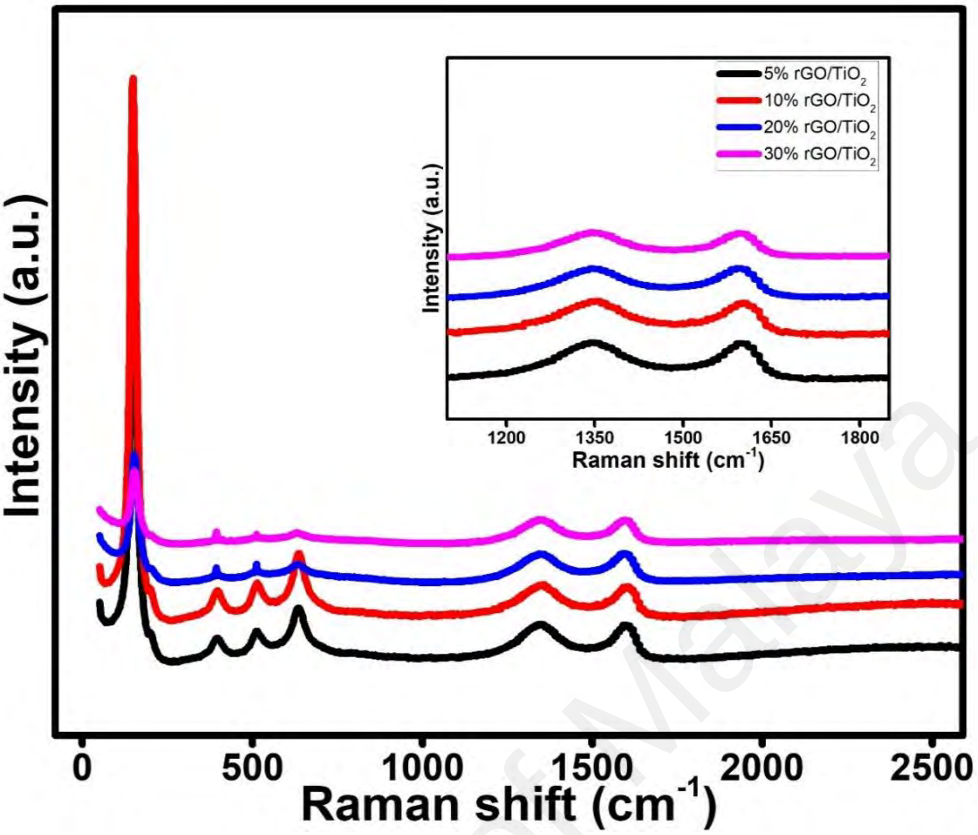

Figure 4.11: Raman spectroscopy of rGO/TiO$_2$ nanocomposites for 5%, 10%, 20%, and 30% with enlarge insert.

4.2.6 BET

The specific surface area and pore size distribution of rGO/TiO_2 nanocomposites were measured and analysed by using Brunauer-Emmett-Teller (BET) instrument. This analysis was performed as critical factors for the determination of supercapacitor performance based on rGO/TiO_2 nanocomposites as the efficient electrodes for a supercapattery system. Figure 4.12 (a-d) present the N_2 adsorption/desorption isotherms of different rGO/TiO_2 nanocomposites. According to IUPAC classification, rGO/TiO_2 nanocomposites displayed typical type IV isotherms accompanied by distinct H_2 type hysteresis loops, suggesting the existence of mesoporous structure (T.-W. Kim & Park, 2017). The BET surface areas of 5%, 10%, 20%, and 30 % rGO/TiO_2 nanocomposites were estimated as 119.3 m^2g^{-1}, 137.2 m^2g^{-1}, 128.1 m^2g^{-1}, and 121.5 m^2g^{-1}, respectively. The recorded BET surface area of 10 % rGO/TiO_2 nanocomposites (137.2 m^2g^{-1}) was slightly greater than the reported surface area of 10 % rGO/TiO_2 nanocomposites (113.0 m^2g^{-1}) (Minella et al., 2017). Besides, the mesoporous features of nanocomposites were further determined by Barrett-Joyner-Halenda (BJH) pore size distribution plotted in Figure 4.12 (e-h). Basically, the BJH is used to determine the pore size distribution of rGO/TiO_2 nanocomposites. Based on understanding, mesoporous nature of pore size was performed in the range of ~2-50 nm (Kumar, Malik, & Purohit, 2018). In fact, the comprehensive work measured that the average pore width of different rGO/TiO_2 nanocomposites was obtained at approximately 7.14-7.19 nm. Hence, the rGO/TiO_2 nanocomposites were mainly mesoporous in structure (Xiao et al., 2016). In contrast, larger specific surface area in 10% rGO/TiO_2 nanocomposites (137.2 m^2g^{-1}) suggested that there were more active sites which facilitated a higher electron transfer kinetics as compared to other composites, and hence enhanced the electron ions transport pathway (Shuhua Yang, Lin, Song, Zhang, & Gao, 2015).

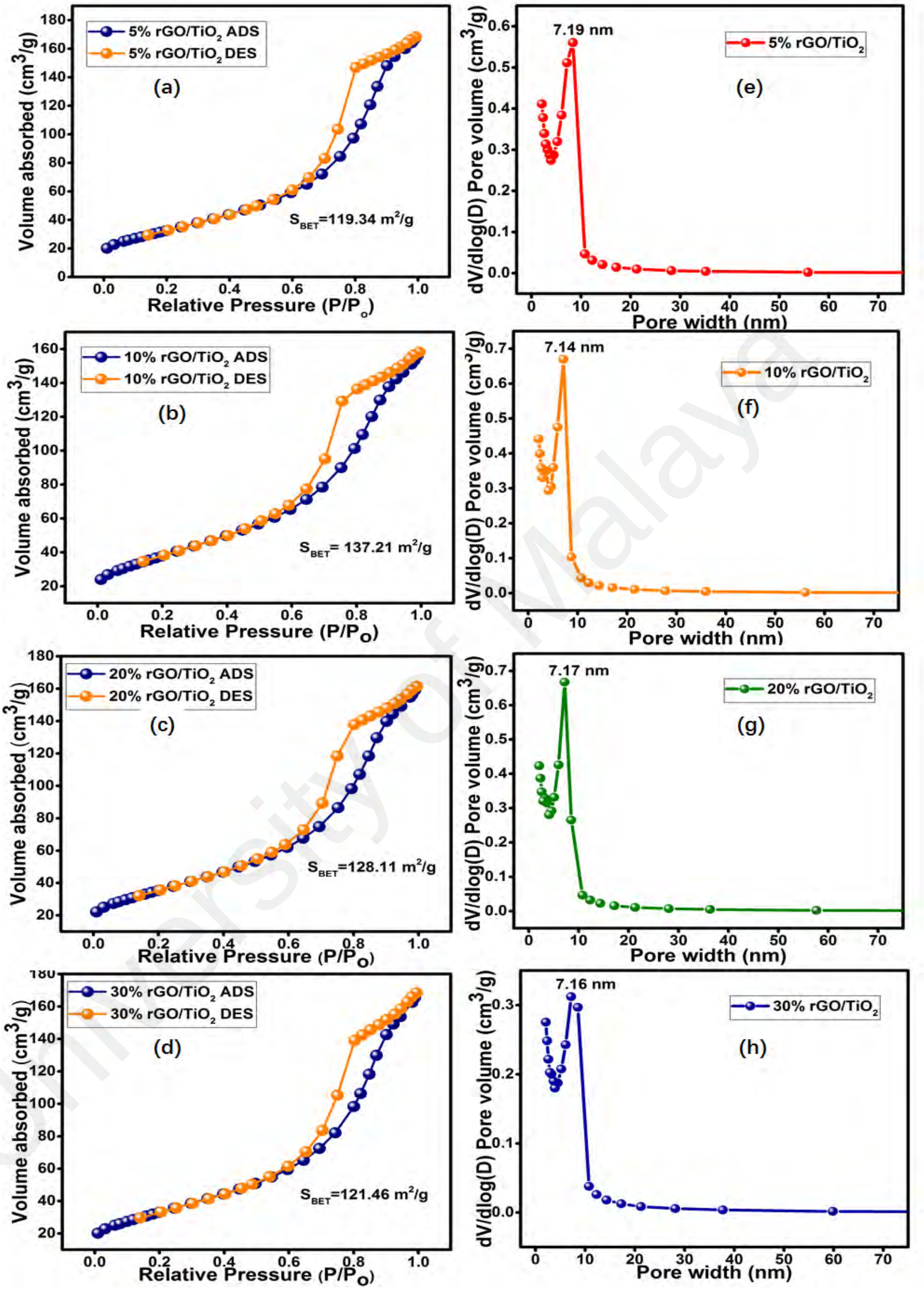

Figure 4.12: (a) – (d) BET surface area of different content of rGO/TiO$_2$ nanocomposites; (e) – (h) Corresponding BJH pore size distribution plots of rGO/TiO$_2$ nanocomposites.

4.2.7 Electrochemistry analysis (Three-electrodes assembly)

4.2.7.1 CV analysis

Electrochemical test, including CV, GCD and EIS, were employed to understand the electrochemical performance of samples. First, the CV curves of GO and rGO were analysed and plotted as shown in Figure 4.13. According to the CV curve, a larger curve of rGO was formed as compared to the GO curve. This suggested that a reduction in hydrothermal process restores electronic conjugation of rGO, enhancing the electrical conductivity and fast electron mobility on electrode surface (Gong, Li, Fu, & Pan, 2015; He & Fang, 2016; Sanchez, Pendashteh, Palma, Anderson, & Marcilla, 2018). The attendance of a stronger electroactivity in rGO would affect rGO/TiO_2 nanocomposites in performing a larger specific capacity performance. The specific capacity value was also measured at the scan rate of 3 mV s^{-1} by using Equation 3.2. The calculated value of rGO electrode was significantly greater than GO electrode, which were 103 C g^{-1} and 74 C g^{-1}, respectively. Therefore, the corporation of rGO could bring positive effect and enhance the capacity values for rGO/TiO_2 nanocomposites.

Electrochemical performance of rGO/TiO_2 nanocomposites were further investigated under a variety of weight percent at different scan rates. These comprehensive works were carried out to obtain the optimum conductivity and capacity performance based on rGO/TiO_2 nanocomposites in supercapattery application. In Figure 4.14 (a-d), CV curves of different % rGO/TiO_2 are collected at a scan rate of 3-50 mV s^{-1} with potential windows ranging from 0 - 0.5 V. All curves in Figure 4.14 (a-d) exhibit a pair of cathodic and anodic peaks addressed to the capacity was exactly referred from a battery faradaic charge storage mechanism of electrodes (Gogotsi & Penner, 2018). The anodic and cathodic peaks were virtually symmetrical over the different scan rates, showing that rGO/TiO_2 electrode exhibits good reversibility of the redox reaction. This resulted in the redox peaks of rGO/TiO_2 being attributed to Faradaic redox reactions of Ti^{4+} and Ti^{3+}, according to Equation 4.3 (Z. Yang et al., 2009):

$$\mathrm{Ti\ (IV)} + \mathrm{e}^- \Leftrightarrow \mathrm{Ti(II)} + 2\mathrm{e}^- \qquad \text{Eq 4.3}$$

As the scan rate is augmented, the anode and cathode peaks will move towards higher and lower potentials, respectively. The phenomenon resulted in an enhanced electric polarization and potential kinetic irreversibility of electrolyte ions access to electrode interfaces (Xia, Tu, Wang, Gu, & Zhao, 2011).

Figure 4.15 shows specific capacity value of different % rGO/TiO_2 nanocomposites at a scan rate of 3 mV s^{-1}. The values of specific capacity for 5%, 10%, 20%, and 30% of rGO/TiO_2 nanocomposites electrodes were calculated at a scan rate of 3 mV s^{-1} at 209, 331, 325, and 257 C g^{-1}, respectively. The highest value obtained for 10% rGO/TiO_2 nanocomposites, as the best capacitive behavior, suggested that increased specific capacity may attribute to the hierarchical structure and large surface area of rGO/TiO_2 nanocomposites, allowing easy penetration of electrolyte into the electrode interface (Ping, Gong, Fu, & Pan, 2017). In addition, the faradaic behavior produced from redox reaction of TiO_2 nanocrystals could further improve the specific capacity. Meanwhile, rGO could provide conductive pathways, facilitating electron transfer within the electrodes (Mondal, Maiti, Singha, Mahanty, & Panda, 2017; Y. Xie, Song, Zhou, Ling, & Wu, 2016).

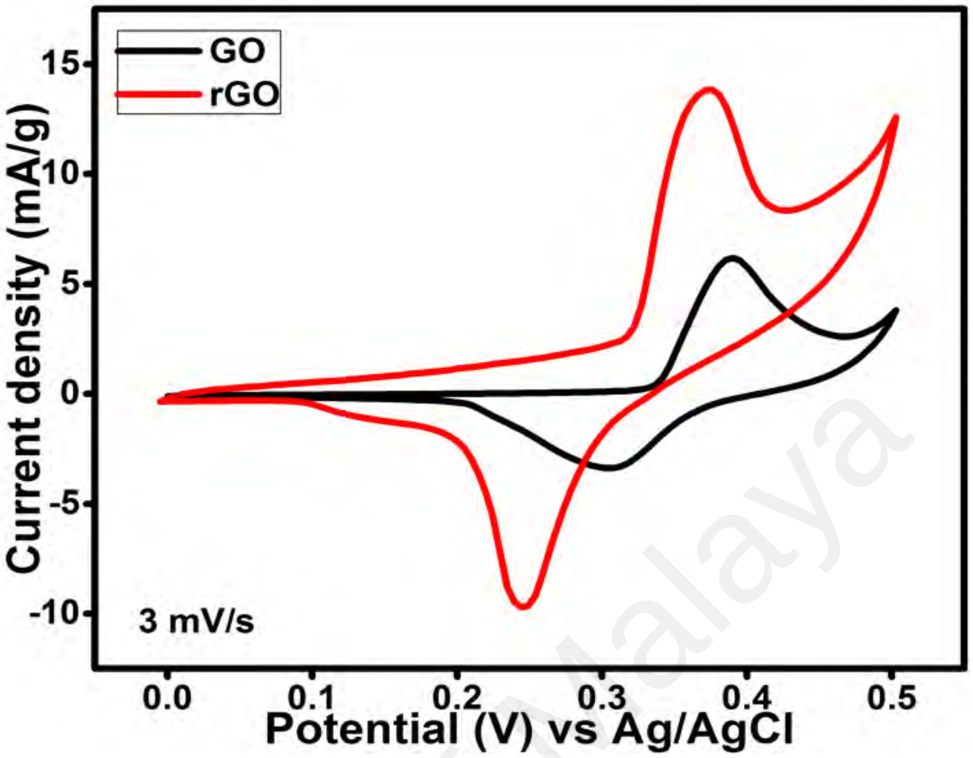

Figure 4.13: CV curves for GO and rGO electrodes at a scan rate of 3 mV s^{-1}.

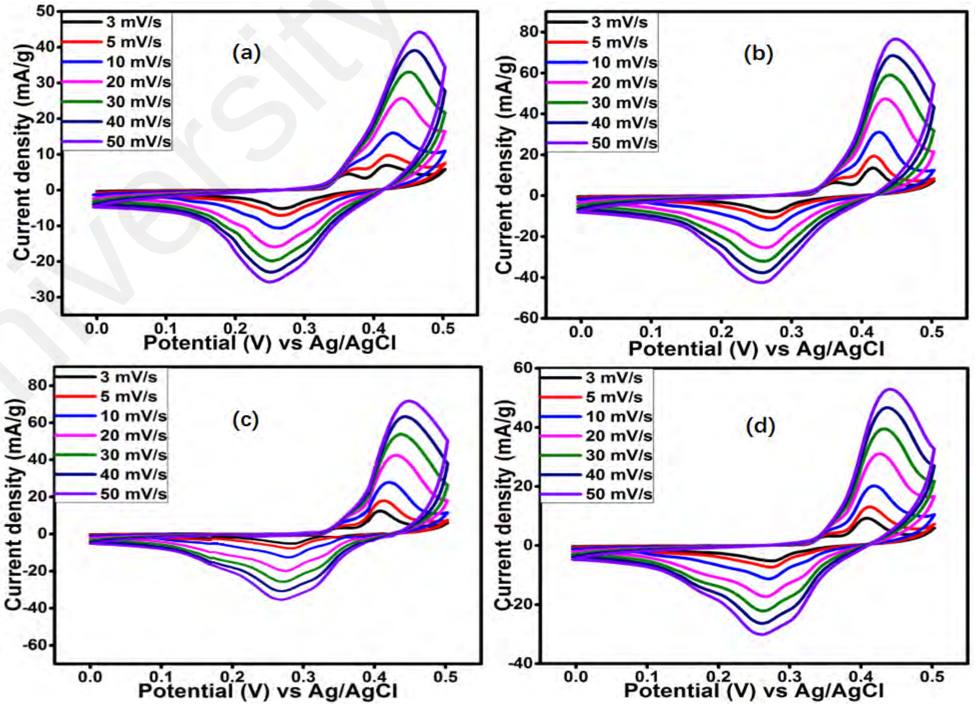

Figure 4.14: CV curves at different scan rates based rGO/TiO_2 nanocomposites electrode of (a) 5%, (b) 10%, (c) 20%, and (d) 30%

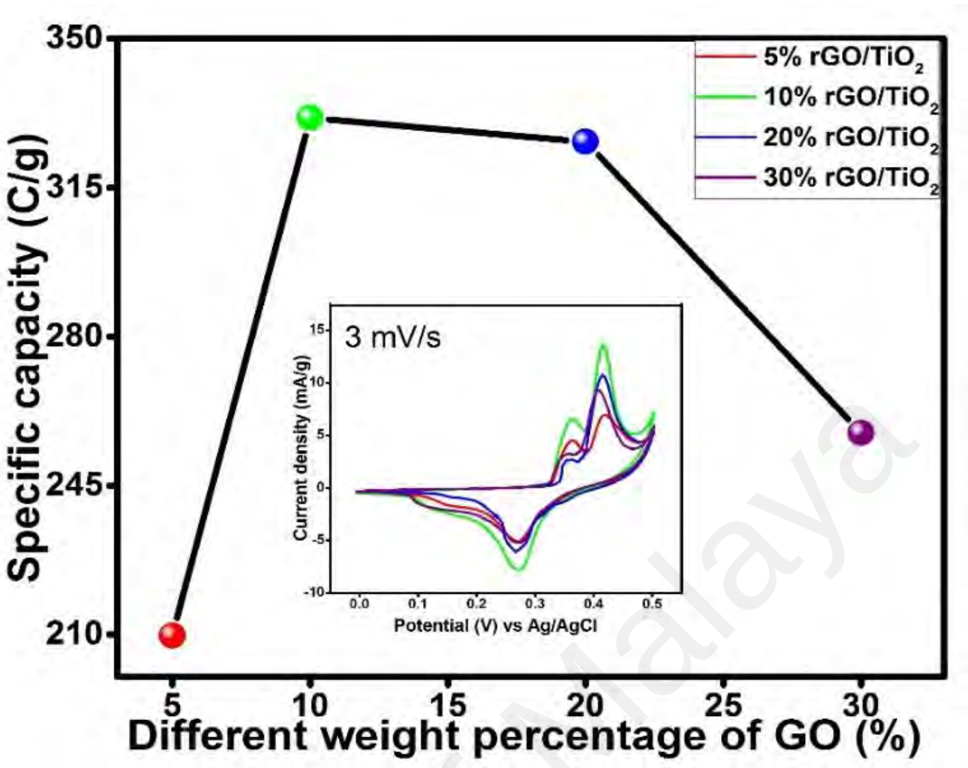

Figure 4.15: Specific capacity values against different % rGO/TiO_2 nanocomposites at a scan rate of 3 mV s^{-1}

4.2.7.2 GCD analysis

GCD analysis was done to study the influences of GO and GO reduction byproducts (rGO) on supercapacitor performance, charge and discharge to analyse the real applicability of the GO and rGO electrodes. In Figure 4.16, the specific capacity value exhibited by the GO electrode was 23.40 C g^{-1} at 0.2 A g^{-1}. The calculated result reflected a poor electrochemical performance. The specific capacity was significantly improved from 23.40 C g^{-1} to 34.20 C g^{-1}, while by using rGO electrode, as shown in Figure 4.16. Therefore, the improved specific capacity had resulted from high intercalation and dispersion of TiO_2 on rGO matrix for electrochemical performance.

Next, different weight percentage of GO incorporated with TiO_2, was identified to determine the optimum specific capacity value for electrochemical performance. Figure 4.17 (a-d) show the GCD plot of different weight percentages of rGO/TiO_2 nanocomposites, which were completely recorded in various current densities from 0.2 A g^{-1} to 1.0 A g^{-1} under a potential range between 0 - 0.42 V. Figure 4.17 (a-d) clearly display that charge-discharge plateaus, suggesting dominance in battery-type faradic behavior of the fabricated composite (Z. Gao et al., 2019). However, Figure 4.18 (a) shows the specific capacity values of rGO/TiO_2 electrode with different loading amounts of GO under various current densities. As a result, an increase in charge/discharge current densities gradually decreased the discharge time due to its limited available duration for ion diffusion through electrodes at higher current densities (W.-w. Liu, Yan, & Xue, 2013; Yao et al., 2018). Apart from that, Figure 4.18 (b) also shows the specific capacity values for as-prepared rGO and several rGO/TiO_2 nanocomposites samples with different content of GO at the current density of 0.2 A g^{-1}. The rGO, 5%, 10%, 20%, and 30% of rGO/TiO_2 nanocomposites corresponded to the calculated specific capacity values of

34.2, 72.50, 116.70, 85.80, and 39.77 C g^{-1}, respectively. This occurrence clearly showed that the specific capacity values of rGO/TiO_2 electrodes performed more efficiently than rGO electrodes. In this manner, it is owing to the incorporation of rGO into TiO_2 which could enhance the electrical properties of TiO_2 and secure the charge transfer pathways (Rajagopal & Ryu, 2018).

Furthermore, Figure 4.18 (b) illustrates that the 10% of rGO incorporated into TiO_2 sample exhibited the highest specific capacity with specific areas as compared to other samples, resulting in more active surface sites. However, lesser electrochemical capacitive value of rGO/TiO_2 was observed with excessive GO loading of 20% and above, resulting a decline in the specific surface area, which limits OH- ion diffusion into the electrode surface (Krishnan, Harilal, Yar, et al., 2017; Y. Xie et al., 2016). As a result, the optimized amount of GO with 10% loading to the TiO_2 was categorized as an efficient electrode for the electrochemical performance study (B. Wang et al., 2017).

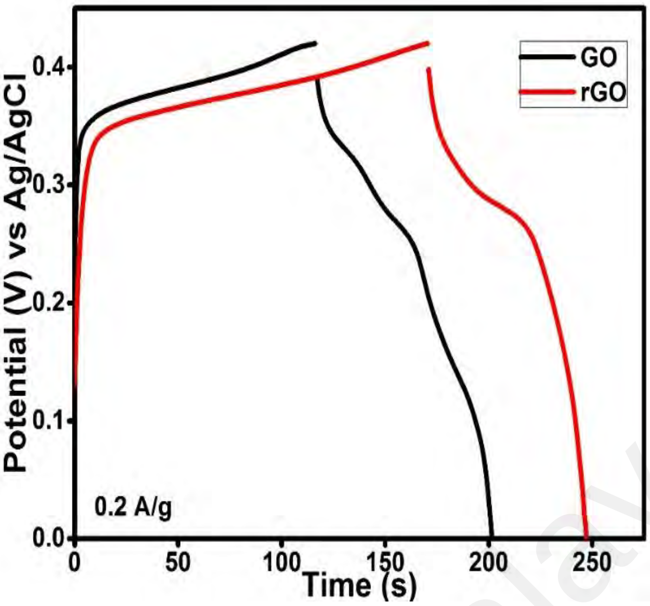

Figure 4.16: GCD curves of GO and rGO electrode at constant current density of 0.2 A g^{-1} under potential range between 0 - 0.42 V.

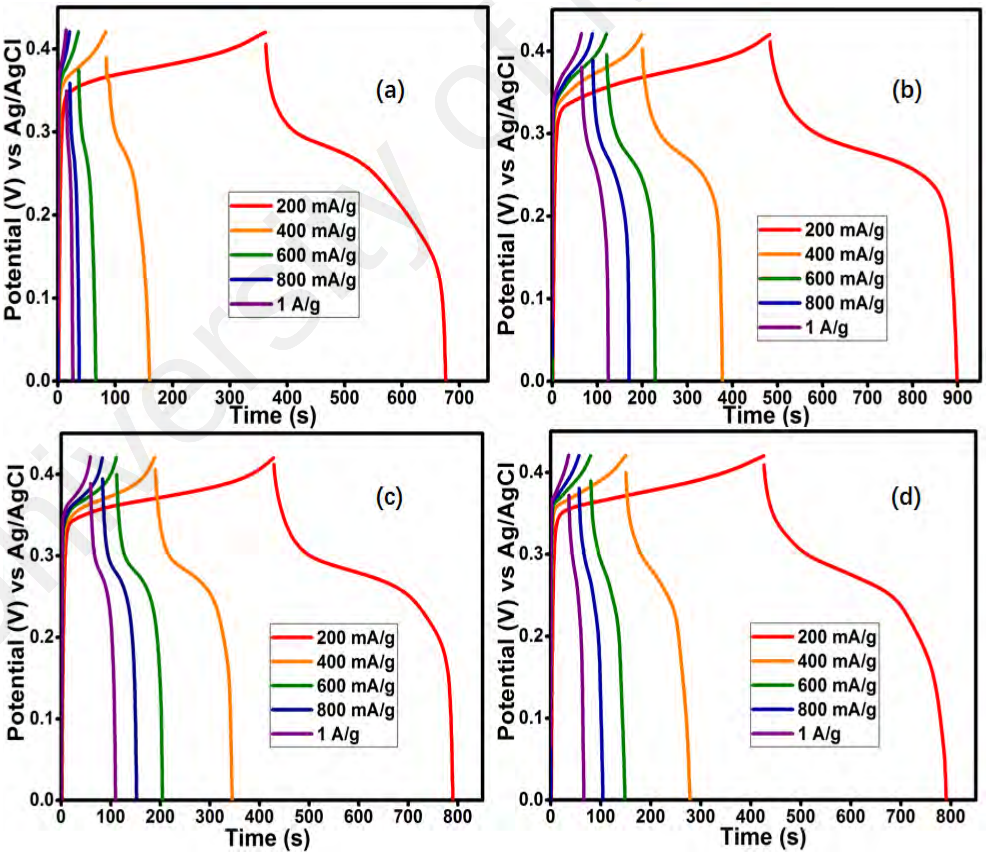

Figure 4.17: GCD curves of rGO/TiO_2 electrode at different current densities under potential range between 0 - 0.42 V for rGO/TiO_2 nanocomposites of (a) 5%, (b)10%, (c) 20%, and (d) 30%.

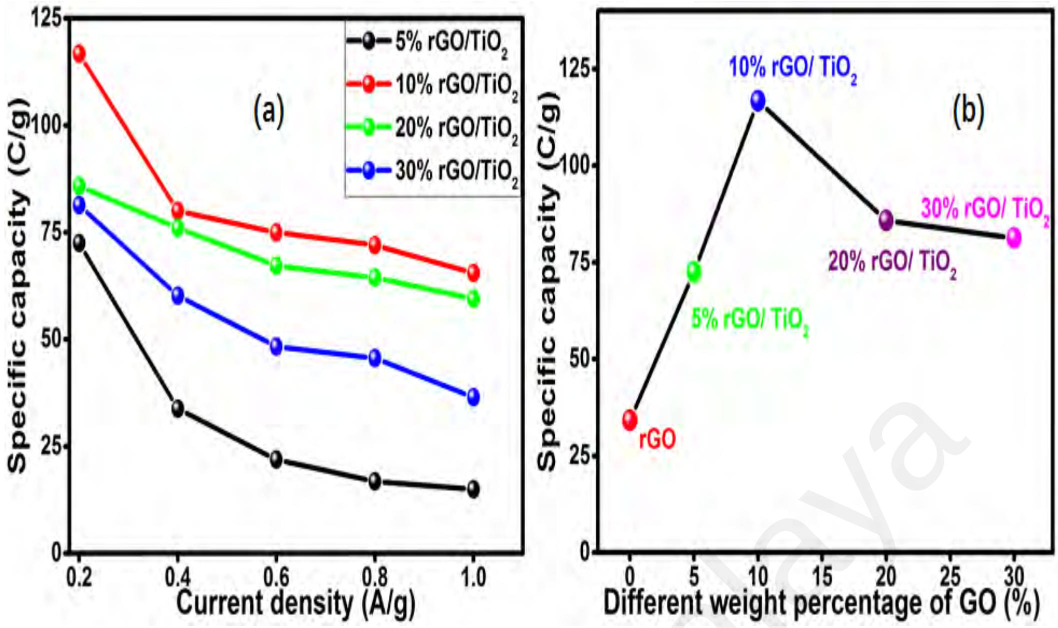

Figure 4.18: (a) The specific capacity value of different rGO/TiO_2 nanocomposites at 0.2 - 1.0 A g^{-1} (b) Comparison of specific capacity values with respect to rGO and different GO loading amount incorporated with TiO_2.

4.2.7.3 EIS analysis

EIS analysis was used to characterize the interfacial electrical properties and potentiality of rGO/TiO_2 nanocomposite electrode as a supercapattery device (Ramadoss & Kim, 2013). EIS reading was recorded between 0.01 - 100 kHz frequency range. Figure 4.19 demonstrates the Nyquist plot of rGO and 10% – 50% rGO/TiO_2 nanocomposites electrodes. Nyquist plots in Figure 4.19 comprise the measured charge transfer resistance (R_{ct}). Basically, the R_{ct} consisted of resistance from KOH electrolyte, the contact resistance at the interface between the nickel foam and electrode material, and intrinsic resistance of electrode material (Heng et al., 2019). Therefore, the calculated R_{ct} values for rGO, 5%, 10%, 20%, and 30% rGO/TiO_2 nanocomposites electrodes were 40, 16.45, 9.84, 10.15, and 14.08 Ω, respectively. Interestingly, rGO electrode exhibited the highest charge transfer/interior resistance as compared to other samples. Therefore, a considerable reduction in resistance and perform well with rGO material after formation with TiO_2. Nevertheless, the smallest R_{ct} value of 10% rGO/TiO_2 nanocomposites (9.84 Ω) was accredited to the rGO to entertain as a conducting/catalyst agent to enhance the electrical conductivity of electrode and also influence the charge carriers in electrochemical performance. In spite of that, well-dispersed TiO_2 and decrease in rGO restacking/defect could establish an efficient electrochemical performance (W. Guo et al., 2017). Finally, 10% rGO/TiO_2 electrode possessed the best capacitive characteristic for fast electron transfer throughout the entire electrodes.

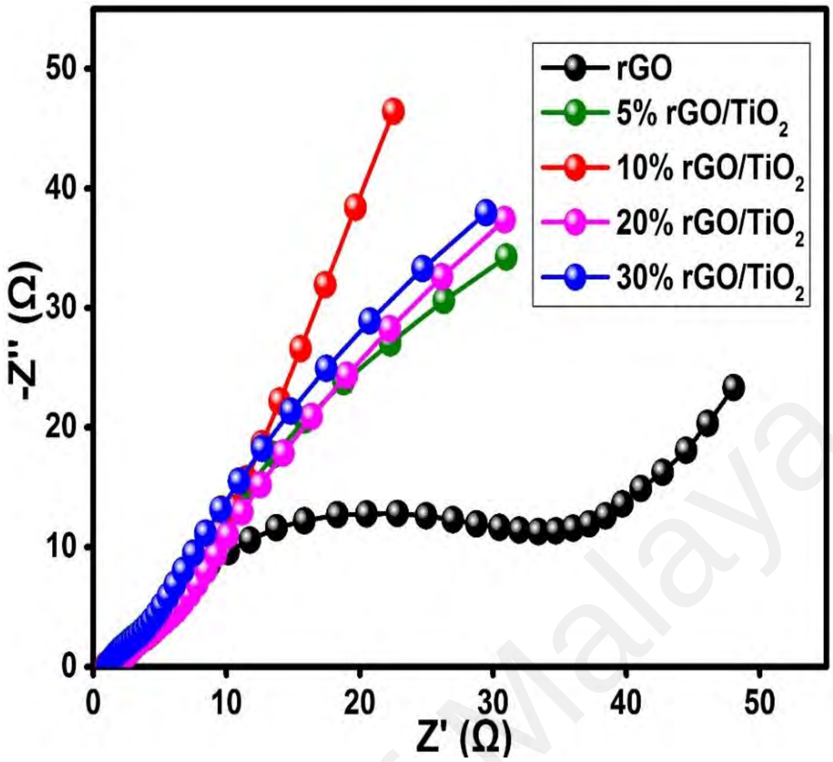

Figure 4.19: Nyquist plot of different rGO/TiO_2 nanocomposites electrodes.

4.2.3 Electrochemistry analysis (Two-electrodes assembly)

Considering the good battery-like electrode, 10% rGO/TiO_2 nanocomposites were further assembled as anode, whereas activated carbon (AC) as cathode for supercapattery application and relatively evaluated its practical field. The CV curves in Figure 4.20 (a) display the CV curves of 10% rGO/TiO_2 nanocomposites electrode with distinct peaks due to the redox reaction of TiO_2, whereas AC electrode illustrates a rectangular CV curve. The CV curves indicate the presence of both battery-like and capacitive reactions which take place in a supercapattery.

Figure 4.20 (b) illustrates CV curves of AC and 10% rGO/TiO_2 nanocomposites electrodes at a scan rate of 20 mV s^{-1}. Based on the CV curves in Figure 4.20 (b), the voltage window of the supercapattery could be enlarged as 0-1.45V. Figure 4.20 (c) shows the GCD plot of the fabricated supercapattery device operated at different current densities. The specific capacity values tested by GCD test are shown in Figure 4.20 (d). The corresponding specific capacity values calculated by using Equation 3.3 were 186.2 C g^{-1}, 165.0 C g^{-1}, 140.0 C g^{-1}, and 120.0 C g^{-1} at 0.4 A g^{-1}, 0.5 A g^{-1}, 1 A g^{-1}, and 2 A g^{-1}, respectively.

To evaluate the stability of supercapattery, GCD cycles were repeated at 3000 cycles. The cycling stability of 10% rGO/TiO_2/AC interfaces-based supercapattery was performed at a current density of 1 A g^{-1}, based on Figure 4.21. As shown in Figure 4.21, the capacity retention was gradually dropped and finally maintained at 92% of its initial value after 3000 cycles, and possessed a superior cycling stability of supercapattery. According to Equation 3.4 and Equation 3.5, a supercapattery achieved a maximum energy density of 54.37 Wh kg^{-1} at power density of 420.48 W kg^{-1}. The reported energy density value was higher than the other reported nanocomposites-based supercapatteries, such as CN-rGO//rGO (42.9 Wh kg^{-1} at 393 W kg^{-1}) (Z. Gao et al., 2019).; CNCS/TNA//AC (45.5 Wh kg^{-1} at 400.5 W kg^{-1}); MnS/rGO//AC (37.9 Wh kg^{-1} at 1500 W kg^{-1}) (X. Xu et al., 2018) and rGO-TiO$_2$//AC(42 Wh kg^{-1} at 800W kg^{-1}) (H. Kim et al., 2013).

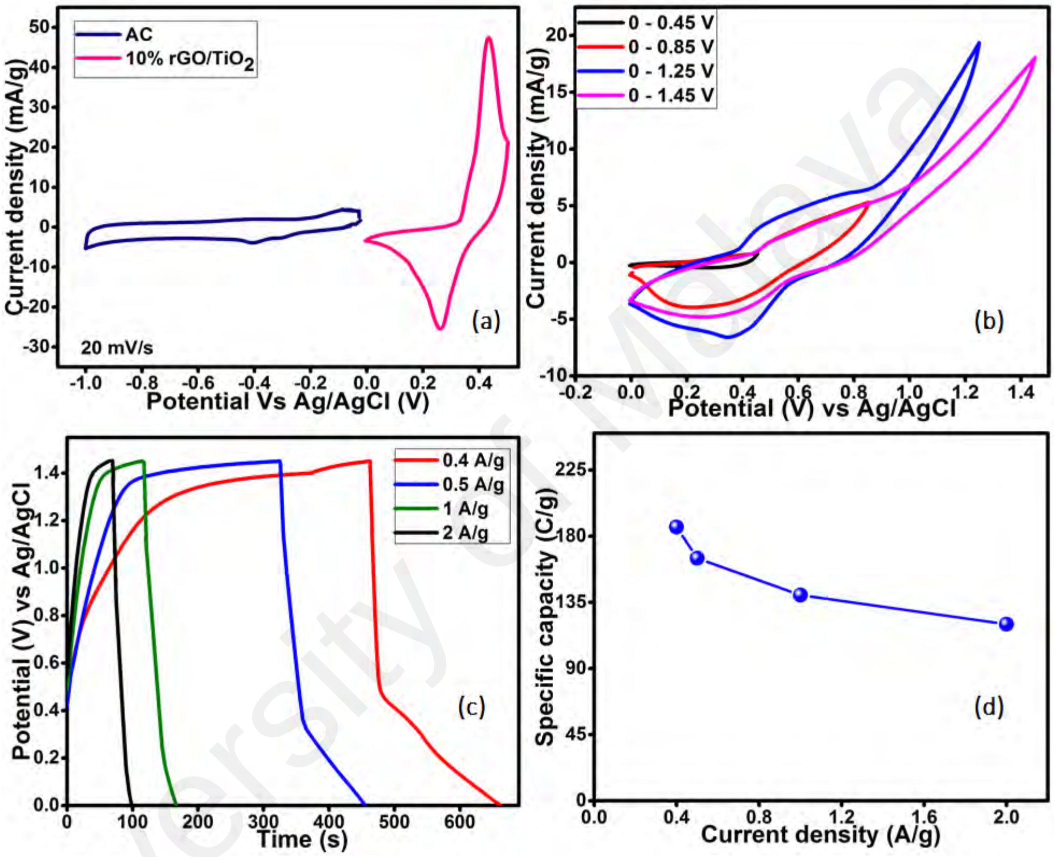

Figure 4.20: (a) CV curves of AC and rGO/TiO$_2$ electrodes at the scan rate of 20 mV s^{-1}, (b) CV curves of supercapattery measured at different voltage potential at a scan rate of 20 mV s^{-1}, (c) GCD plot of a supercapattery, and (d) Specific capacity value of supercapattery at different current densities.

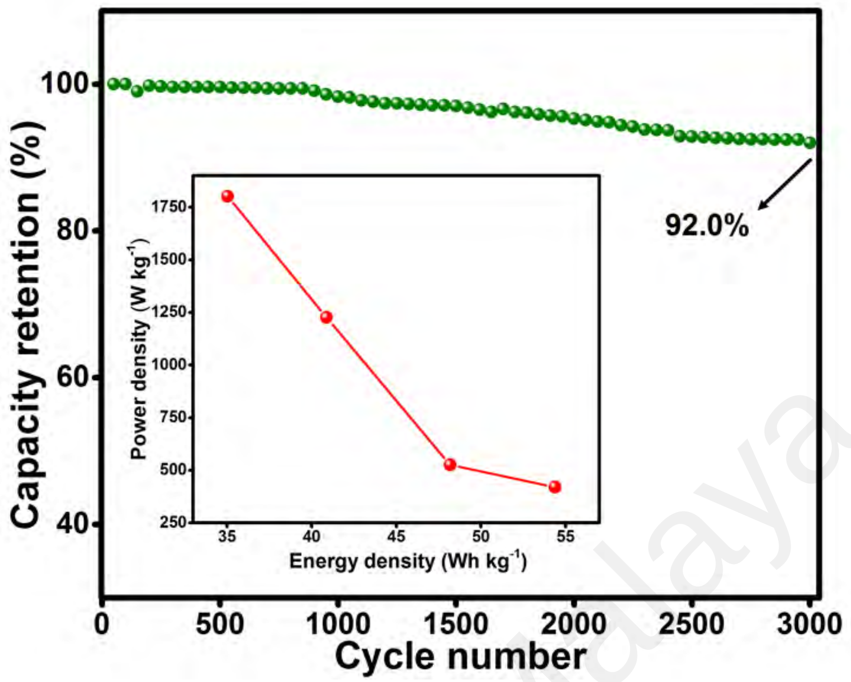

Figure 4.21: Cycling stability of supercapattery with insert of ragone plot.

CHAPTER 5: CONCLUSION

5.1 Conclusion

With the aim of studying the phase transition and electrochemical characteristics of TiO_2 nanocrystals synthesized by the peroxo sol gel method, intermediate phase of amorphous and anatase of TiO_2 nanocrystals with diameter 12 nm calcined at low temperature 200 ºC exhibited the highest capacity. The main reason is attributed to increase of calcination temperature which transformed the structure of TiO_2 nanocrystals from amorphous to crystalline at the same time increasing the particles size. Besides that, the fine crystallites of as prepared TiO_2 nanocrystals and TiO_2 calcined at 200 ºC with smaller particle size enabled faster interaction between electrode and electrolyte, resulting in higher electrochemical active sites and consequently enhanced the electrochemical performance. Calcination temperature affects the crystallinity of the TiO_2 nanocrystals, particle size and electrochemical performance. In short, TiO_2 nanocrystals calcined at 200 ºC possesses excellent electrochemical performance.

The sol-gel hydrothermal process of rGO/TiO_2 nanocomposites for supercapacitor application was successfully achieved. Throughout this method, GO could be reduced into rGO without any toxicity from the reducing agent. In the same time, TiO_2 has the ability to transform into the anatase phase from its original phase (rutile phase). In short, this facile hydrothermal method provided a green and environmental friendly process for rGO/TiO_2 nanocomposites formation. In the analysis part, the effects of GO loading in rGO/TiO_2 nanocomposite found that a suitable amount of rGO led to an increased efficiency in supercapacitor application. A 10% rGO/TiO_2 nanocomposites electrode exhibited a maximum specific capacity of 116.70 C g^{-1} in 1M KOH electrolyte at the current density of 0.2 A g^{-1} for electrochemical performance. Finally, a current density of

1 A g^{-1} was obtained from the cycling stability test based on 10% rGO/TiO_2//AC interface electrodes and the capacitance potential remained up to 92% after 3000 cycles for supercapattery performance, resulting in an efficient charge transfer performance.

5.2 Recommendation for future research

To comply with future needs regards to development of energy storage green devices, several perspectives and suggestions were proposed as follows:

(1) Ternary composite composed of multicomponent materials are foreseen as remarkable electrode materials with synergistic electrochemical properties. Therefore, the suggested materials like silver, manganese oxide or ferric oxide are added to form ternary composites with rGO/TiO_2 supercapacitor electrode. Incorporation of redox electroactive materials into rGO/TiO_2 electrodes could provide additional capacitance. Meanwhile, metal oxides hinder the restacking of rGO nanosheets and preserve the good properties of rGO.

(2) Increasing the potential window of the cell by using organic electrolyte, ionic liquid or combination of organic electrolyte and ionic liquid, which can expand the potential window up to 3.5-4 V. Besides that, combination of ionic liquid and organic electrolyte could realize safety issue due to low volatility and high thermal stability of ionic liquid.

(3) Using redox additive electrolyte is a cost-effective and user-friendly way to enhance the electrochemical performance. Small size of redox additive exhibit higher diffusion rate and able to gain and loss of electrons. Besides that, electrode can store extra energy from the redox reaction of redox additives within the electrode surface and electrolyte. Redox additives suggested such as potassium iodide, methylene blue, indigo carmine, hydroquinone and phenylenediamine that could increase specific capacitance of rGO/TiO_2 electrodes.

REFERENCES

Abdollahifar, M., Huang, S.-S., Lin, Y.-H., Lin, Y.-C., Shih, B.-Y., Sheu, H.-S., Liao, Y.-F., & Wu, N.-L. (2018). High-performance carbon-coated $ZnMn_2O_4$ nanocrystallite supercapacitors with tailored microstructures enabled by a novel solution combustion method. *Journal of Power Sources, 378*, 90-97.

Agharezaei, P., Abdizadeh, H., & Golobostanfard, M. R. (2018). Flexible supercapacitor electrodes based on TiO_2/rGO/TiO_2 sandwich type hybrids. *Ceramics International, 44*(4), 4132-4141.

Akhavan, O., Ghaderi, E., Aghayee, S., Fereydooni, Y., & Talebi, A. (2012). The use of a glucose-reduced graphene oxide suspension for photothermal cancer therapy. *Journal of Materials Chemistry, 22*(27), 13773-13781.

Akhavan, O., Kalaee, M., Alavi, Z., Ghiasi, S., & Esfandiar, A. (2012). Increasing the antioxidant activity of green tea polyphenols in the presence of iron for the reduction of graphene oxide. *Carbon, 50*(8), 3015-3025.

Ali, R., Daut, I., & Taib, S. (2012). A review on existing and future energy sources for electrical power generation in Malaysia. *Renewable and Sustainable Energy Reviews, 16*(6), 4047-4055.

Ammam, M. (2012). Electrophoretic deposition under modulated electric fields: a review. *RSC Advances, 2*(20), 7633-7646.

Ashnani, M. H. M., Johari, A., Hashim, H., & Hasani, E. (2014). A source of renewable energy in Malaysia, why biodiesel? *Renewable and Sustainable Energy Reviews, 35*, 244-257.

Augustyn, V., Simon, P., & Dunn, B. (2014). Pseudocapacitive oxide materials for high-rate electrochemical energy storage. *Energy & Environmental Science, 7*(5), 1597-1614.

Bao, W., Miao, F., Chen, Z., Zhang, H., Jang, W., Dames, C., & Lau, C. N. (2009). Controlled ripple texturing of suspended graphene and ultrathin graphite membranes. *Nature nanotechnology, 4*(9), 562.

Brodie, B. (1860). Sur le poids atomique du graphite. *Ann. Chim. Phys, 59*(466), e472.

Brousse, T., Bélanger, D., & Long, J. W. (2015). To be or not to be pseudocapacitive? *Journal of the Electrochemical Society, 162*(5), A5185-A5189.

Cao, Y., Lin, B., Sun, Y., Yang, H., & Zhang, X. (2015). Symmetric/Asymmetric Supercapacitor Based on the Perovskite-type Lanthanum Cobaltate Nanofibers with Sr-substitution. *Electrochimica Acta, 178*, 398-406.

Chang, Y.-C., Lee, C.-Y., & Chiu, H.-T. (2013). Porous inorganic materials from living porogens: channel-like TiO_2 from yeast-assisted sol–gel process. *ACS applied materials & interfaces, 6*(1), 31-35.

Chen, H., Guo, Y.-c., Wang, F., Wang, G., Qi, P.-r., Guo, X.-h., Dai, B., & Yu, F. (2018). An activated carbon derived from tobacco waste for use as a supercapacitor electrode material. *Carbon, 130*, 848.

Chen, J., Wang, Y., Cao, J., Liu, Y., Ouyang, J.-H., Jia, D., & Zhou, Y. (2015). Flexible and solid-state asymmetric supercapacitor based on ternary graphene/MnO_2/carbon black hybrid film with high power performance. *Electrochimica Acta, 182*, 861-870.

Chen, L., Xu, Z., Li, J., Min, C., Liu, L., Song, X., Chen, G., & Meng, X. (2011). Reduction and disorder in graphene oxide induced by electron-beam irradiation. *Materials Letters, 65*(8), 1229-1230.

Chen, Z., Gao, Y., Zhang, Q., Li, L., Ma, P., Xing, B., Cao, J., Sun, G., Bala, H., & Zhang, C. (2019). TiO_2/NiO/reduced graphene oxide nanocomposites as anode materials for high-performance lithium ion batteries. *Journal of Alloys and Compounds,* *774*, 873-878.

Conway, B. E. (2013). *Electrochemical supercapacitors: scientific fundamentals and technological applications*: Springer Science & Business Media.

Dai, C., Wan, J., Yang, J., Qu, S., Jin, T., Ma, F., & Shao, J. (2018). H_3PO_4 solution hydrothermal carbonization combined with KOH activation to prepare argy wormwood-based porous carbon for high-performance supercapacitors. *Applied Surface Science, 444*, 105-117.

Danks, A., Hall, S., & Schnepp, Z. (2016). The evolution of 'sol–gel'chemistry as a technique for materials synthesis. *Materials Horizons, 3*(2), 91-112.

Dong, H., Wang, A., & Koenig, G. M. (2018). Role of coprecipitation and calcination of precursors on phase homogeneity and electrochemical properties of battery active materials. *Powder Technology, 335*, 137-146.

Dong, L., Li, M., Zhao, M., Feng, J., Han, Y., Deng, J., Li, X., Li, D., & Sun, X. (2014). Hydrothermal synthesis of mixed crystal phases TiO_2–reduced graphene oxide nanocomposites with small particle size for lithium ion batteries. *international journal of hydrogen energy, 39*(28), 16116-16122.

Down, M. P., Rowley-Neale, S. J., Smith, G. C., & Banks, C. E. (2018). Fabrication of Graphene Oxide Supercapacitor Devices. *ACS Applied Energy Materials, 1*(2), 707-714.

Etacheri, V., Seery, M. K., Hinder, S. J., & Pillai, S. C. (2011). Oxygen rich titania: A dopant free, high temperature stable, and visible‐light active anatase photocatalyst. *Advanced Functional Materials, 21*(19), 3744-3752.

Fabregat-Santiago, F., Barea, E. M., Bisquert, J., Mor, G. K., Shankar, K., & Grimes, C. A. (2008). High carrier density and capacitance in TiO_2 nanotube arrays induced by electrochemical doping. *Journal of the American Chemical Society, 130*(34), 11312-11316.

Feng, J.-M., Dong, L., Han, Y., Li, X.-F., & Li, D.-J. (2016). Facile synthesis of graphene-titanium dioxide nanocomposites as anode materials for Na-ion batteries. *International Journal of Hydrogen Energy, 41*(1), 355-360.

Fic, K., Platek, A., Piwek, J., & Frackowiak, E. (2018). Sustainable materials for electrochemical capacitors. *Materials Today*.

Fu, Y., Wei, Q., Wang, X., Shu, H., Yang, X., & Sun, S. (2015). Porous hollow α-Fe_2O_3@ TiO_2 core–shell nanospheres for superior lithium/sodium storage capability. *Journal of Materials Chemistry A, 3*(26), 13807-13818.

Galiński, M., Lewandowski, A., & Stępniak, I. (2006). Ionic liquids as electrolytes. *Electrochimica Acta, 51*(26), 5567-5580.

Gao, Y., Masuda, Y., & Koumoto, K. (2004). Micropatterning of TiO_2 thin film in an aqueous peroxotitanate solution. *Chemistry of materials, 16*(6), 1062-1067.

Gao, Z., Wang, Z., Chang, J., Chen, L., Wu, D., Xu, F., Wang, X., & Jiang, K. (2019). Micelles directed preparation of ternary cobalt hydroxide carbonate-nickel hydroxide-reduced graphene oxide composite porous nanowire arrays with superior faradic capacitance performance. *Journal of colloid and interface science, 534*, 563-573.

Ge, L., Xu, M., & Sun, M. (2006). Synthesis and characterization of TiO_2 photocatalytic thin films prepared from refluxed PTA sols. *Materials Letters, 60*(2), 287-290.

Ghamsari, M. S., Radiman, S., Hamid, M. A. A., Mahshid, S., & Rahmani, S. (2013). Room temperature synthesis of highly crystalline TiO_2 nanoparticles. *Materials Letters, 92*, 287-290.

Ghorbani, M., Abdizadeh, H., & Golobostanfard, M. (2015). Reduction of graphene oxide via modified hydrothermal method. *Procedia Materials Science, 11*, 326-330.

Gogotsi, Y., & Penner, R. M. (2018). Energy Storage in Nanomaterials–Capacitive, Pseudocapacitive, or Battery-like? : ACS Publications.

Gong, Y., Li, D., Fu, Q., & Pan, C. (2015). Influence of graphene microstructures on electrochemical performance for supercapacitors. *Progress in Natural Science: Materials International, 25*(5), 379-385.

Gu, C., Ge, X., Wang, X., & Tu, J. (2015). Cation–anion double hydrolysis derived layered single metal hydroxide superstructures for boosted supercapacitive energy storage. *Journal of Materials Chemistry A, 3*(27), 14228-14238.

Guo, P., Song, H., & Chen, X. (2009). Electrochemical performance of graphene nanosheets as anode material for lithium-ion batteries. *Electrochemistry Communications, 11*(6), 1320-1324.

Guo, W., Li, Y., Tang, Y., Chen, S., Liu, Z., Wang, L., Zhao, Y., & Gao, F. (2017). TiO_2 nanowire arrays on titanium substrate as a novel binder-free negative electrode for asymmetric supercapacitor. *Electrochimica Acta, 229*, 197-207.

Hamid, S. B. A., Tan, T. L., Lai, C. W., & Samsudin, E. M. (2014). Multiwalled carbon nanotube/TiO_2 nanocomposite as a highly active photocatalyst for photodegradation of Reactive Black 5 dye. *Chinese Journal of Catalysis, 35*(12).

He, J., & Fang, L. (2016). Controllable synthesis of reduced graphene oxide. *Current Applied Physics, 16*(9), 1152-1158.

Heimböckel, R., Kraas, S., Hoffmann, F., & Fröba, M. (2018). Increase of porosity by combining semi-carbonization and KOH activation of formaldehyde resins to prepare high surface area carbons for supercapacitor applications. *Applied Surface Science, 427*, 1055-1064.

Heng, I., Lai, C. W., Juan, J. C., Numan, A., Iqbal, J., & Teo, E. Y. L. (2018). Low-temperature synthesis of TiO_2 nanocrystals for high performance electrochemical supercapacitors. *Ceramics International*.

Heng, I., Lai, C. W., Juan, J. C., Numan, A., Iqbal, J., & Teo, E. Y. L. (2019). Low-temperature synthesis of TiO_2 nanocrystals for high performance electrochemical supercapacitors. *Ceramics International, 45*(4), 4990-5000.

Hosseinpour, A., Abdizadeh, H., & Golobostanfard, M. R. (2017). Comparing the electrophoretic deposition process of graphene oxides synthesized through different methods. *Thin Solid Films, 631*, 118-123.

Huang, K., Yan, C., Wang, K., Zhang, Y., & Ju, Z. (2016). Phases hybriding and graphene-like TiO2 for high-performance Na-ion batteries. *Journal of Alloys and Compounds, 687*, 683-688.

Hummers Jr, W. S., & Offeman, R. E. (1958). Preparation of graphitic oxide. *Journal of the American Chemical Society, 80*(6), 1339-1339.

Iqbal, J., Numan, A., Rafique, S., Jafer, R., Mohamad, S., Ramesh, K., & Ramesh, S. (2018). High performance supercapattery incorporating ternary nanocomposite of multiwalled carbon nanotubes decorated with Co_3O_4 nanograins and silver nanoparticles as electrode material. *Electrochimica Acta, 278*, 72-82.

Jagadale, A. D., Guan, G., Li, X., Du, X., Ma, X., Hao, X., & Abudula, A. (2016). Ultrathin nanoflakes of cobalt–manganese layered double hydroxide with high reversibility for asymmetric supercapacitor. *Journal of Power Sources, 306*, 526-534.

Jahromi, S. P., Pandikumar, A., Goh, B. T., Lim, Y. S., Basirun, W. J., Lim, H. N., & Huang, N. M. (2015). Influence of particle size on performance of a nickel oxide nanoparticle-based supercapacitor. *RSC Advances, 5*(18), 14010-14019.

Jiang, L.-l., Lu, X., Xie, C.-m., Wan, G.-j., Zhang, H.-p., & Youhong, T. (2015). Flexible, free-standing TiO_2–graphene–polypyrrole composite films as electrodes for supercapacitors. *The Journal of Physical Chemistry C, 119*(8), 3903-3910.

Jiao, Y., Pei, J., Yan, C., Chen, D., Hu, Y., & Chen, G. (2016). Layered nickel metal–organic framework for high performance alkaline battery-supercapacitor hybrid devices. *Journal of Materials Chemistry A, 4*(34), 13344-13351.

Jung, H., Wang, H., & Hu, T. (2014). Control design for robust tracking and smooth transition in power systems with battery/supercapacitor hybrid energy storage devices. *Journal of Power Sources, 267*, 566-575.

Kanezaki, E., Sakamoto, T., Ookubo, A., & Ooi, K. (1992). Solid-state chemistry of thermally induced yellow colouring in synthetic hydrous titanium oxide from $TiCl_3$. *Journal of the Chemical Society, Faraday Transactions, 88*(24), 3583-3586.

Kate, R. S., Khalate, S. A., & Deokate, R. J. (2017). Overview of nanostructured metal oxides and pure nickel oxide (NiO) electrodes for supercapacitors: a review. *Journal of Alloys and Compounds*.

Kierzek, K., Frackowiak, E., Lota, G., Gryglewicz, G., & Machnikowski, J. (2004). Electrochemical capacitors based on highly porous carbons prepared by KOH activation. *Electrochimica Acta, 49*(4), 515-523.

Kim, H., Cho, M. Y., Kim, M. H., Park, K. Y., Gwon, H., Lee, Y., Roh, K. C., & Kang, K. (2013). A Novel High‐Energy Hybrid Supercapacitor with an Anatase TiO_2‐Reduced Graphene Oxide Anode and an Activated Carbon Cathode. *Advanced Energy Materials, 3*(11), 1500-1506.

Kim, J., Khoh, W.-H., Wee, B.-H., & Hong, J.-D. (2015). Fabrication of flexible reduced graphene oxide–TiO_2 freestanding films for supercapacitor application. *RSC Advances, 5*(13), 9904-9911.

Kim, J. H., Choi, W., Jung, H.-G., Oh, S. H., Chung, K. Y., Cho, W. I., Oh, I. H., & Nah, I. W. (2017). Anatase TiO2-reduced graphene oxide nanostructures with high-rate sodium storage performance. *Journal of Alloys and Compounds, 690*, 390-396.

Kim, T.-W., & Park, S.-J. (2017). Synthesis of reduced graphene oxide/thorn-like titanium dioxide nanofiber aerogels with enhanced electrochemical performance for supercapacitor. *Journal of colloid and interface science, 486*, 287-295.

Krishnan, S. G., Harilal, M., Pal, B., Misnon, I. I., Karuppiah, C., Yang, C.-C., & Jose, R. (2017). Improving the symmetry of asymmetric supercapacitors using battery-type positive electrodes and activated carbon negative electrodes by mass and charge balance. *Journal of Electroanalytical Chemistry, 805*, 126-132.

Krishnan, S. G., Harilal, M., Yar, A., Vijayan, B. L., Dennis, J. O., Yusoff, M. M., & Jose, R. (2017). Critical influence of reduced graphene oxide mediated binding of M (M= Mg, Mn) with Co ions, chemical stability and charge storability enhancements of spinal-type hierarchical MCo_2O_4 nanostructures. *Electrochimica Acta, 243*, 119-128.

Krivtsov, I., Ilkaeva, M., Avdin, V., Khainakov, S., Garcìa, J. R., Ordòñez, S., Dìaz, E., & Faba, L. (2015). A hydrothermal peroxo method for preparation of highly crystalline silica–titania photocatalysts. *Journal of colloid and interface science, 444*, 87-96.

Kruse, A., & Dahmen, N. (2018). Hydrothermal biomass conversion: Quo vadis? *The Journal of Supercritical Fluids, 134*, 114-123.

Kumar, K. T., Sundari, G. S., Kumar, E. S., Ashwini, A., Ramya, M., Varsha, P., Kalaivani, R., Andikkadu, M. S., Kumaran, V., & Gnanamuthu, R. (2018). Synthesis of nanoporous carbon with new activating agent for high-performance supercapacitor. *Materials Letters, 218*, 181-184.

Kumar, S., Malik, M., & Purohit, R. (2018). Synthesis of high surface area mesoporous silica materials using soft templating approach. *Materials Today: Proceedings,* *5*(2), 4128-4133.

Le, Z., Liu, F., Nie, P., Li, X., Liu, X., Bian, Z., Chen, G., Wu, H. B., & Lu, Y. (2017). Pseudocapacitive sodium storage in mesoporous single-crystal-like TiO_2–graphene nanocomposite enables high-performance sodium-ion capacitors. *ACS nano, 11*(3), 2952-2960.

Lee, D.-S., & Liu, T.-K. (2002). Preparation of TiO_2 sol using $TiCl_4$ as a precursor. *Journal of Sol-Gel Science and Technology, 25*(2), 121-136.

Lee, S., Cho, I.-S., Lee, J. H., Kim, D. H., Kim, D. W., Kim, J. Y., Shin, H., Lee, J.-K., Jung, H. S., & Park, N.-G. (2010). Two-step sol− gel method-based TiO_2 nanoparticles with uniform morphology and size for efficient photo-energy conversion devices. *Chemistry of Materials, 22*(6), 1958-1965.

Leong, K. H., Sim, L. C., Bahnemann, D., Jang, M., Ibrahim, S., & Saravanan, P. (2015). Reduced graphene oxide and Ag wrapped TiO_2 photocatalyst for enhanced visible light photocatalysis. *APL Materials, 3*(10), 104503.

Li, G., Li, L., Boerio-Goates, J., & Woodfield, B. F. (2005). High purity anatase TiO_2 nanocrystals: near room-temperature synthesis, grain growth kinetics, and surface hydration chemistry. *Journal of the American Chemical Society, 127*(24), 8659-8666.

Li, J., Huang, J., Li, J., Cao, L., Qi, H., Cheng, Y., Xi, Q., & Dang, H. (2017). Improved Li-ion diffusion process in TiO_2/rGO anode for lithium-ion battery. *Journal of Alloys and Compounds, 727*, 998-1005.

Li, S., Jiang, H., Yang, K., Zhang, Z., Li, S., Luo, N., Liu, Q., & Wei, R. (2018). Three-dimensional hierarchical graphene/TiO_2 composite as high-performance electrode for supercapacitor. *Journal of Alloys and Compounds, 746*, 670-676.

Li, X., & Wei, B. (2013). Supercapacitors based on nanostructured carbon. *Nano Energy,* *2*(2), 159-173.

Li, X., Zheng, F., Luo, Y., Wu, Y., & Lu, F. (2017). Preparation and electrochemical performance of TiO_2-SnO_2 doped RuO_2 composite electrode for supercapacitors. *Electrochimica Acta, 237*, 177-184.

Li, Z., Zhu, Y., Wang, L., Wang, J., Guo, Q., & Li, J. (2015). A facile method for the structure control of TiO_2 particles at low temperature. *Applied Surface Science, 355*, 1051-1056.

Liu, W.-w., Yan, X.-b., & Xue, Q.-j. (2013). Multilayer hybrid films consisting of alternating graphene and titanium dioxide for high-performance supercapacitors. *Journal of Materials Chemistry C, 1*(7), 1413-1422.

Liu, X., Iocozzia, J., Wang, Y., Cui, X., Chen, Y., Zhao, S., Li, Z., & Lin, Z. (2017). Noble metal–metal oxide nanohybrids with tailored nanostructures for efficient solar energy conversion, photocatalysis and environmental remediation. *Energy & Environmental Science, 10*(2), 402-434.

Liu, Y.-J., Aizawa, M., Wang, Z.-M., Hatori, H., Uekawa, N., & Kanoh, H. (2008). Comparative examination of titania nanocrystals synthesized by peroxo titanic acid approach from different precursors. *Journal of colloid and interface science, 322*(2), 497-504.

Lokhande, V., Lokhande, A., Lokhande, C., Kim, J. H., & Ji, T. (2016). Supercapacitive composite metal oxide electrodes formed with carbon, metal oxides and conducting polymers. *Journal of Alloys and Compounds, 682*, 381-403.

Lorenzen, A. L., Rossi, T. S., Riegel-Vidotti, I. C., & Vidotti, M. (2018). Influence of cationic and anionic micelles in the (sono) chemical synthesis of stable $Ni(OH)_2$ nanoparticles:“in situ” zeta-potential measurements and electrochemical properties. *Applied Surface Science*.

Low, F. W., Lai, C. W., & Hamid, S. B. A. (2015). Easy preparation of ultrathin reduced graphene oxide sheets at a high stirring speed. *Ceramics International, 41*(4), 5798-5806.

Low, F. W., Lai, C. W., & Hamid, S. B. A. (2017). Study of reduced graphene oxide film incorporated of TiO_2 species for efficient visible light driven dye-sensitized solar cell. *Journal of Materials Science: Materials in Electronics, 28*(4), 3819-3836.

Low, W., & Boonamnuayvitaya, V. (2013). A study of photocatalytic graphene–TiO_2 synthesis via peroxo titanic acid refluxed sol. *Materials Research Bulletin, 48*(8), 2809-2816.

Lu, S., Song, Y., Guo, K., Chen, X., Xu, J., & Zhao, L. (2018). Effect of aqueous electrolytes on the electrochemical behaviors of ordered mesoporous carbon composites after KOH activation as supercapacitors electrodes. *Journal of Electroanalytical Chemistry, 818*, 58-67.

Luo, D., Li, Y., Liu, J., Feng, H., Qian, D., Peng, S., Jiang, J., & Liu, Y. (2013). One-step solution-phase synthesis of a novel RGO–Cu_2O–TiO_2 ternary nanocomposite with excellent cycling stability for supercapacitors. *Journal of Alloys and Compounds, 581*, 303-307.

Minella, M., Versaci, D., Casino, S., Di Lupo, F., Minero, C., Battiato, A., Penazzi, N., & Bodoardo, S. (2017). Anodic Materials for Lithium-ion Batteries: TiO_2-rGO Composites for High Power Applications. *Electrochimica Acta, 230*, 132-140.

Mirzaeian, M., Abbas, Q., Ogwu, A., Hall, P., Goldin, M., Mirzaeian, M., & Jirandehi, H. F. (2017). Electrode and electrolyte materials for electrochemical capacitors. *International Journal of Hydrogen Energy, 42*(40), 25565-25587.

Mohammad-Rezaei, R., & Razmi, H. (2016). Preparation and Characterization of Reduced Graphene Oxide Doped in Sol-Gel Derived Silica for Application in

Electrochemical Double-Layer Capacitors. *International Journal of Nanoscience and Nanotechnology, 12*(4), 233-241.

Mondal, A., Maiti, S., Singha, K., Mahanty, S., & Panda, A. B. (2017). TiO_2-rGO nanocomposite hollow spheres: large scale synthesis and application as an efficient anode material for lithium-ion batteries. *Journal of Materials Chemistry A, 5*(45), 23853-23862.

Morimoto, N., Kubo, T., & Nishina, Y. (2016). Tailoring the oxygen content of graphite and reduced graphene oxide for specific applications. *Scientific reports, 6*, 21715.

Mu, X., Liu, X., Zhang, K., Li, J., Zhou, J., Xie, E., & Zhang, Z. (2016). Molybdenum dioxide-anchored graphene foam as a negative electrode material for supercapacitors. *Electronic Materials Letters, 12*(2), 296-300.

Munir, M. T., Mansouri, S. S., Udugama, I. A., Baroutian, S., Gernaey, K. V., & Young, B. R. (2018). Resource recovery from organic solid waste using hydrothermal processing: Opportunities and challenges. *Renewable and Sustainable Energy Reviews, 96*, 64-75.

Navarro-Suárez, A. M., Van Aken, K. L., Mathis, T., Makaryan, T., Yan, J., Carretero-González, J., Rojo, T., & Gogotsi, Y. (2018). Development of asymmetric supercapacitors with titanium carbide-reduced graphene oxide couples as electrodes. *Electrochimica Acta, 259*, 752-761.

Nguyen-Phan, T.-D., Liu, Z., Luo, S., Gamalski, A. D., Vovchok, D., Xu, W., Stach, E. A., Polyansky, D. E., Fujita, E., & Rodriguez, J. A. (2016). Unraveling the Hydrogenation of TiO_2 and Graphene Oxide/TiO_2 Composites in Real Time by in Situ Synchrotron X-ray Powder Diffraction and Pair Distribution Function Analysis. *The Journal of Physical Chemistry C, 120*(6), 3472-3482.

Omar, F. S., Numan, A., Duraisamy, N., Bashir, S., Ramesh, K., & Ramesh, S. (2016).

Ultrahigh capacitance of amorphous nickel phosphate for asymmetric supercapacitor applications. *RSC Advances, 6*(80), 76298-76306.

Pal, B., Vijayan, B. L., Krishnan, S. G., Harilal, M., Basirun, W. J., Lowe, A., Yusoff, M. M., & Jose, R. (2018). Hydrothermal syntheses of tungsten doped TiO_2 and TiO_2/WO_3 composite using metal oxide precursors for charge storage applications. *Journal of Alloys and Compounds, 740*, 703-710.

Pham, V. H., Nguyen-Phan, T.-D., Tong, X., Rajagopalan, B., Chung, J. S., & Dickerson, J. H. (2018). Hydrogenated TiO_2@ reduced graphene oxide sandwich-like nanosheets for high voltage supercapacitor applications. *Carbon, 126*, 135-144.

Ping, Y., Gong, Y., Fu, Q., & Pan, C. (2017). Preparation of three-dimensional graphene foam for high performance supercapacitors. *Progress in Natural Science: Materials International, 27*(2), 177-181.

Police, A. K. R., Chennaiahgari, M., Boddula, R., Vattikuti, S. P., Mandari, K. K., & Chan, B. (2018). Single-step hydrothermal synthesis of wrinkled graphene wrapped TiO $_2$ nanotubes for photocatalytic hydrogen production and supercapacitor applications. *Materials Research Bulletin, 98*, 314-321.

Poonguzhali, R., Shanmugam, N., Gobi, R., Senthilkumar, A., Viruthagiri, G., & Kannadasan, N. (2015). Effect of Fe doping on the electrochemical capacitor behavior of MnO_2 nanocrystals. *Journal of Power Sources, 293*, 790-798.

Prasannalakshmi, P., Shanmugam, N., & Kannadasan, N. (2016). Phase-dependent electrochemistry of TiO_2 nanocrystals for supercapacitor applications. *Journal of Electroanalytical Chemistry, 775*, 356-363.

Rajagopal, R., & Ryu, K.-S. (2018). Synthesis of rGO-doped Nb_4O_5–TiO_2 nanorods for photocatalytic and electrochemical energy storage applications. *Applied Catalysis B: Environmental, 236*, 125-139.

Rakhi, R., & Lekshmi, M. (2017). Reduced graphene oxide based ternary nanocomposite cathodes for high-performance aqueous asymmetric supercapacitors. *Electrochimica Acta, 231*, 539-548.

Ramadoss, A., & Kim, S. J. (2013). Improved activity of a graphene–TiO_2 hybrid electrode in an electrochemical supercapacitor. *Carbon, 63*, 434-445.

Rasul, S., Alazmi, A., Jaouen, K., Hedhili, M. N., & Costa, P. (2017). Rational design of reduced graphene oxide for superior performance of supercapacitor electrodes. *Carbon, 111*, 774-781.

Regonini, D., Bowen, C. R., Jaroenworaluck, A., & Stevens, R. (2013). A review of growth mechanism, structure and crystallinity of anodized TiO_2 nanotubes. *Materials Science and Engineering: R: Reports, 74*(12), 377-406.

Saha, S., Samanta, P., Murmu, N. C., & Kuila, T. (2018). A review on the heterostructure nanomaterials for supercapacitor application. *Journal of Energy Storage, 17*, 181-202.

Salari, M., Aboutalebi, S. H., Chidembo, A. T., Nevirkovets, I. P., Konstantinov, K., & Liu, H. K. (2012). Enhancement of the electrochemical capacitance of TiO_2 nanotube arrays through controlled phase transformation of anatase to rutile. *Physical Chemistry Chemical Physics, 14*(14), 4770-4779.

Sanchez, J. S., Pendashteh, A., Palma, J., Anderson, M., & Marcilla, R. (2018). Synthesis and application of $NiMnO_3$-rGO nanocomposites as electrode materials for hybrid energy storage devices. *Applied Surface Science*.

Sarma, B. K., Pal, A. R., Bailung, H., & Chutia, J. (2013). Growth of nanocrystalline TiO_2 thin films and crystal anisotropy of anatase phase deposited by direct current reactive magnetron sputtering. *Materials Chemistry and Physics, 139*(2-3), 979-987.

Sasirekha, N., Rajesh, B., & Chen, Y.-W. (2009). Synthesis of TiO_2 sol in a neutral solution using $TiCl_4$ as a precursor and H_2O_2 as an oxidizing agent. *Thin Solid Films, 518*(1), 43-48.

Sawczak, M., Sobaszek, M., Siuzdak, K., Ryl, J., Bogdanowicz, R., Darowicki, K., Gazda, M., & Cenian, A. (2015). Formation of highly conductive boron-doped diamond on TiO_2 nanotubes composite for supercapacitor or energy storage devices. *Journal of the Electrochemical Society, 162*(10), A2085-A2092.

Sharavath, V., Sarkar, S., & Ghosh, S. (2018). One-pot hydrothermal synthesis of TiO_2/graphene nanocomposite with simultaneous nitrogen-doping for energy storage application. *Journal of Electroanalytical Chemistry, 829*, 208-216.

Shavdina, O., Berthod, L., Kampfe, T., Reynaud, S., Veillas, C., Verrier, I., Langlet, M., Vocanson, F., Fugier, P., & Jourlin, Y. (2015). Large Area Fabrication of Periodic TiO_2 Nanopillars Using Microsphere Photolithography on a Photopatternable Sol–Gel Film. *Langmuir, 31*(28), 7877-7884.

Shen, J., Shi, M., Yan, B., Ma, H., Li, N., & Ye, M. (2011). Ionic liquid-assisted one-step hydrothermal synthesis of TiO_2-reduced graphene oxide composites. *Nano Research, 4*(8), 795.

Shin, H. J., Kim, K. K., Benayad, A., Yoon, S. M., Park, H. K., Jung, I. S., Jin, M. H., Jeong, H. K., Kim, J. M., & Choi, J. Y. (2009). Efficient reduction of graphite oxide by sodium borohydride and its effect on electrical conductance. *Advanced Functional Materials, 19*(12), 1987-1992.

Shoaib, A., Huang, Y., Liu, J., Liu, J., Xu, M., Wang, Z., Chen, R., Zhang, J., & Wu, F. (2017). Ultrathin single-crystalline TiO_2 nanosheets anchored on graphene to be hybrid network for high-rate and long cycle-life sodium battery electrode application. *Journal of Power Sources, 342*, 405-413.

Sobczyk-Guzenda, A., Owczarek, S., Szymanowski, H., & Gazicki-Lipman, M. (2015). Amorphous and crystalline TiO_2 coatings synthesized with the RF PECVD technique from metalorganic precursor. *Vacuum, 117*, 104-111.

Staudenmaier, L. (1898). Verfahren zur darstellung der graphitsäure. *European Journal of Inorganic Chemistry, 31*(2), 1481-1487.

Sun, J., & Gao, L. (2002). pH Effect on Titania - Phase Transformation of Precipitates from Titanium Tetrachloride Solutions. *Journal of the American Ceramic Society, 85*(9), 2382-2384.

Sykam, N., & Rao, G. M. (2017). Room temperature synthesis of reduced graphene oxide nanosheets as anode material for supercapacitors. *Materials Letters, 204*, 169-172.

Tang, Y., Wu, D., Chen, S., Zhang, F., Jia, J., & Feng, X. (2013). Highly reversible and ultra-fast lithium storage in mesoporous graphene-based TiO_2/SnO_2 hybrid nanosheets. *Energy & Environmental Science, 6*(8), 2447-2451.

Tao, L., Li, J., Zhou, Q., Zhu, H., Hu, G., & Huang, J. (2018). Composition, microstructure and performance of cobalt nickel phosphate as advanced battery-type capacitive material. *Journal of Alloys and Compounds*.

Thakur, S., & Karak, N. (2012). Green reduction of graphene oxide by aqueous phytoextracts. *Carbon, 50*(14), 5331-5339.

Thirugnanam, L., & Sundara, R. (2018). Few layer graphene wrapped mixed phase TiO_2 nanofiber as a potential electrode material for high performance supercapacitor applications. *Applied Surface Science, 444*, 414-422.

Tiron, V., Velicu, I.-L., Dobromir, M., Demeter, A., Samoila, F., Ursu, C., & Sirghi, L. (2016). Reactive multi-pulse HiPIMS deposition of oxygen-deficient TiOx thin films. *Thin Solid Films, 603*, 255-261.

Tomita, K., Petrykin, V., Kobayashi, M., Shiro, M., Yoshimura, M., & Kakihana, M. (2006). A water‐soluble titanium complex for the selective synthesis of nanocrystalline brookite, rutile, and anatase by a hydrothermal method. *Angewandte Chemie International Edition, 45*(15), 2378-2381.

Torres, G. R., Lindgren, T., Lu, J., Granqvist, C.-G., & Lindquist, S.-E. (2004). Photoelectrochemical study of nitrogen-doped titanium dioxide for water oxidation. *The Journal of Physical Chemistry B, 108*(19), 5995-6003.

Triampo, W., Yodyingyong, S., Panijpan, B., & Triampo, D. (2009). An Inexpensive Furnace for Calcination: Simple TiO_2 Synthesis. *Journal of chemical education, 86*(8), 950.

Vinny, R., Chaitra, K., Venkatesh, K., Nagaraju, N., & Kathyayini, N. (2016). An excellent cycle performance of asymmetric supercapacitor based on bristles like α-MnO_2 nanoparticles grown on multiwalled carbon nanotubes. *Journal of Power Sources, 309*, 212-220.

Vu, T. H. T., Tran, T. T. T., Le, H. N. T., Nguyen, P. H. T., Bui, N. Q., & Essayem, N. (2015). A new green approach for the reduction of graphene oxide nanosheets using caffeine. *Bulletin of Materials Science, 38*(3), 667-671.

Wang, B., Xie, Y., Liu, T., Luo, H., Wang, B., Wang, C., Wang, L., Wang, D., Dou, S., & Zhou, Y. (2017). $LiFePO_4$ quantum-dots composite synthesized by a general microreactor strategy for ultra-high-rate lithium ion batteries. *Nano Energy, 42*, 363-372.

Wang, J., Dou, W., Zhang, X., Han, W., Mu, X., Zhang, Y., Zhao, X., Chen, Y., Yang, Z., & Su, Q. (2017). Embedded Ag quantum dots into interconnected Co_3O_4 nanosheets grown on 3D graphene networks for high stable and flexible supercapacitors. *Electrochimica Acta, 224*, 260-268.

Wang, W., Wang, Z., Liu, J., Luo, Z., Suib, S. L., He, P., Ding, G., Zhang, Z., & Sun, L. (2017). Single-step one-pot synthesis of TiO_2 nanosheets doped with sulfur on reduced graphene oxide with enhanced photocatalytic activity. *Scientific reports, 7*, 46610.

Wang, Y., Song, Y., & Xia, Y. (2016). Electrochemical capacitors: mechanism, materials, systems, characterization and applications. *Chemical Society Reviews, 45*(21), 5925-5950.

Wellia, D. V., Xu, Q. C., Sk, M. A., Lim, K. H., Lim, T. M., & Tan, T. T. Y. (2011). Experimental and theoretical studies of Fe-doped TiO_2 films prepared by peroxo sol–gel method. *Applied Catalysis A: General, 401*(1-2), 98-105.

Wu, H., Wang, X., Jiang, L., Wu, C., Zhao, Q., Liu, X., & Yi, L. (2013). The effects of electrolyte on the supercapacitive performance of activated calcium carbide-derived carbon. *Journal of Power Sources, 226*, 202-209.

Wu, Z., Li, L., Yan, J. m., & Zhang, X. b. (2017). Materials Design and System Construction for Conventional and New‐Concept Supercapacitors. *Advanced Science, 4*(6), 1600382.

Xia, X.-h., Tu, J.-p., Wang, X.-l., Gu, C.-d., & Zhao, X.-b. (2011). Hierarchically porous NiO film grown by chemical bath deposition via a colloidal crystal template as an electrochemical pseudocapacitor material. *Journal of Materials Chemistry, 21*(3), 671-679.

Xiao, H., Guo, W., Sun, B., Pei, M., & Zhou, G. (2016). Mesoporous TiO_2 and Co-doped TiO_2 nanotubes/reduced graphene oxide composites as electrodes for supercapacitors. *Electrochimica Acta, 190*, 104-117.

Xie, H., Zhang, Q., Xi, T., Wang, J., & Liu, Y. (2002). Thermal analysis on nanosized TiO_2 prepared by hydrolysis. *Thermochimica acta, 381*(1), 45-48.

Xie, Y., Song, J., Zhou, P., Ling, Y., & Wu, Y. (2016). Controllable synthesis of TiO_2/graphene nanocomposites for long lifetime lithium storage: nanoparticles vs. nanolayers. *Electrochimica Acta, 210*, 358-366.

Xu, K., Ding, M. S., & Jow, T. R. (2001). Quaternary onium salts as nonaqueous electrolytes for electrochemical capacitors. *Journal of the electrochemical Society, 148*(3), A267-A274.

Xu, X., Zhang, X., Zhao, Y., & Hu, Y. (2018). An efficient hybrid supercapacitor based on battery-type MnS/reduced graphene oxide and capacitor-type biomass derived activated carbon. *Journal of Materials Science: Materials in Electronics, 29*(10), 8410-8420.

Yan, J., Wang, Q., Wei, T., & Fan, Z. (2014). Recent advances in design and fabrication of electrochemical supercapacitors with high energy densities. *Advanced Energy Materials, 4*(4).

Yang, M., Liu, W., Jiang, C., He, S., Xie, Y., & Wang, Z. (2018). Fabrication of superhydrophobic cotton fabric with fluorinated TiO_2 sol by a green and one-step sol-gel process. *Carbohydrate Polymers*.

Yang, S., Dong, W., Shen, D., Li, S., Sun, W., Hong, X., Wang, M., & Mao, Y. (2017). Composite of nonexpansion reduced graphite oxide and carbon derived from pitch as anodes of Na-ion batteries with high coulombic efficiency. *Chemical Engineering Journal, 309*, 674-681.

Yang, S., Lin, Y., Song, X., Zhang, P., & Gao, L. (2015). Covalently coupled ultrafine H-TiO_2 nanocrystals/nitrogen-doped graphene hybrid materials for high-performance supercapacitor. *ACS applied materials & interfaces, 7*(32), 17884-17892.

Yang, Z., Choi, D., Kerisit, S., Rosso, K. M., Wang, D., Zhang, J., Graff, G., & Liu, J.

(2009). Nanostructures and lithium electrochemical reactivity of lithium titanites and titanium oxides: A review. *Journal of Power Sources, 192*(2), 588-598.

Yao, D., Ouyang, Y., Jiao, X., Ye, H., Lei, W., Xia, X., Lu, L., & Hao, Q. (2018). Hierarchical NiO@ $NiCo_2O_4$ core–shell nanosheet arrays on Ni foam for high-performance electrochemical supercapacitors. *Industrial & Engineering Chemistry Research, 57*(18), 6246-6256.

Yoon, D., Hwang, J., Kim, D. H., Chang, W., Chung, K. Y., & Kim, J. (2017). One-pot route for uniform anchoring of TiO_2 nanoparticles on reduced graphene oxides and their anode performance for lithium-ion batteries. *The Journal of Supercritical Fluids, 125*, 66-78.

Yu, H.-F. (2007). Photocatalytic abilities of gel-derived P-doped TiO_2. *Journal of Physics and Chemistry of Solids, 68*(4), 600-607.

Yu, J., Wang, G., Cheng, B., & Zhou, M. (2007). Effects of hydrothermal temperature and time on the photocatalytic activity and microstructures of bimodal mesoporous TiO_2 powders. *Applied Catalysis B: Environmental, 69*(3-4), 171-180.

Yun, T. K., Park, S. S., Kim, D., Shim, J.-H., Bae, J. Y., Huh, S., & Won, Y. S. (2012). Effect of the rutile content on the photovoltaic performance of the dye-sensitized solar cells composed of mixed-phase TiO_2 photoelectrodes. *Dalton Transactions, 41*(4), 1284-1288.

Zhang, L., Candelaria, S. L., Tian, J., Li, Y., Huang, Y.-x., & Cao, G. (2013). Copper nanocrystal modified activated carbon for supercapacitors with enhanced volumetric energy and power density. *Journal of Power Sources, 236*, 215-223.

Zhang, R., Wang, Y., Zhou, H., Lang, J., Xu, J., Xiang, Y., & Ding, S. (2018). Mesoporous TiO_2 nanosheets anchored on graphene for ultra long life Na-ion batteries. *Nanotechnology, 29*(22), 225401.

Zhang, Y., Foster, C. W., Banks, C. E., Shao, L., Hou, H., Zou, G., Chen, J., Huang, Z., & Ji, X. (2016). Graphene‐Rich Wrapped Petal‐Like Rutile TiO_2 tuned by Carbon Dots for High‐Performance Sodium Storage. *Advanced Materials, 28*(42), 9391-9399.

Zhang, Y., Wang, F., Zhu, H., Zhang, D., & Chen, J. (2017). Elongated TiO_2 nanotubes directly grown on graphene nanosheets as an efficient material for supercapacitors and absorbents. *Composites Part A: Applied Science and Manufacturing, 101*, 297-305.

Zhang, Z., Wang, L., Li, Y., Wang, Y., Zhang, J., Guan, G., Pan, Z., Zheng, G., & Peng, H. (2017). Nitrogen‐Doped Core‐Sheath Carbon Nanotube Array for Highly Stretchable Supercapacitor. *Advanced Energy Materials, 7*(5), 1601814.

Zhao, C., Ju, P., Wang, S., Zhang, Y., Min, S., & Qian, X. (2016). One-step hydrothermal preparation of TiO_2/RGO/$Ni(OH)_2$/NF electrode with high performance for supercapacitors. *Electrochimica Acta, 218*, 216-227.

Zhao, L., Tang, T., Chen, W., Feng, X., & Mi, L. (2018). Carbon coated ultrasmall anatase TiO2 nanocrystal anchored on N, S-RGO as high-performance anode for sodium ion batteries. *Green Energy & Environment*.

Zhong, C., Deng, Y., Hu, W., Qiao, J., Zhang, L., & Zhang, J. (2015). A review of electrolyte materials and compositions for electrochemical supercapacitors. *Chemical Society Reviews, 44*(21), 7484-7539.

Zhou, Y., Bao, Q., Tang, L. A. L., Zhong, Y., & Loh, K. P. (2009). Hydrothermal dehydration for the "green" reduction of exfoliated graphene oxide to graphene and demonstration of tunable optical limiting properties. *Chemistry of materials, 21*(13), 2950-2956.

Zhu, J., Sakaushi, K., Clavel, G., Shalom, M., Antonietti, M., & Fellinger, T.-P. (2015). A general salt-templating method to fabricate vertically aligned graphitic carbon nanosheets and their metal carbide hybrids for superior lithium ion batteries and water splitting. *Journal of the American Chemical Society, 137*(16), 5480-5485.

Zhu, X., Yu, S., Xu, K., Zhang, Y., Zhang, L., Lou, G., Wu, Y., Zhu, E., Chen, H., & Shen, Z. (2018). Sustainable activated carbons from dead ginkgo leaves for supercapacitor electrode active materials. *Chemical Engineering Science, 181*, 36-45.

Zou, J., Gao, J., & Xie, F. (2010). An amorphous TiO_2 sol sensitized with H_2O_2 with the enhancement of photocatalytic activity. *Journal of Alloys and Compounds, 497*(1-2), 420-427.

LIST OF PUBLICATIONS AND PAPERS PRESENTED

Research Articles:

1. Heng. I., Lai, C.W., Juan, J.C., Arshid. N., J. Iqbal., Teo. E.Y.L. (2019)
   Low temperature synthesis of TiO_2 nanocrystals for high performance electrochemical supercapacitors. *Ceramics International*, 45(1), 4990-5000. (Q1, Impact factor = 3.450)
2. Heng.I, Lai, C.W., Juan, J.C., Low F.W., Amin N., Tiong S.K. (2019)
   High performance supercapattery with rGO/TiO_2 nanocomposites anode and activated carbon cathode. *Journal of Alloys and Compounds*, 796(1), 13-24. (Q1, Impact factor = 4.175)

Presentation in Conference:

1. **Association of South-East Asian Nations Emerging Researchers Conference (ASEAN ERC) 2018**, Sunway University, 3rd Dec 2018
   Oral Presenter- Preliminary Study on Hybrid Supercapacitor Based on TiO_2 Nanocrystals and Activated Carbon.
2. **UMRC 2018 Poster Competition**, University of Malaya, 15-17th Nov 2018.
   Oral Presenter- Phase Controlled Synthesis of Engineered Nano-Hybrid Composites with Reduced Occupational Health Hazards for Potable Water Supply.